Design and Characterisation of Soft Biomaterials and Interfaces for Bio-Adhesives and Cell Culture

William Valentine Megone

Submitted to the School of Engineering and Material Science Queen Mary University of London in partial fulfilment of the requirements of the Degree of Doctor of Philosophy in Engineering

Acknowledgments

First, I would like to thank my supervisor Dr Julien Gautrot for all of his guidance help and support over the past 4 years. It has been a real pleasure working with him and I have thoroughly enjoyed the atmosphere he has cultivated in his group. I am extremely grateful for all of his guidance and without his help and support completing this project would not have been possible

I would also like the thank all of my friends and colleagues within QMUL and above all within my group. I would especially like to thank Dexu Kong, Burcu Colak and Lihui Peng for all their help with my experiments. I would also like to thank Matt Dibble, Emma Butterworth, Gaston Primo, Luis Flores, Gannian Zhang, Miguel Quetzeri and Jorge Fuentes for all the delicious shared luncheon foods and company.

I am extremely grateful to all the support staff who have helped me so much along the way, in particular I'd especially like to thank Chris Mole, Alice Williams and Russell Bailey for all their technical support making my research possible. I would also like to extend my thanks to Dr Nima Roohpour for all his technical expertise, advice and support.

I am extremely thankful to all those who have helped me throughout my academic career. In particular the Mech Eng Footy guys from Imperial, Hyung, Santhosh, Dat, Yang, Sim, Wai Hong, Dan and co. I was also extremely lucky to make great friends during my undergraduate without whom I wouldn't be where I am today, so thanks a lot Tino, Rostocki, Jay and TK. I would also like to extend my thanks and gratitude to Adriana and her family for the huge amounts of support and guidance they offered me through some of my most formative years.

I am especially grateful to everyone at the London Japanese RFC, there are too many of you to name but playing with you has given me huge amounts of joy and I am incredibly proud to pull on the jersey with you and to call you my teammates and friends

I would like to thank my close friends, Kit, Ginbob, Stef, Beatty, Imogen, Danny T, Ele, King Pez and Seb you have all supported me hugely over the past years. I am incredibly grateful to you all and hope our friendships will carry on through our future endeavours.

Finally I would like to thank my Granny, Mum and Alex. I know you have all sacrificed so much for me throughout my life to help me get where I am today. I am so grateful for all the love and support you have given me.

Abstract

This thesis consists of three chapters which can be split into studies of (1) the impact of length scale, surface adhesion and heterogeneity on the mechanical characterisation of soft biomaterials, (2) the effect of non-covalent cross-linking chemistry on the mechanics of CMC hydrogels and (3) analytical characterisation of the interfacial mechanics of liquid-liquid interfaces.

The mechanical properties of soft materials used in the biomedical field play an important role on their performance. In the field of tissue engineering, it is known that cells sense the mechanical properties of their environment, however some materials, such as Sylard 184 PDMS (poly(dimethylsiloxane)), have failed to elicit such response. It was proposed that differences in the mechanical properties of such soft materials, at different scales, could account for these discrepancies. Indeed, the variation in the elastic moduli obtained for soft materials characterised at different scales can span several orders of magnitude. This called for a side-by-side comparison of the mechanical behaviour of soft materials at different scales. Here we use indentation, rheology and atomic force microscopy nanoidentation (using different tip geometries) to characterise the mechanical properties of PDMS, poly(acrylamide) (PAAm) and carboxymethyl cellulose (CMC) hydrogels at different length scales. Our results highlight the importance of surface adhesion and the resulting changes in contact area, and sample microstructural heterogeneity, in particular for the mechanical characterisation of ultra-soft substrates at the nano- to micro-scale.

Next the impact of inorganic divalent cationic and organic cationic polyelectrolyte cross-linkers on the rheological and adhesive properties of CMC hydrogels was studied. The inorganic cations used in this study were Sr^{2+} and Ca^{2+} resulted in no

significant change in the bulk rheological properties and apparent chain collapse, but an increase in the adhesive strength. The introduction of organic polyelectrolytes caused complex coacervation with the CMC polymer chains. Some CMC chain bridging occurred, but the interactions between the polyelectrolytes and CMC chains caused complexes to form, resulting in polymer rich complexes to form within a more dilute matrix. The introduction of organic polyelectrolyte cross-links failed to increase the bulk mechanical properties studied by rheology but did increase the adhesive strength.

Finally the impact of protein adsorption on interfacial mechanics was studied. The interfacial mechanics was studied by interfacial shear rheology and interfacial nanoindentation by AFM, and PLL, BSA and lysozyme were the proteins chosen for this study. Proteins adsorbed at the interface resulted in a significant increase in the interfacial shear moduli, however this was not seen by nanoindentation. By modelling the interfacial mechanics as the superposition of the film forces and the interfacial surface tension forces we showed that when testing by nanoindentation changes in surface tension and surface potential have a significant impact on the interfacial mechanics. The addition of protein films was shown to have a surfactant effect on interfaces essentially softening them, this results in the films essentially having soft substrates and is proposed as the main cause of discrepancies between interfacial rheology and nanoindentation by AFM.

Disclaimer

I, William Valentine Megone, confirm that the research included within this thesis is my own work or that where it has been carried out in collaboration with, or supported by others, that this is duly acknowledged below and my contribution indicated. Previously published material is also acknowledged below.

I attest that I have exercised reasonable care to ensure that the work is original, and does not to the best of my knowledge break any UK law, infringe any third party's copyright or other Intellectual Property Right, or contain any confidential material.

I accept that the College has the right to use plagiarism detection software to check the electronic version of the thesis.

I confirm that this thesis has not been previously submitted for the award of a degree by this or any other university.

William Megone

1st November 2018

"*You know what I think? I think that we're all in our private traps, clamped in them, and none of us can ever get out. We scratch and claw... but only at the air, only at each other, and for all of it, we never budge an inch.*"

Norman Bates, Psycho, 1960
Dir. Alfred Hitchcock

"The passage of time
Is flicking dimly up on the screen
I can't see the lines
I used to think I could read between
Perhaps my brains have turned to sand"

Brian Eno, Golden Hours, 1975

"To stay apart when others have fun,
But being happy all the time,
Gladly carrying out the most sacred task,
Renouncing in a noble way one's personal desires,
Living in darkness from the sun but shining like a star,
That is the art that only one whose soul is bent on heaven can understand"

Miss Juliet, Land of Silence and Darkness, 1971
Dir. Werner Herzog

Table of Contents

List of Figures

the ratios of CMC: organic cations the same as those used for the rheology and lap shear experiments. A minimum of three samples per experiment were tested. All error bars are standard deviations.

Figure 4.1 Mechanical characterisation of fluorinated oil – PBS interfaces, done by Dr Dexu Kong, with and without protein films by oscillatory rheology146, 148, showing a) the frequency sweeps performed on the dif-ferent interfaces with an oscillating displacement of 10-4 rad, from 0.01 – 100 Hz, and b) a summary comparing the storage moduli for the different conditions tested. All error bars are standard deviations. The surfactant used was PFBC at 0.01 mg/mL and the PLL and BSA concentrations were 1 mg/mL and 0.1 mg/mL respectively.

Figure 4.2 Mechanical characterisation of fluorinated oil – PBS interfaces, done by Dr Dexu Kong, with and without protein films by oscillatory rheology144, 146, showing, a) representative stress relaxation data on fluorinated oil + [s] – PBS + PLL interfaces with the PLL deposited at pH 10.5 and 7.4 and c) comparison of protein film adsorption at fluorinated oil + [s] – PBS interfaces for BSA, PLL at pH 7.4 and PLL at pH 10.5.

Figure 4.3 Nanoindentation by AFM on fluorinated oil – PBS interfaces with and without protein using a plain pyramidal AFM tip showing a) – f) histograms of the interfacial stiffness for fluorinated oil – PBS only, fluorinated oil – PBS + BSA, fluorinated oil + [s] – PBS, fluorinated oil + [s] – PBS + BSA, fluorinated oil + [s] – PBS + PLL at pH 7.4 and fluorinated oil + [s] – PBS + PLL at pH 10.5 respectively, g) box plot summarising the distribution of the moduli for the fore mentioned conditioned and h) summary of the interfacial stiffness obtained for the different interfaces. PFBC was used as the surfactant with a concentration of 0.01 mg/mL and the BSA and PLL concentrations were 1 mg/mL and 0.1 mg/mL respectively. AFM experiments were conducted on a minimum of three sam-ples with each sample being tested in three 1 mm X 1 mm squares performing 100 indents in each area. All error bars are standard errors and all values are significantly different apart from those labelled n.s. with $p < 0.01$

Figure 4.4 Nanoindentation by AFM with a 20 mm diameter colloidal tip on fluorinated oil – PBS interfaces with and without protein using a plain pyramid AFM tip showing a) – f) histograms of the inter-facial stiffness for fluorinated oil – PBS only, fluorinated oil – PBS + BSA, fluorinated oil + [s] – PBS, fluorinated oil + [s] – PBS + BSA, fluorinated oil + [s] – PBS + PLL at pH 7.4 and fluorinated oil + [s] – PBS + PLL at pH 10.5 respectively, g) box plot summarising the distribution of the moduli for the fore mentioned conditioned and h) summary of the interfacial stiffness obtained for the different interfaces. The surfactant used was PFBC at a con-centration of 0.01 mg/mL and the proteins used were BSA and PLL at concentrations of 1 mg/mL and n0.1 mg/mL respectively. AFM experiments were conducted on a minimum of three samples with each sample being tested in three 1 mm X 1 mm squares performing 100 indents in each area. All error bars are standard errors and all values are significantly different, apart from those labelled n.s. with $p < 0.01$

Figure 4.5 Comparison of the normalised interfacial stiffness of fluorinated oil – PBS interfaces, with and without protein, when tested using a colloidal AFM tip against a plain pyramid tip. All error bars are stand-ard errors.

Figure 4.6 Representative raw AFM nanoindentation curves on fluorinated oil – PBS, fluorinated oil + [s] – PBS and fluori-nated oil – PBS + BSA interfaces using a) a plain pyramid tip and b) a colloidal tip and raw AFM curves on fluor-inated oil + [s] – PBS + BSA/PLL at pH 7.4/PLL at pH 10.5 using c) a plain pyramid tip and d) a colloidal tip). The surfactant used was PFBC at a concentration of 0.01 mg/mL and the BSA and PLL concentration were 1 mg/ml and 0.1 mg/mL respectively.

Figure 4.7 Image showing emulsions made using mineral oil and PBS with BSA and Lysozyme as the proteins and benzoyl chloride (marked A) or sebacoyl chloride (marked B) as the surfactant. The surfactant was always used at a con-centration of 0.1 mg/ml and the protein concentration was kept at 10 mg/ml

Figure 4.8 Oscillatory rheology characterisation of mineral oil – PBS interfaces by a) Oscillating frequency sweep with a oscillating displacement of 10-4 rad from 0.01 – 10 Hz on mineral oil – PBS interfaces with and without lysozyme (used at a concentration of 10 mg/mL) and benzoyl chloride (used at a concentration of 0.1 mg/mL)respectively, where the solid dots are G' and hollow dots are G'', b) stress relaxation data on interfaces showing the impact of protein on the relaxation profile, c) representative time sweep showing the formation of a lysozyme protein film on a mineral oil – PBS interface (solid line showing G' and the dotted line G''), d) summary of the interfacial

me-chanics of mineral oil – PBS interfaces comparing films with and without surfactant and lysozyme respectively. A minimum of three samples was tested per test. All error bars are standard deviations.

Figure 4.9 a) – c) Histograms showing the distribution of interfacial stiffness obtained by interfacial nanoindentation by AFM using a colloidal probe on mineral oil – PBS, mineral oil + [s] – PBS, and mineral oil + PBS – PBS + lysozyme interfaces respectively, formed at pH 7.4 with benzoyl chloride and lysozyme concentrations of 0.1 and 10 mg/ml respectively and d) boxplot summarising the distribution of the interfacial stiffness of the mineral oil systems, showing the spread in data for the plain mineral oil – PBS interface, mineral oil + [s] – PBS and mineral oil + [s] – PBS + lysozyme interfaces. A minimum of three samples for each condition were tested, three 1mm X 1mm areas on each sample were tested with 100 indentation curves taken at each location. The colloidal AFM tip used had a diameter of 20mm. All the data is significantly different with $p < 0.01$ unless labelled not significant (n.s.).

Figure 4.10 Summary of the interfacial stiffness of the mineral oil systems, showing the average stiffness of the plain mineral oil – PBS interface, mineral oil + [s] – PBS and mineral oil + [s] – PBS + lysozyme interfaces. A minimum of three samples for each condition were tested, three 1mm X 1mm areas on each sample were tested with 100 inden-tation curves taken at each location. The colloidal AFM tip used had a diameter of 20mm.All error bars are stand-ard errors and all the data is significantly different with $p < 0.01$ unless labelled not significant (n.s.).

Figure 4.11 Representative pendent droplet images of fluorinated oil droplets in PBS and PBS in mineral oil with and without surfactant. The surfactant used for the fluorinated and mineral oil were PFBC and benzoyl chloride respec-tively at concentrations of 0.01 mg/mL and 0.1 mg/mL respectively. The image of the fluorinated oil – PBS droplet has a representative fit (red line) used to characterise the surface tension.

Figure 4.12 Representative pendent droplet images showing the impact of protein absorption on the drop profile initially, $t = 0$, and after 14 h allowing for the films to fully deposit. For the fluorinated oil PFBC and PLL were used as the sur-factant and protein respectively at concentrations of .0.01 mg/mL and 0.1 mg/mL respectively. For the mineral oil 0.1 mg/mL benzoyl chloride was used as the surfactant and 10 mg/mL lysozyme was used as the protein.

for the lower quartile and blue the average. The modelled data is shown by the black dotted line with yellow error bars showing the standard error of the estimate. Details of the values for the variables used for the numerical model are shown in table 4.5. Note: for PLL the upper quartile is not included as the overlap between the average and the upper quartile made it difficult to read the graph.

Figure 4.21 Effect of changing the interfacial surface tension on modelled data for a) PLL b) BSA and c) Lysozyme protein films deposited at oil-PBS interfaces (mineral oil in the case of lysozyme and fluorinated oil for BSA and PLL). The orange curves here are the same as the fits shown in figure 4.21 and the blue and green curves show theoretical values with varying surface tension according to the legend.

Figure 4.22 Effect of changing the surface potential on modelled data for a) PLL b) BSA and c) Lysozyme protein films depos-ited at oil-PBS interfaces (mineral oil in the case of lysozyme and fluorinated oil for BSA and PLL). The orange curves here are the same as the fits shown in figure 4.21 and the blue and green curves show theoretical values with varying surface potential according to the legend.

Figure 4.23 Effect of changing the shear moduli used in the FEA on modelled data for a) PLL b) BSA and c) Lysozyme protein films deposited at oil-PBS interfaces (mineral oil in the case of lysozyme and fluorinated oil for BSA and PLL). The orange curves here are the same as the fits shown in figure 4.21 and the blue and green curves show theoretical values with the modulus increased or decreased by 20% respectively.

List of Tables

Nomenclature

A	Cross Sectional Area
a	Contact Radius
AFM	Atomic Force Microscopy
ATRP	Atom Transfer Radical Polymerisation
BSA	Bovine Serum Albumin
CMC	Carboxymethyl Cellulose
D	Interfacial Gap
DETA	Diethyl Triamine
Dfl	Cantilever Deflection
DMA	Dynamic Mechanical Analysis
DMT	Derjaguin, Muller and Toporov
DVLO	Dejaguin Landau Verwey Overbeek
DVS	Divinyl Sulfone
E	Young's Modulus
ECM	Extra Cellular Matrix
FEA	Finite Element Analysis
G	Shear Modulus
γ	Surface Tension
G'	Shear Storage Modulus
G"	Shear Loss Modulus
G*	Complex Shear Modulus
h	Indentation Depth

HCl	Hydrochloric Acid
JKR	Johnson, Kendall and Roberts
MSC	Mesenchymal Stem Cell
P	Indentation Load
Π	Disjoining Pressure
PAAm	Polyacrylamide
PBS	Phosphate Buffered Saline
PDMS	Polydimethylsiloxane
PEG	Poly(ethylene glycol)
PEHA	Pentaethylenehexamine
PEO	Poly(ethylene oxide)
PEtOx	Polyoxazoline
PFBC	Pentafluorobenzoyl chloride
PLL	Poly-l-lysine
SEM	Scanning Electron Microscopy
ω	Angular Viscosity
W	Work of Adhesion
ε	Strain
η	Viscosity
λ	Stretch
ν	Poisson's Ratio
σ	Stress
τ	True Stress

Chapter One

Introduction

This thesis consists of three chapters covering a broad range of topics, with some through narratives and themes. It is split into studies of (1) the impact of length scale, surface adhesion and heterogeneity on the mechanical characterisation of soft biomaterials, (2) the effect of non-covalent cross-linking chemistry on the mechanics of CMC hydrogels and (3) analytical characterisation of the interfacial mechanics of liquid-liquid interfaces.

Soft materials are ubiquitous in the field of bioengineering, human tissue varies from having moduli in the range of kPa, like brain tissue, to MPa in the case of cartilage. Furthermore tissue often have high performance properties arising from their heterogeneous structure. Beyond soft heterogeneous materials occurring frequently in nature, current thinking with respect to *in vitro* cell culture and tissue engineering shows a relationship between cell spreading, adhesion and fate and the mechanics of their substrate. As a result being able to reliably characterise soft materials both macroscopically and on length scales relevant to what cells sense is clearly very important. In the first experimental chapter of this work the agreement between frequently used macroscale (rheology and microindentation testing) and local (nanoindentation) mechanical testing methods is investigated on a series of materials with differing structure and properties across a range of stiffnesses.

The motivation for the third experimental chapter is similar to that mentioned for the first experimental chapter, however here the mechanics of interfaces occurring

between two immiscible fluids is considered. Recent research within the Gautrot laboratory has shown how cells can proliferate at liquid-liquid interfaces. Considering the obviously weak bulk mechanics of oil droplets this finding is quite striking. Hence the desire to fully understand what is being sensed at by cells at these interfaces and how the localised mechanical strength is being derived. As such understanding the shear and in plain mechanical response at these interfaces is studied.

Finally, carboxymethyl cellulose (CMC) is a very commonly used polysaccharide hydrogel, particularly as a denture adhesive. Denture adhesives have quite specific design criteria, needing to last for around 12 h securely, while remaining easily removable and easy to clean. As a result being able to tine the mechanics of CMC gels is important to ensuring they can be best utilised effectively as denture adhesives and other potential uses. The use of ionic crosslinks to tune hydrogels in this context is particularly interesting as these are non-permanent bonds and hence can be broken with relative ease. The use of ionic crosslinks can result in numerous different structures forming, from inter-chain crosslinking in an egg-box model to phase separating chain clustering like in coacervates. Hence studying the impact of divalent cationic crosslinkers on CMC gels mechanics and structure is of great interest.

The literature on these subjects will now be considered in an extensive literature review. Here we aim to give an overview and outlook on current opinion on: the techniques and models used to characterise the mechanics of soft biomaterials; the design and characterisation of hydrogels utilising non-covalent cross-linking; the current experimental methods used to mechanically characterise liquid-liquid interfaces and the models used to understand interfacial mechanics.

1.1 Multiscale Mechanical Properties of Soft Biomaterials

Interest in the study of mechanical properties of soft materials in the field of biomedical engineering has grown significantly in recent years. It has been studied across many applications including, tissue engineering[1, 2], drug delivery[2, 3], wound healing[2, 4, 5], and cell culture substrates for *in vitro* studies[6-8]. However, typical engineering methods for mechanical characterisation are tuned for use with traditional engineering materials, where the moduli is typically in the range of MPa – GPa. As a result the mechanical characterisation of soft biomaterials is not trivial, both in terms of the measurement of mechanical data and the interpretation of the data. In terms of measurement, it can be difficult to grip soft materials without damaging them, and furthermore materials like hydrogels can be difficult to machine into specific sample shapes used for testing, like 'dog bones'. The materials themselves also often have complex structures making the interpretation of data more challenging, for example, consisting of two phases (a solid phase and a liquid phase)[9], having a heterogeneous structure[10-12] or displaying strong time scale dependent properties[13, 14].

The complexity of the mechanics of soft biomaterials also has a significant impact on their application. This is particularly striking with respect to cell culture, where cell spreading, fate and differentiation are strongly influenced by the mechanical microenvironment. To illustrate the importance of soft biomaterial mechanics the impact of cell microenvironment mechanics on cell culture will now be explored in greater detail.

1.1.2 Impact of Biomaterial Mechanics on Cell Culture

The cells which make up the tissue of complex organisms are normally found embedded within a fibrous extracellular matrix (ECM). The matrix provides not only

structural integrity to cells allowing them to withstand daily stresses, but also plays a part in the regulation of numerous cellular functions, including cell spreading, migration, proliferation and stem cell differentiation[15-17]. The ECM therefore plays an important role in many biological processes such as embryonic development, adult tissue homeostasis and pathogenesis of diseases such as fibrosis and cancer[6, 17-19].

There has been much work showing that substrate mechanics play an important role in determining cell behaviour, however the techniques to study this phenomenon all have their limitations. The most immediate problem faced is the fact that changing the stiffness of the matrix often results in changing one or more other material properties, like surface chemistry, topography or the availability of adhesive ligands. As a result it is not convincingly demonstrable to claim that the stiffness is exclusively responsible for the observed effects[6].

The most prominent adhesions found in cultured cells are focal adhesions areas of the cultured cells which have strongly adhered to the underlying ECM through the plasma membrane, as shown in figure 1.1. The recruitment of actin microfilament bundles, or stress fibres, at the cytoplasmic interface is enabled by focal adhesions. Focal adhesions are made up of numerous large protein complexes of transmembrane adhesion receptors and cytoplasmic proteins, and the main proteins involved are talin, vinculin, paxillin and α-actinin and these link the adhesion receptors to the actin cytoskeleton[20, 21]. Focal adhesions play a vital role in providing the tools for actomyosin contractility which is essential for cell migration. The focal adhesions bridge across the cell membrane such that the integrins can bind to ligands, like the ECM protein fibronectin, allowing for the transmission of forces between the cells and their microenvironment. This allows for cells to integrate both biochemical and mechanical signals to control the organisation of their cytoskeleton.

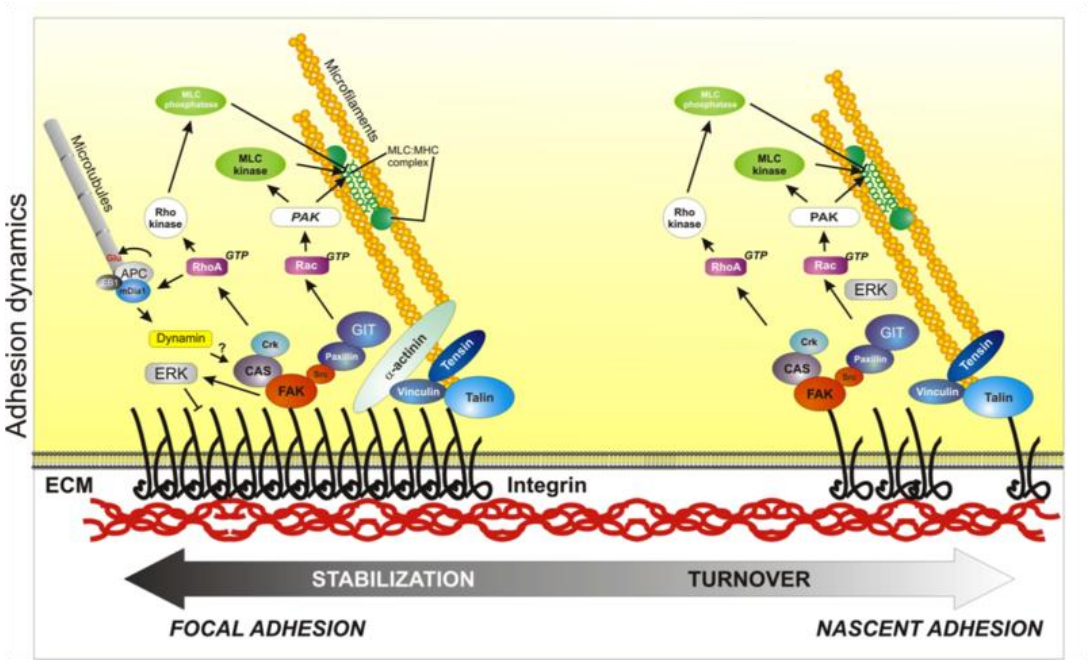

Figure 1.1 Diagram showing the structure of focal adhesions[22]

The interactions between cells and the ECM appear to be of significant influence on cell behaviour. Along with cellular interactions with soluble molecules and cell-cell interactions, physical stimuli have been shown to be very important with respect to cell structure and function[15]. The determination of stem cell function appears to be particularly influenced by the cell microenvironment. More recent studies on the influence of physical parameters on cell fate have focused on the effect of cell shape, substrate stiffness and surface topography[6, 15]. These factors are explored next.

Physical Parameter Effects on Cell Behaviour

Influence of cell shape on behaviour

The shape cells take within their natural microenvironment depends upon the type of cell and its function. Connective tissue cells provide a clear example of this phenomenon, as they all derive from a single mesenchymal stem cell (MSC) precursor but their shape is varied based upon the lineage they differentiate into, in order to serve their specific function and to promote their multicellular organisation. Other examples

of how cells take a certain shape in order to optimise for their specific function include adipocytes which take a spherical shape to offer maximum storage capacity as they specialise in storing energy as fat, and osteoblasts which in order to promote the deposition of ECM spread, take on a cuboidal shape which is essential for the remodelling of bone[23]. The difference in cell morphology is determined at the early stages of stem cell commitment where the fate is decided and results in changes in the expression of integrins, cadherins and cytoskeletal proteins[16].

Despite having been known for a long time that cell morphology is affected by differentiation, it is only recently that studies on the effects of cell shape on stem cell determination have been executed. Studies have been performed on numerous cell types to see what affect cell shape has on lineage and cell function. The effects of cell shape on cell function have been studied using micro-patterned substrates using different sized adhesive islands[24]. The results showed that cells are forced into a circular shape on smaller islands, between 5 and 10μm in diameter, causing apoptosis, while on larger islands cells spread and hence proliferation is induced. Further studies on cell shape affects have shown that human MSCs cultured in a mixed media that promotes both fat and bone differentiation will result in osteoblasts if given the space to flatten and spread on their substrate but will become adipocytes if there is no room to spread[25].

The effects of cell shape on terminal differentiation, with respect to human skin cells, has also been studied[26]. Cell shape was controlled by patterning single cells onto different sized adhesive islands, on large islands the cells spread, whereas on the small islands adhesion was restricted and cells took a more rounded shape. This study showed how cell shape also triggers terminal differentiation as the rounded cells exhibited inhibition of DNA synthesis and the differentiation marker involucrin and

hence the cell shape triggers terminal differentiation in keratinocytes. The aforementioned studies have shown how changes in cell shape have a direct influence on cytoskeleton and mechanotransduction apparatus on numerous different types of cells.

Studies have also been performed to look at the effects of cell symmetry, cell polarisation, and the spatial distribution of ECM molecules on cell migration and stem cell determination[27, 28]. The effects of geometrical constraints on architectures and tissues containing numerous types of cells have also been examined. Studies on how tissue geometry can determine organ morphology have been performed using micropatterning to reproduce the initial three dimensional structure of mouse mammary epithelial tubules in culture, showing that tubule geometry directs the position of branches[29].

Influence of substrate mechanics on cell behaviour

When culturing cells outside of tissue, the cells need to be supported by a substrate. The cells will need to be able to anchor and pull on this substrate to make decisions based on the mechanotransduction. The anchorage transduction of cells to their substrate is dependent on actomyosin-based contractility, transcellular adhesion mediated by the integrin and cadherin classes of molecules, as well as focal adhesion proteins and focal adhesion kinases[15]. Tissue cells also sense the mechanical resistance of the substrate, as opposed to merely transmitting force to the substrate, and depending upon the mechanical response organise their cytoskeleton accordingly[30].

Within their natural environment, cells mechanically interact with materials across a wide range of stiffness, from very soft ~100 Pa, like fat tissue or brain, to stiffer ~ 10 kPa, like muscle, to very stiff ~100 kPa, like cartilage or collagenous bone.

To perform *in vitro* studies on the effects of substrate stiffness on cell response, tuneable materials with elastic moduli covering the range of natural tissue are needed. Materials that are frequently used for this purpose include PDMS, PAAm, poly(ethylene glycol) (PEG), and alginate[31-33]. Many studies have shown how substrate stiffness plays an important role in cell differentiation and the development of tissue and organs. This is of great practical importance as ECMs that have abnormal stiffness could play an significant role in the development of diseases like cancer[34]. Therefore having a greater understanding of mechanotransduction will not only give a useful insight into *in vitro* cell culture but could also help progress the field of regenerative medicine. One issue with much research in the field is the use of substrates that are far stiffer than that which cells would experience in their natural environment.

The first gels used to study the effects of substrate mechanics on cell behaviour were based on natural ECMs, like collagen and fibrin. These proteins self-assemble into nanofibrous structures which can mimic cells' natural microenvironment. The studies on these systems showed that increasing the substrate stiffness impacts integrin signalling and actomyosin mediated cellular tension, parameters which impact on tumour growth[17, 34]. Normal cells have also been shown to regulate their differentiation and proliferation based on the stiffness of their protein gel substrate[17].

PAAm substrates with stiffness from 1-100 kPa have been used to study the effect of substrate stiffness on rat kidney epithelial cells by Pelham *et al.*[30]. The study showed how on soft substrates, stiffness ~1 kPa, the cells formed scattered and dynamic adhesions whereas on stiffer substrates (~30 kPa to 100 kPa) stable focal adhesions are found as shown in figure 1.2. The adhesions were traced by microinjecting the cells with fluorescently labelled vinculin. The more stable adhesions formed on stiff substrates coincided with an increase in tyrosine phosphorylation on multiple

proteins. The study also found that the motility of fibroblasts varies with substrate stiffness, on soft substrates cells migrate ten time faster than those on stiff substrates. This is due to the lack of stability of the focal adhesions and hence the ability of the cells to exert force onto the substrate. Immunostaining was also performed and showed an increase in F-actin organisation and stress fibres with increased substrate stiffness. This study showed how cells have the ability to control their adhesion structures and motility as a result of the mechanical response of the microenvironment[30].

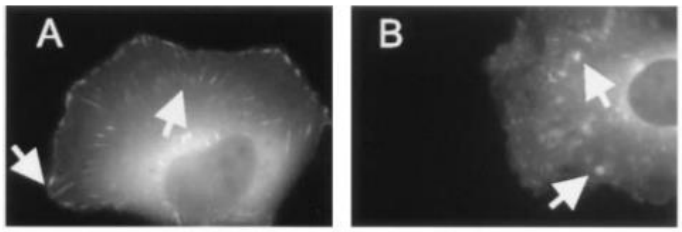

Figure 1.2 Focal adhesion formation in normal rat kidney epidermal cells on PAAm substrates of differing stiffness. Distribution of vinculin on A) stiff and B) soft substrates[30].

Further studies on the role of substrate stiffness have shown how cells organise by mechanotaxis, by culturing endothelial cells and fibroblasts on PDMS substrates patterned with micrometer-scale regions of compliant and stiff material. The results showed that both these cell types preferred accumulation on stiffer areas[32]. AFM has been used to show the direct relationship between the cell and the substrate mechanics. The study demonstrated how fibroblasts alter their own stiffness to match that of the substrate, where the substrate stiffness was varied from 0.5 to 20 kPa, hence highlighting changes in the cytoskeletal tension[35].

Beyond cell spreading and cytoskeletal changes, substrate stiffness also has a major influence on cell lineage. Engler *et al.* have studied the effects of substrate stiffness on MSC lineage selection[7]. MSCs can develop into numerous different cell types, including neurons, myoblasts and osteoblasts, depending upon their anchorage to the

substrate. On soft substrates, with an elastic modulus similar to brain tissue, the MSCs spread disparately into cells resembling primary neurons after a week. While on stiffer substrates, with a modulus similar to muscle, they developed into cells similar to myoblasts and on the stiffest substrates, resembling the stiffness of a cross-linked collagen network, the cells developed into cells resembling osteoblasts. When left to culture for several weeks these cells committed to the lineage specified by the matrix stiffness[7]. Work on cell lineage in 3D hydrogels does not corroborate with work on 2D substrates as it has been shown that cell fate does not correlate with matrix stiffness. The matrix stiffness does, however, direct integrin binding and hence, on the nanoscale, controls organisation of adhesion ligands[36].

Influence of substrate surface topography on cell behaviour

The substrates which cells interact with within their natural environment, often have a fibrillary nature and show topographical features on the nano to micrometer length scale. Collagen is a regularly occurring ECM protein and a single collagen molecule is around 300 nm in length and 1.5 nm wide. When collagen fibres undergo self-assembly they can reach lengths of up to tens of micrometers, and widths of up to 410 nm, as has been shown on bovine tendons[37].

A clear example of the influence of nano topography is given when considering *in vivo* cell adhesions with basal membranes. The large range in surface topography of the basal matrix is thought to be a driving force in the determination of cell lineage. The influence on cells of the underlying substrate topography has been described as the phenomenon of contact guidance. Cells reacting to the surface topography of the substrate has been shown by studies on anisotropic topographic features, where the cells will migrate in the direction of the anisotropy[38-40].

The most extensively studied topographies on 2D substrates are nanograting, nanopost and nanopit arrays[41] as shown in figure 1.3 below. It has been shown that cells take the shape of the substrate topography they are cultured on, Teixeira *et al.*[40] showed human epithelial cells cultured on a substrate patterned with grooves and ridges, similar to nanograting, elongated along the length of the features, while cells cultured on a plane substrate took a rounded shape. The cell elongation coincided with an alignment of actin filaments and FAs in the direction of the anisotropy[40].

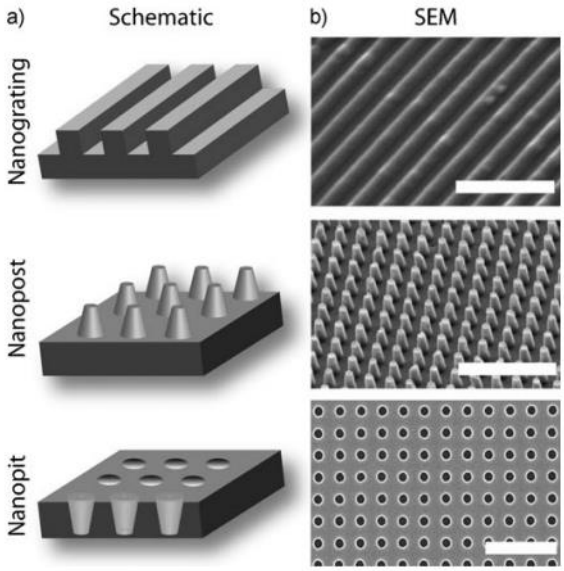

Figure 1.3 Schematic (a) and SEM images (b) of commonly studied nano-topographies for cell culture[41]

It is clear that cell shape, substrate mechanics and substrate topography, along with the interplay between these three parameters, play a crucial role in the development, lineage and spreading behaviour of cells. Understanding the relationship between cells and their mechanical environment is therefore very important in order to gain a full understanding of cell behaviour. It follows that having thorough and robust methods for mechanically characterising the cellular microenvironment is essential to understand these relations.

Engineered materials to study the effects of cell shape and matrix mechanics on cell behaviour

The effects of the physical microenvironment on cell behaviour, as discussed, are clearly very important. Hence, understanding the types of materials used in the study of cells and how they are used will inform the question of how we should characterise these materials. As a result in order to be able to perform useful *in vitro* experiments on substrate effects on cells, it is clearly very important to develop materials that allow for functional and mechanical diversity and robust reproducible tools for cell study. Some materials and patterns currently employed for cell study will now be examined.

Microcontact printing on substrates

Two common ways of patterning substrates with molecules are, *via* soft lithography[42] and microcontact printing[43]. Microcontact printing is commonly used to create patterns on a sub-micron length scale and is simple, quick and inexpensive. In microcontact printing self-assembled monolayers, like peptides, are deposited onto the substrate using a topographically patterned elastomeric stamp as shown in figure 1.4[44, 45]. The steps followed for microcontact printing shown in figure 1.4 are as follows, (a) a master is created by generating a mask to be reproduced using lithography or other methods. (b) PDMS is poured onto the pattern and cured, (c) then peeled away. (d) The stamp is then inked with molecules, (e) and then brought into contact with the surface (f) to transfer the molecules leaving the desired pattern[44].

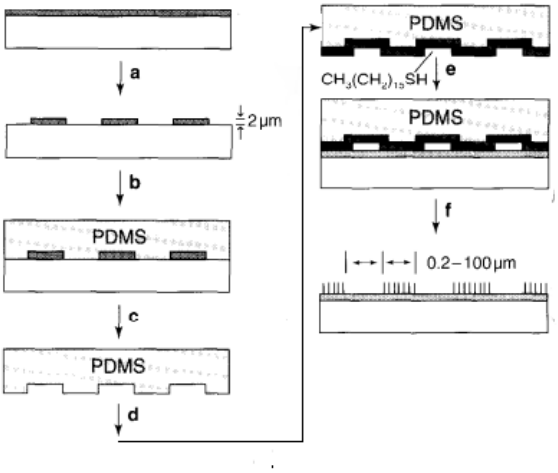

Figure 1.4 Schematic of microcontact printing adapted from[44]

Microcontact printing allows for substrate surfaces to be patterned with complex organic functional groups in a specific pattern. The functional groups would include ligands for protein recognition, attachment point for proteins, peptides, carbohydrates and other relevant groups that allow biosensors to function. Microcontact printing thus gives excellent control over surface properties at a molecular level[44].

Polymer brushes

The use of polymer brushes to coat substrates allows for control over the surface chemistry, topography and physical properties making them extremely useful for biotechnology. Polymer brushes are essentially an assembly of polymer chains that are covalently bound to a desired surface from one end[46]. The polymer chains are forced to stretch out away from the surface due to the dense packing of the chains in order to avoid physically interfering or overlapping with each other[47]. Polymer brushes can have functional groups easily introduced into their structure, are mechanically robust and have both high molecular weight and low polydispersity. There are many ways to synthesis polymer brushes, one widely used, robust method to produce brushes of well-defined thickness, composition and grafting density is surface initiated atom transfer radical polymerisation (ATRP)[48]. ATRP is in essence a catalytic

process in which a transition metal complex reversibly activates the dormant polymer chains via halogen atom transfer reaction[49].

Polymer brushes with non-fouling properties are frequently utilised for biomedical and bioanalytical uses as they exhibit suppression of non-specific protein absorption and cell adhesion[50]. When compared to self-assembled monolayers, brushes which have been used show more prolonged stability, improved surface coverage and protein resistance[51]. By microcontact printing ATRP initiators to the surface of substrates, brushes can then be used to pattern islands of ECM proteins onto substrate surfaces. This allows control over cell shape and position on substrates in a controlled chemical environment[50].

Elastic substrates

The ability to generate substrates with easily and precisely controlled mechanics and surface properties is essential to study the role of substrate stiffness on cell behaviour. Proteins that occur within cells' natural environment, like collagen, have been frequently been used for this application as they have similar macromolecular properties[17, 52]. The stiffness of collagen substrates can be controlled by varying its concentration, which has been shown to influence cell function in 3D matrices[53]. One problem associated with changing the collagen concentration is that this will not only change the modulus of the substrate but also the spatial density of ligands and substrate topography as shown in figure 1.5[17].

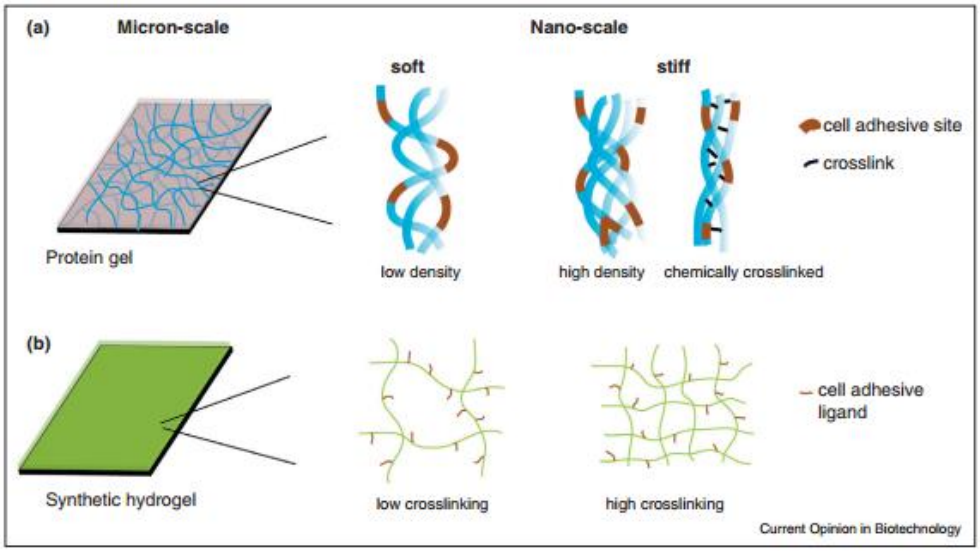

Figure 1.5 Schematic of structural features of protein gels (a) and synthetic hydrogels (b) showing how substrate mechanics influence matrix and ligand density and hydrogel pore size[17].

Using synthetic polymer hydrogels the mechanics and ligand density can be varied independently of each other, making them potentially more useful than naturally occurring ECM proteins for the study of matrix stiffness effects on cell behaviour. Unlike naturally occurring fibrous materials used to make gels, synthetic gels are typically considered linear visco-elastic solids where the mechanics is considered to be independent of deformation magnitude or rate[17]. Polyacrylamide (PAAm) is a hydrogel frequently used in the study of cell behaviour as the modulus can be changed easily and precisely over several orders of magnitude. The stiffness of PAAm can be varied from between 0.1 and 100kPa by adjusting the amount of base monomer and cross-linker, similar to the stiffness of naturally occurring tissue[7, 54]. Beyond being easily tuneable, PAAm also offers excellent optical properties allowing observation of the living cells via immunofluorescence with high magnifications. Finally PAAm is has a structure that closely resembles that of natural tissue due to its porous and swollen nature[55].

PAAm gels can be used in conjunction with fluorescent beads to follow the traction forces cell enact on the substrate to quantify the distribution of force at the

cell-substrate interface[56]. One problem associated with using PAAm as a substrate is that cells do not adhere to unmodified PAAm, however this can be overcome by conjugating ECM proteins to the PAAm matrix[57].

Another frequently used material for cell culture substrates is PDMS. PDMS is particularly useful when trying to mimic stiffer naturally occurring substrates, like blood vessel walls which have elastic moduli in the region of MPa. PDMS is much stiffer than PAAm and can have an elastic moduli reaching up to 2 MPa. Furthermore it is well understood how the surface of PDMS interacts with aqueous solution making it easy to perform surface characterisation with standard techniques. One major disadvantage when using PDMS substrates is that it is difficult to culture cells on PDMS over long periods due to difficulties with surface modification[58].

PDMS chains are highly mobile resulting in permanent surface reorganisation and hence surface modification with cell-adhesive molecules is not efficient. Poor coating of the substrate with ECM proteins is, however, only problematic for long-term cell culturing experiments (experiments lasting over 3 days). Ways to manipulate PDMS to overcome this problem have also been developed, like using a layer-by-layer self-assembly to alternately adsorb positively and negatively charged polymers onto the surface, which has been shown to achieve cell growth for over a week[59]. Finally PDMS is very good for studying the effects of topographical features on cell behaviour as it can be cured in a master mould to leave the desired micro-pattern on the substrate hence allowing for the combined study of rigidity and topography[60, 61].

Given the sensitivity of cells to their physical microenvironment and developments in materials used as cell substrates, it is clear that having robust and thorough techniques to characterise the mechanics of cell culture substrates is essential to

properly understand cell culture work. As shown above, the materials used as substrates are becoming more sophisticated and it is important that the differences between the local and bulk properties of the materials are also understood.

1.1.3 Mechanical Characterisation of Soft Biomaterials

Mechanical characterisation consists of obtaining mechanical data for the material tested, normally in the form of force-displacement-time or stress-strain-time, and translating this into material properties. There are many different methods and techniques used to collect mechanical data, along with many different material models to understand it. Here common testing techniques used to characterise soft materials and typical models used to translate the experimental data into material properties are discussed.

Mechanical Testing Methods

One major difficulty in the mechanical characterisation of soft biomaterials arises from their poor mechanical strength compared to traditional engineering materials, and this is particularly striking in the case of hydrogels. Not only does this make mechanical characterisation difficult, but it also limits their adoption in biomedical applications[62, 63]. The low modulus of hydrogels coupled with the fact that hydrogels have the properties of something that is neither solid nor liquid makes both measuring and interpreting mechanical data non-trivial. The most immediate problem faced when trying to get mechanical measurements is the difficulty gripping hydrogels for testing. There is also the issue that most hydrogels have a modulus of the order of kPa while the majority of mechanical testing rigs have been optimised to work in the region of MPa or GPa. Hydrogels are also often very heterogeneous, especially physical gels, and as a result the bulk material properties vary significantly from the local properties

at any given point on the material[10-12]. Accurate mechanical characterisation of hydrogels and soft biomaterials on both a local and macroscale, and understanding the reasons behind any discrepancies between the two, is essential in order to fully exploit their potential in biomedical applications.

The apparatus and testing techniques used to analyse soft materials is essentially the same as those used for mechanical analyses of typical engineering materials. Soft biomaterials are typically polymers and hence have a time dependant mechanical response due to the viscoelasticity of the polymer matrix, in the case of hydrogels this is coupled with the time dependant response of the fluid flow through the solid matrix. As a result hydrogels are very sensitive to the time scales of testing used and are typically tested in either the time or frequency domain[62]. Selected methods of testing hydrogels' and other soft polymers' bulk and local properties will now be analysed.

Bulk Mechanical Properties

Universal Test Frame

The universal test frame is the most common tool used for mechanical analyses. They are able to carry out numerous different tests and most can operate in only one axis, although biaxial test frames are becoming more common. The actuation of the motion or force varies but is typically servo hydraulic or electromechanical or, less commonly, systems driven by speaker coils. Universal test frames come in a wide range of sizes and it is important that the rig used is optimised for the load scales needed. Larger test frames will operate at extremely high forces often in the mega-Newton range, whereas smaller rigs are optimised for soft biological tissue and have load cells with a maximum load in the region of 5-10 N. These test frames can operate in both tension and compression using different hardware at the point of sample contact[62]. A critical condition for good tensile testing is good gripping which is extremely

difficult to achieve with hydrogels and soft materials due to how compliant and hydrated they are. There has been some work done to overcome this problem and potential solutions include the use of cardboard tabs, double sided tape and glue to achieve sufficient gripping[64].

Compression testing can be performed using one of two different configurations, confined or unconfined. Confined compression involves enclosing the sample in a nonporous container and compressing it with a porous plate[65], unconfined compression involves compressing the sample between two nonporous parallel flat plates[64, 66, 67]. Confined compression is a testing set up unique to multiphase materials as the flow of the liquid phase through the porous plate allows deformation of the sample[62].

Both compression and tensile testing give load *vs* displacement data and for tensile testing and unconfined compression this data is typically converted to stress vs strain using basic geometric relations[68]. This data can then be used to obtain the Young's modulus and failure strength. Tests are typically performed at a set rate and samples tested until failure; when testing hydrogels it may also be necessary to try a series of strain rates in order to account for their time dependant nature.

In order to obtain meaningful material properties from force-displacement-time data, it is typically converted to stress-strain-time, where stress is the force divided by the cross-sectional area it is acting over and strain is the extension divided by the original length. The simplest interpretation of this data would be for a linear elastic isotropic material in which the gradient of the linear slope of a stress-strain curve, from uniaxial tensile or compression test, is taken as the elastic modulus, *E*. Soft biomaterials, like hydrogels respond in a far more complex manner and as a result

more sophisticated models are needed to interpret the data. For soft biomaterials, models include large strain elasticity and time dependant response.

The structure of polymers makes them fundamentally time dependant in their mechanical behaviour. The ways to characterise this time dependence varies from more simple empirical measurements to more complex models such as those that consider the interactions between the solid and fluid phases in hydrogels explicitly using the coupled equations of poroelasticity[62]. However time independent models can still be useful especially when considering highly cross-linked polymers. In the case of highly cross-linked polymers the elastic and hyperelastic models have been used as very good approximations in the past.

Theories of rubber elasticity can often be used to characterise the polymer network of soft polymers and hydrogels. This approximation is most accurate when studying highly cross-linked gel networks to the point where the polymer network can be considered a single molecule thanks to the level of interconnectivity. Assuming that the polymer network can be considered a single molecule, then entropic elasticity dominates and the elastic modulus, E (note in rubber theory this is normally denoted by G, but E is used so as not to confuse it with the shear modulus), in the unswollen state can be expressed as a function of the number of chains per unit volume and hence related to the cross-link density, swelling ratio and network mesh size[69-72].

This model assumes that when loaded the macroscopic deformations translate directly to the molecular level. The most significant question of this model is whether the assumption of affine deformation holds. This assumption has already been called into question for polyacrylamide gels[62, 73].

When considering swollen hydrogels, the swollen modulus can be considered proportional to the unswollen modulus multiplied by the volume swelling ration to the power of 1/3. This model assumes a perfect polymer network, however for real gels the modulus is expected to decrease proportionally to the number of defects present. Defects are typically defined as loops and free ends[62].

Within rubber elasticity theory the force displacement relationship is typically given in terms of true stress, τ and stretch, λ, where

$$\lambda = \frac{l_{current}}{l_{original}} \quad [1.1]$$

$$\tau = E(\lambda^2 - \lambda^{-1}) \quad [1.2]$$

Using the relationship between true stress and stretch, rather than the standard engineering stress, σ and strain, ε, is useful when considering materials with very large deformations to failure. The equation of engineering stress, as shown in equation 1.6, is quite different to that of true stress and upon closer inspection is clearly Hooke's law when the stretch is small. The most significant difference between rubber elasticity and elasticity theory is the fact that within rubber elasticity there is only one constant, E, whereas within elasticity theory there are two, E and the Poisson's ratio, v.

$$\sigma = E(\lambda - \lambda^{-2}) \quad [1.3]$$

The biggest issue with using elastic and hyperelastic models is the fact that these models ignore the time dependence of the mechanical response. The elastic modulus is an equilibrium modulus and to approximate it, for time dependant polymer and gel materials, compressive or tensile tests must be performed at very low strain rates.

To study the intrinsic time dependence of polymers gels, due to both the viscoelasticity of the polymer network and the fluid flow through the network, different mechanical models must be used.

The viscoelastic model is essentially the same as the elastic model, but the elastic constants are replaced with time dependant functions[74]. A common assumption in viscoelasticity is that volumetric deformation is independent of time and only the shear modulus is time dependant, *G(t)*. The simplest models of viscoelasticity assume the mechanical response can be characterised by the lumped characteristics of springs and dashpots. A more general model characterises polymer viscoelasticity using summed exponential functions, known as a Prony series, to describe the time dependant mechanical response.

The most common material characteristics obtained from these models are the instantaneous, *E(0)*, and equilibrium, *E(∞)*, modulus and the time constant. Taking the ratio of the instantaneous and equilibrium modulus values, *f=E(0)/E(∞)*, gives a useful parameter for determining the elasticity of the sample, where if f=1 the sample is a perfectly elastic solid and if *f=0* it is a perfectly viscous liquid. The stress/strain history also has an effect on the modulus obtained and for samples that have undergone complicated loading histories then Boltzmann superposition or hereditary integrals can be used to characterise samples more precisely[62, 74].

Viscoelastic models can also be used to characterise samples in the frequency domain, using testing set ups like Dynamic mechanical analysis (DMA)[75], and Rheometry[76]. Simple spring-dashpot models can be utilised to interpret data in the frequency domain or more sophisticated approaches like fractional derivative models[75] have been used. It has been shown how viscoelastic data can be translated between

the frequency and time domains as the physical functions are the same in each, describing a single viscoelastic response[74]. However it is very uncommon to see conversion of data from the frequency to time domain or *vice versa.* Frequency dependant data obtained via rheology or DMA is typically exhibited as plots of the storage and loss moduli, *G'* and *G''* respectively, against frequency without further analysis. Attempts to link the viscoelastic properties to physical properties or explicit physical processes have had very little success to date[62].

The poroelastic, or biphasic[77], model is a time dependant model that models a material's time dependence due to fluid flow through the elastic, or viscoelastic solid structure. The poroelastic model is typically used to obtain the following material properties, the elastic properties of the solid matrix, including the shear modulus, drained and undrained Poisson's ratios, and the level of fluid-solid interactions.

The two major advantages of the poroelastic model compared to the viscoelastic model are, first that the model explicitly accounts for the multiphase nature of hydrated materials, and second that the material characteristics obtained directly relate to the microstructure of the material, as opposed to being empirical fits to experimental data. A good example of how the poroelastic model relates directly to the materials microstructure is intrinsic permeability which can also be calculated from first principles based on the solid fraction and a characteristic length scale.

A major complication associated with the poroelastic model is the fact that the governing equations are highly interlinked and as a result for the majority of mechanical tests, closed form solutions which can easily fit to the data do not exist. The main exception to this is confined compression. When using confined compression the test-

ing conditions of either step loading or constant rate ramp loading followed by a constant load hold period have relatively simple solutions where the data can be matched to a series of summed exponentials[14]. For most other mechanical tests the data will typically need to be analysed by numerical or computational models. Indentation testing has been used both successfully and frequently in recent years to obtain poroelastic properties like the elastic modulus and intrinsic permeability[13, 14, 78, 79].

Dynamic Mechanical Analysis

DMA is a frequency based test where the sample is loaded with sinusoidal actuation. DMA can be performed in a range of testing modes, including shear, tension and bending. Samples typically must be prepared specifically for the testing method or machine used and can be tested using numerous different types of 'sweep'. The most commonly used test is the frequency sweep in which the sample is tested over a range of frequencies keeping the amplitude of oscillation or stress constant but the frequency is varied. From these tests, the elastic (or storage) and viscous (or loss) moduli are obtained, *G'* and *G''* respectively. Together the storage and loss moduli make up the complex modulus, *G**, defined as[62, 80-82],

$$G^* = G' + iG'' \qquad [1.4]$$

DMA is also often used to investigate temperature effects on samples giving transition temperatures, like the glass transition temperature, and additionally allowing for the manipulation of time-temperature superposition which extends the scales of frequency possible to study far beyond what is practical experimentally[62, 81, 82]. DMA is a method for studying solid polymers, however dynamic analysis of polymer melts and very soft polymers is possible *via* rheometry. As rheometry can be used to

study both viscous liquids and viscoelastic solids it has been used widely to study the gelation process[62, 76, 82, 83].

Dynamic testing methods utilising sinusoidal loading have now spread beyond just DMA and rheology, and now have been used in sinusoidal indentation[84, 85] and dynamic confined compression[65]. Micro-rheology is another field that is growing in popularity in which embedded beads are oscillated and then motion tracked to give the local viscoelastic properties of a material[86].

Rheology

Rheology is defined as the study of the flow and deformation of a material[76, 80]. Rheology utilises material models to describe materials, with its foundation in theories used to define ideal materials, like Hookean solids and Newtonian liquids. In reality materials are neither ideal solids nor liquids but exhibit characteristics of both solids and liquids behaving in a viscoelastic manner. The microstructure of soft materials gives rise to non-trivial responses to mechanical loading and as a result the relationship between stress and strain are not merely defined by elastic and viscous constants, but also time scale, direction and scale of deformation. Rheology aims to offer a method to characterise the dynamic viscoelastic response over a wide range of time and deformation length scales[80].

When looking into the fundamentals of rheology it is easiest to look at the response and interpretation of results for ideal materials first, and then to move on to more complex real materials. To start, ideal Newtonian solids will be considered before moving onto ideal fluids and then finally looking at the response of viscoelastic solids.

When elastic solids are loaded it results in a stress being applied which causes the material to deform, or strain, proportionally to the applied stress. An example of tension on a rectangle is shown in figure 1.6a, while the application of shear stress on a cube is shown in figure 1.6b. The tensile stress-strain relationship is very simple, shown in equation 1.5, while the shear stress-shear strain response is slightly more complex, as shown in equation 1.6,

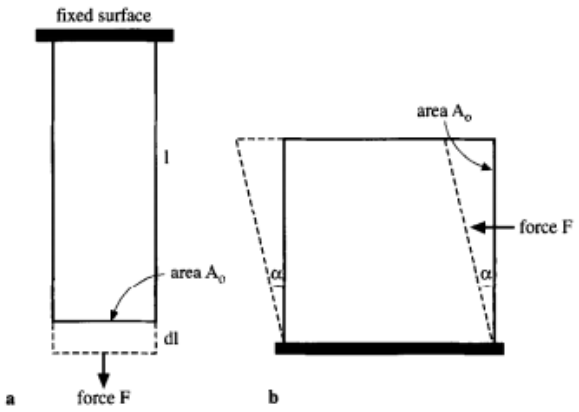

Figure 1.6 Schematic of stress-strain (or force extension) relations in tension (a) and shear (b) [76]

$$E = \frac{\sigma}{\varepsilon} = \frac{F/A_0}{dl/l} \qquad [1.5]$$

$$G = \frac{\tau}{\gamma} = \frac{F/A_0}{\tan\alpha} \qquad [1.6]$$

where, E is the Young's modulus, σ is the tensile stress, ε is the tensile strain, G is the shear modulus, τ is the shear stress, and γ is the shear strain. Under shear loading when the stain is only small, tan α can be approximated as equal to α at which point $G \simeq F/A_0\alpha$. However in practice, and when conducting rheometry, it is seldom that shear testing is performed on a simple block of material, figure 1.7 shows typical testing set ups for rheometry using parallel plate geometry and cone and plate geometry.

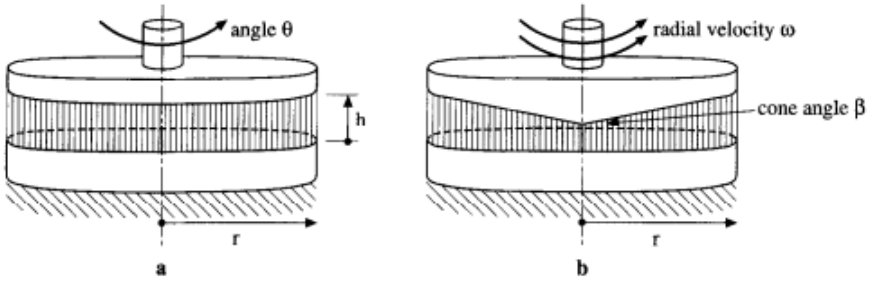

Figure 1.7 Schematic of a rheology set up with parallel plate geometry (a) and cone and plate geometry (b)[76]

With linear elastic deformation the stress-strain relationship is independent of time, however for fluids the stress is a function of the strain rate, such that,

$$\eta = \frac{\tau}{d\gamma/dt} = \frac{\tau}{\dot{\gamma}} \qquad [1.7]$$

where, η is the viscosity of the fluid. Cone and plate rheometry is particularly useful when studying the viscosity of fluids as the shear rate is constant across the sample and is given by, $\dot{\gamma} = \omega/\beta$, where $\dot{\gamma}$ is the shear rate, ω is the angular velocity and β is the plate angle. Based on the shape of the shear vs stress-shear rate or viscosity-shear rate traces it is possible to observe several different types of behaviour as shown in figure 1.8.

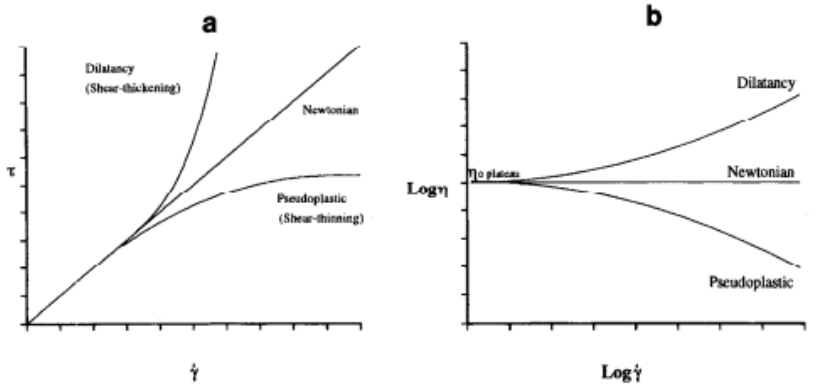

Figure 1.8 Traces of shear-stress vs shear rate (a) and viscosity vs shear rate (b) showing different types of fluid behaviour[76]

However most materials are not ideal elastic solids or ideal viscous liquids but behave in a manner that combines these two models, exhibiting both an instantaneous recoverable elastic response and a time dependant viscous response and are known as viscoelastic solids. Rheology is a very good way of obtaining the mechanical properties of viscoelastic materials and is most frequently used to perform dynamic mechanical analyses. Samples are loaded in a sinusoidal manner and the strain response is recorded. The phase angle between the torque and the displacement, δ, is used to show how viscous or how elastic the response is, with a phase angle of 0° representing an ideal elastic material and a phase angle of 90° representing a viscous fluid. A typical loading curve and strain response is shown in figure 1.9.

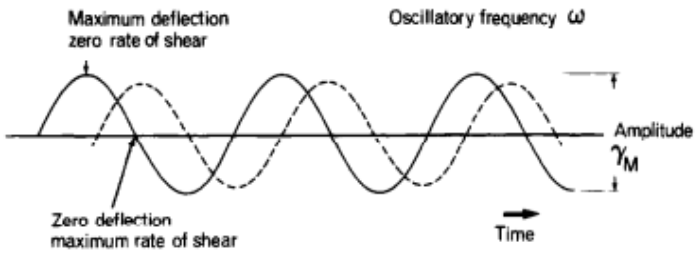

Figure 1.9 Typical sinusoidal loading curve and strain response for oscillatory rheometry

Based on the strain response to displacement, the complex modulus, *G**, can be obtained. The complex modulus can be broken down into the in phase shear storage, or elastic, modulus, *G'*, and the out of phase viscous, or loss, modulus, *G''*. Where the *G** is represented by,

$$G^* = \frac{\tau^*}{\gamma_M} = (G'^2 + iG''^2)^{1/2} \qquad [1.8]$$

where, τ^* is the complex shear modulus and γ_M is the maximum shear strain. When using rheology, the values of elastic and viscous moduli are normally directly output by the machine software and very little data analysis is needed. As a result rheology

is not often used to get further information with respect to the material microstructure, but is more used to get information such as the role of frequency on the stress-strain relations.

While these methods are useful at gauging the bulk characteristics of materials they do not give any information regarding their local (or nano-scale) characteristics. Some materials behave very differently on a local scale compared to their bulk characteristics, for example where there is small scale heterogeneity in the sample[11], and these differences can have a significant influence in practical applications. As such local mechanical characterisation will now be examined.

Local Mechanical Properties

Indentation Testing

In instrumented indentation testing (referred to more commonly as indentation testing), a probe of known size and geometry is brought into contact with the surface of a sample, pressed then retracted again and the force, displacement and time data is recorded for material property deconvolution[62]. The indenter geometry is significantly smaller than that of the sample being tested. The fact that the indenter is significantly smaller than the sample being tested gives rise to plane strain conditions, where due to the surrounding material fixing strain perpendicular to the direction of the indentation strain only occurs normal to the loading, and hence a very different strain field to that observed by compression testing. Indentation tests are used most commonly to obtain the reduced modulus, E_R, and relates to the Young's modulus by the following equation,

$$E_R = \frac{E}{1 - \upsilon^2} \qquad [1.9]$$

where υ is the Poisson's ratio[68].

A major benefit of indentation testing is the lack of a need of much sample preparation. This is especially useful for testing hydrogel materials as they are difficult to produce or machine to a regular shape. Indentation testing also removes the problem of how to grip the specimen that is often occurs when testing hydrated samples in tension and compression[62]. Indentation testing also provides a very useful method of obtaining local properties when studying heterogeneous or patterned materials, using mapping techniques across the sample surface[87]. Finally it is also very easy to keep samples hydrated throughout the duration of indentation tests.

Indentation can be performed across a large range of length scales, from mm, at the larger end[66, 88], down to nm or µm, at the smaller end[14, 54, 84, 85, 89, 90]. Indentation is incredibly malleable to different length scales as the indenter geometry and contact area can both be tuned to match the resolution of force and displacement of the instrument used[91].

The use of indentation tests at small scales, or nanoindentation as it is commonly known, has become increasingly popular recently for mechanical analysis of a wide range of biomaterials[90]. Atomic force microscopy (AFM) rigs are now frequently adopted for use as nanoindentors[54, 84, 86, 89]. AFM can be utilised as indenters by actuating the tip indirectly with a calibrated cantilever[62], hence the cantilever system used by AFM nanoindentors can easily be tuned to specific samples by simply switching the cantilever with either higher or lower stiffness.

Localised Testing Applications of Atomic Force Microscopy

Nanoindentation performed using AFM is becoming of increasing interest and importance in the field of biomaterials and for the characterisation of soft materials. There are three main reasons for the rise in popularity of this testing method, first, the

loading of an indenter tip over a micro-nano length scale with constant monitoring onto a specimen surface make it ideal for characterising the local mechanics and heterogeneity of non-homogenous samples. Secondly, AFM is very easy to use practically as very little sample preparation in required. And finally AFM allows for the study of a variety of different deformation modes depending upon the time scale, indenter tip geometry used and loading conditions[9292].

AFM nanoindentation can be used to either explore structural characteristics, for example indenting a cell membrane, or to study the material properties of a single material, essentially using AFM as a universal test frame with a local contact[92, 93]. Indentation data by AFM is recorded, as shown in figure 1.10, as cantilever deflection, in nA, against piezo electric crystal movement, in nm. A laser is shone against the top of the cantilever and the reflected beam is recorded by a sensor to record the deflection, while the piezoelectric crystal is controlled. In order to convert the deflection from nA into nm the cantilever must be calibrated against a hard material, such that the entire piezo movement can be considered as the deflection, typically a silicon wafer is used. As the spring constant of the cantilever is known the cantilever deflection can then be converted to the force and the total indentation is simply the cantilever deflection subtracted from the piezo movement. For each indentation test the 'land' (approach), and 'lift' (retraction) curves are recorded, a typical land curve is shown in figure 1.10b and c. In figure 1ab the key stages of the land curve are highlighted; 1) shows the initial approach, 2) snap into contact due to short range forces, and 3) the indentation. The retraction would follow a similar path but both depend on the sample – tip interaction (if adhesion is present or repulsive forces due to surface chemistry *etc*.). The deflection is nA is hence the same as in nm just scaled relative to the spring constant and deflection calibration.

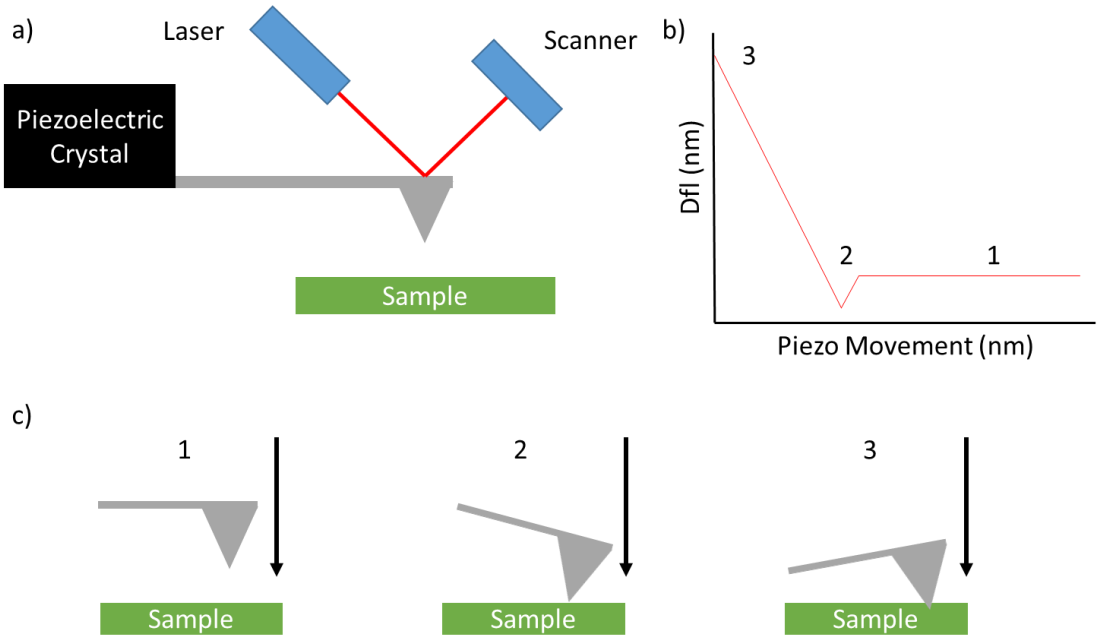

Figure 1.10 a) schematic of the experimental setup for nanoindentation by AFM b) typical land curve with the key stages numbered 1-3 and c) schematic of the sample tip interactions at the 3 stages previously highlighted.

The ease of use of AFM for nanoindentation is one of the most attractive features of this technique, however to get meaningful information from the results is not trivial. Methods to obtain the elastic modulus working with hard elastic materials are the best defined and have been extensively used, the Oliver Pharr method being a good example[94]. The Oliver Pharr method was introduced in 1992 to obtain the elastic modulus of samples at small length scales. The method gained traction as it allowed mechanical properties to be obtained from load-displacement curves without the need to image the indentation scar[95].

The Oliver and Pharr[94] method was originally developed to obtain the hardness and elastic modulus of a material from load-displacement data obtained by indentation testing. The foundation of this method is the general relationship between contact area, load and displacement developed by Sneddon[96] for simple punch geometry. Based on Sneddon's analysis the load-displacement relationship using simple punch geometry is given by,

$$P = \alpha h^m \quad [1.10]$$

where P is the indenter load, h is the elastic displacement and α and m are constants. The value of m is dependent on the geometry of the punch, and equals 1 for a flat cylinder, 2 for cones and is 1.5 for spheres and paraboloids of revolution.

Introducing plasticity to the analysis makes the problem much more complex as the constitutive equations are non-linear and more material parameters must be known, including the yield stress and work hardening coefficient, and as a result analytical solutions are not readily available. Hence the analysis done by Oliver and Pharr is largely based on experimental data and finite element analysis. Tabor[97], and Stilwell and Tabor[98] performed fundamental early work examining indentation using spherical and conical indenters, respectively, to deform metals. The importance of these experiments lies in that they show that elastic solutions exist for these geometries despite also causing plastic deformation (leaving a perturbed surface) as long as the shape of the perturbed surface is considered in the elastic analysis as shown in figure 1.11b. This analysis also showed that where the indenter used is non-rigid the elastic behaviour can be accounted for by defining a reduced modulus, E_r where,

$$\frac{1}{E_r} = \frac{(1-v^2)}{E} + \frac{(1-v_i{}^2)}{E_i} \quad [1.11]$$

where, E_i and v_i are the Young's modulus and poisons ratio for the indenter respectively. Finally, the work of Bulychev *et al.*[99] showed the relationship between the retraction slope of load-displacement data (as shown in figure 1.11a), S, is related to the reduced modulus and contact area by the following equation,

$$S = \frac{dP}{dh} = \frac{2}{\sqrt{\pi}} E_r \sqrt{A} \quad [1.12]$$

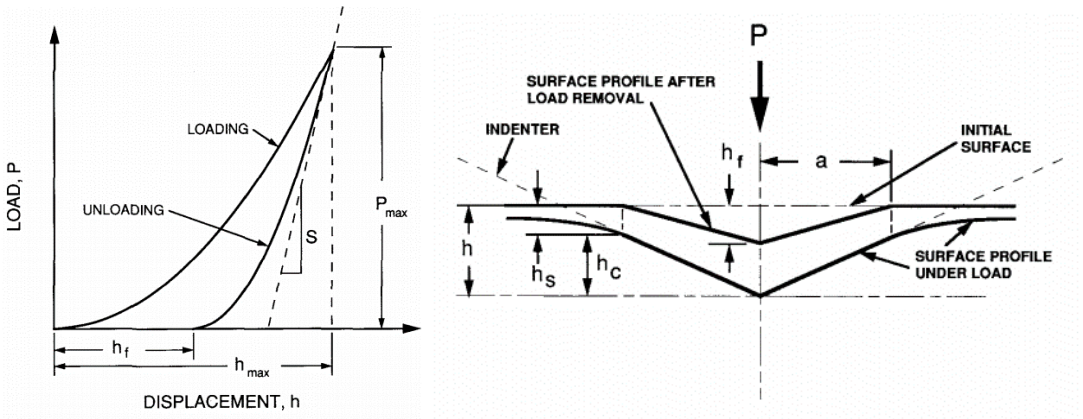

Figure 1.11 schematics of (left) indentation load-displacement highlighting the important measured parameters and (right) of the punch unloading highlighting the parameters that characterise the contact geometry[94]

Oliver and Pharr showed that this force-displacement relationship held for numerous different indenter geometries as long as the contact is elastic, however, when studying biological material or soft gel materials it is highly unlikely that these models will be representative of the materials being characterised. Most biological tissue or soft gel materials exhibit time dependant mechanical response which cannot be described using linear elastic models. The appropriate model to be used can often be discovered by examining the load displacement data, figure 1.12 below illustrates the appropriate models to use based on the load displacement data obtained from the nanoindentation test[9292, 93].

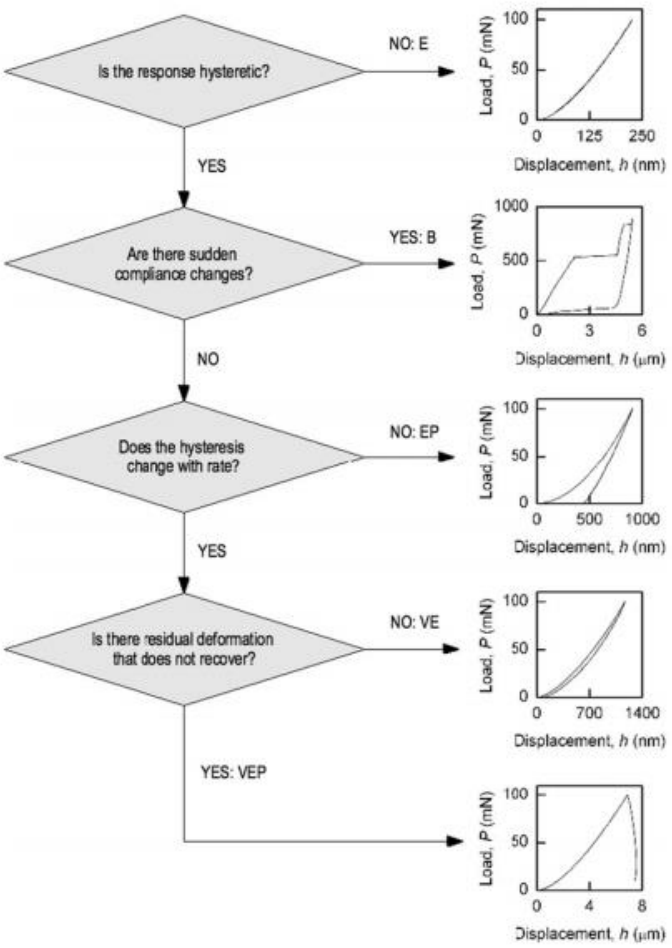

Figure 1.12 Decision tree to identify the deformation mode based on the load-displacement data from nanoindentation, where in the results, E stands for elastic, P for plastic, B for Brittle and V for viscous[92]

Another key parameter that needs to be decided before testing has begun is what indenter tip geometry to use. This choice can have a significant effect on the results obtained. Most AFM tips have a Berkovich indenter geometry as the 'default', however by using more or less acute geometries different results will be obtained. Using a broader tip, like a spherical tip, can reduce or eliminate any plastic deformation, while using a sharper indenter tip will promote plastic or even brittle deformation, thus it is important to match the tip used to the expected mechanical properties[92]. A schematic of some of the different tip geometries is shown in figure 1.13 below.

Based on the load displacement data it is essential that care is taken to ensure the correct model is used for the data analyses, otherwise the mechanical properties obtained will not be realistic. Ensuring the best tip geometry for the material is also of the utmost importance as in order to process the data accurately, it is essential that the mechanical contact is well understood[92].

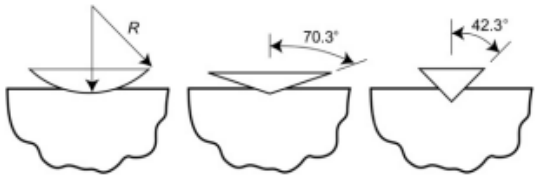

Figure 1.13 Schematic of different indenter with increasing acuity (increasing from left to right), a sphere of radius R, Berkovich pyramid, and cube corner pyramid[92]

Beyond problems selecting the correct indenter tip, there are also problems defining the contact area accurately when studying soft materials due to wetting and adhesive effects. The three dominant models used to describe adhesion between indenters and surfaces are the Herztian contact model, the Johnson, Kendall and Roberts (JKR) model and the Derjaguin, Muller and Toporov (DMT) model[100-103]. The nature of the tip-sample interaction can normally be seen in the force-displacement traces, as shown in figure 1.14. The Hertzian contact model is only applicable for homogenous, isotropic, linear elastic materials that exhibit no attractive surface forces, and assumes a circular contact area of radius a, defined as shown in equation 1.17,

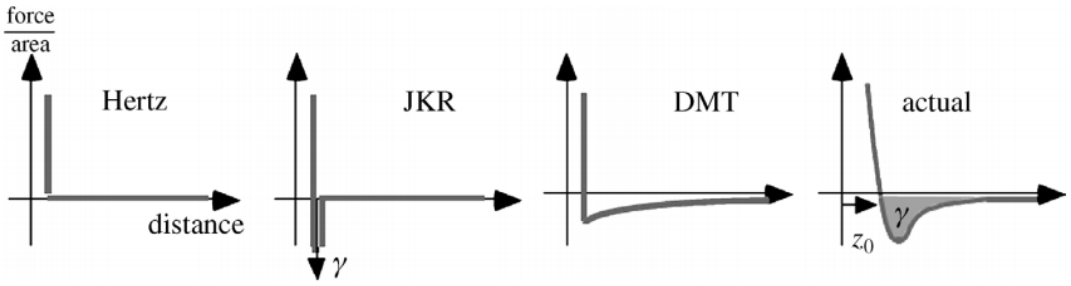

Figure 1.14 Typical force displacement curves by nanoindentation assuming Hertzian, JKR, or DMT contact[100].

$$a = \left(\frac{PR}{K}\right)^{\frac{1}{3}} \quad [1.13]$$

where, P is the normal load, R is the radius of the sphere and K is a function of the moduli of the two materials in contact and their respective Poisson's ratios.

The JKR model is an adaptation of the Hertzian contact model that accounts for adhesion between the two elastic bodies, assuming a larger contact area than the Herztian model defined as,

$$a = \left(\frac{R}{K}\left(P = 3\gamma\pi R + \sqrt{6\gamma\pi RP + (3\gamma\pi R)^2}\right)\right)^{1/3} \quad [1.14]$$

where, γ is the Dupré energy of adhesion, which represents the energy needed to completely detach a unit area of the interface.

While the DMT model also includes the adhesion between elastic bodies adding to the load, it differs from the JKR model as it assumes the contact area remains the same as in the Hertzian model[100, 102] and is given by,

$$a = \left(\frac{R}{K}(P + 2\pi\gamma R)\right)^{1/3} \quad [1.15]$$

Models used to obtain the moduli of samples after indentation rely on having an accurate value for the radius of indenter-sample contact, if there is adhesion this contact is not easily measureable and assuming the contact radius is the tip radius will lead to very inaccurate values for the moduli[104]. Models that are used to characterise indentation data, like the Oliver-Pharr model[94] assume Hertzian contact, which is not appropriate for most soft materials, however there are methods to overcome this issue like that developed by Sirghi and Rossi[104], which takes into account adhesion at the probe sample interface and accounts for it. What is clear is the need to make sure the

model being used is appropriate for the indentation data obtained and that the contact mechanics have been factored into this model in order to obtain reliable mechanical parameters

1.2 Polysaccharide Gel Review

1.2.1 Hydrogel Microstructure

Hydrogels are highly hydrophilic polymer materials with very high water content, upwards of 70% and often over 99%. The water within hydrogels can either be tightly bound or free to move within the polymer network. The large water content of hydrogels gives them excellent biocompatibility[105-107]. Hydrogels were first used for biomedical applications in the 1960s as soft contact lenses[108] and have since been developed for numerous other applications such as wound dressings[109], drug delivery[110, 111], tissue engineering[52] and cell culture[7] to name a few. In recent years the scope of potential applications, and hence research into hydrogels, has expanded significantly into fields such as tissue engineering, 3D cell substrates and nanoparticle coatings[63, 107, 112-114]. Hydrogels could have a lot of potential in studying the effects of substrate stiffness on stem cell differentiation as many hydrogels have very easily tuneable mechanical properties and closely mimic biological tissue[6, 7, 86, 89]. Hydrogels have been synthesised from numerous different synthetic and natural polymers, the structure of some commonly used hydrogel monomers is shown in figure 1.15. As hydrogels are used in so many applications it is important to understand their structure in order to tune them for any given application. Understanding their structure and the methods to manipulate their structure to achieve the desired characteristics is therefore essential to effectively use hydrogels.

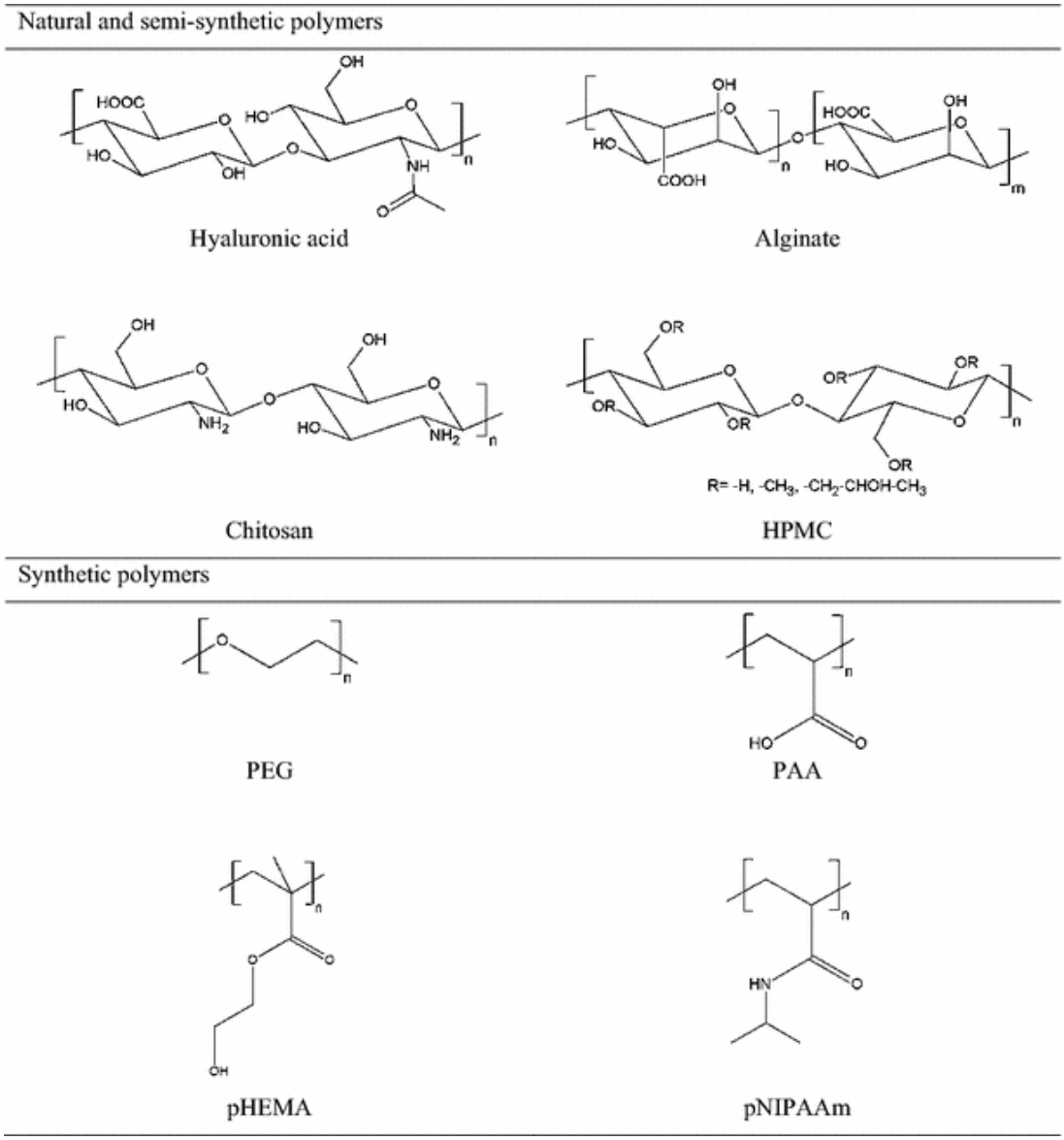

Figure 1.15 Repeat units of commonly used natural, semi-synthetic and synthetic hydrogels[115]

In order to understand how to tune hydrogels for given applications it is important to understand the underlying structure of hydrogel materials. Understanding the structure and composition of hydrogels also allows for a better understanding of how hydrogels can be utilised and manipulated for specific functions.

There are a number of ways to categorise hydrogels based on the nature of their polymer network. These include categorisation by polymer chemistry, details of preparation and type of polymer chemical bonding[106]. The three major classes of hydrogel based on their network origin are synthetic, natural and hybrid gels (hybrid gels

being made up of a combination of natural and synthetic polymers)[106]. Some polymers that have been frequently used for hydrogel study include, poly(ethylene oxide) (PEO), poly(ethylene glycol) (PEG) and poly(acrylamide) (PAAm)[14, 54, 116]. Frequently studied natural polymers used for hydrogels include, protein derivatives such as collagen[117], denatured proteins such as gelatin[118] and polysaccharides like cellulose, agar[64, 66, 84] and alginate[119]. Like synthetic polymers, natural polymers are also often used as multicomponent polymers, either as grafted block copolymers, or as interpenetrating networks of two or more polymers[62]. There are numerous ways of manipulating the polymer chemistry of gels to make them fit for given purposes, from adding degradable cross-linkers for controlled drug delivery[111] to grafting biological recognition motifs to synthetic polymers to enhance their cellular biocompatibility[120].

The most important distinction when categorising hydrogels when considering their mechanical properties is between the nature of the cross-links. Hydrogels can either be chemical (or permanent) gels, where the cross-links are permanent covalent bonds, or physical gels, where the cross-links are not permanent but are a result of physical entanglement of the polymer network or from secondary bonding like ionic or van der Waals bonds, as shown in figure 1.16. Chemical gels are not always perfectly cross-linked and often have defects, like polymer chain self-loops or free ends. Chemical gels can also be made of interpenetrating networks where two distinct networks (where polymer chains only cross-link with like chains) entwine. The apparent cross-links in physical gels arise from physical chain entanglements or non-covalent bonding. Physical gels have also been show to cross-link through the formation of helices, where the ionic interactions between the cations and acid chains link to form

complex joints as shown in figure 1.16[121]. The most fundamental mechanical difference between chemical and physical gels is the mobility of the cross-links under load, with physical cross-links being far more mobile than chemical cross-links under load.

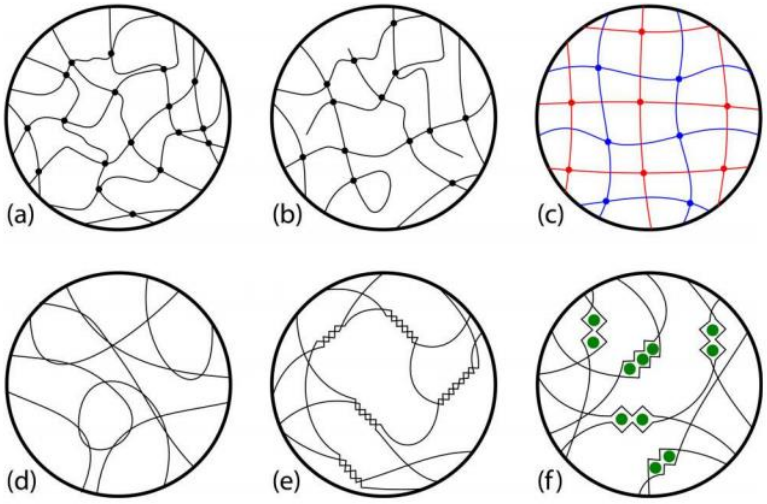

Figure 1.16 Schematic of hydrogel matrices for ideal (a) non ideal (b) and interpenetrating chemical gels (c) and entangled (d) helix entangled (e) and ionically cross-linked physical gels (f)[62]

Hydrogels can be thought of as essentially a molecular scale, porous, solid network with the pore spaces filled with water[112]. Strictly speaking a hydrogel must have the chemical network formed before it is hydrated, or swollen, in water[110], however there are gels in which the network formation occurs in solution. There are numerous ways to activate the cross-links in chemical gels, including chemical reaction, photopolymerisation with UV or irradiation. For physical gels the cross-linking methods include setting from a polymer melt and reversible bridging reactions, for example the use of divalent Ca^{2+} ions to bridge alginate chains[112].

The fluid phase within hydrogels and their swelling behaviour are important when considering gel mechanics, both under equilibrium conditions and dynamically. The volume swelling coefficient is fundamental to hydrogel behaviour and defines many characteristics including the mechanical and transport properties. The swelling

properties of hydrogels are related to numerous physical and chemical factors, including molecular weight between crosslinks and mesh size[62].

The aforementioned parameters discussed are all of fundamental importance to hydrogels and their mechanical behaviour. The swelling ratios are the most straightforward to determine, while the other parameters, like the mesh size and molecular weight between crosslinks, are much more challenging to obtain. This is due to the fact that the length scales when considering hydrogel pore size are very small, of the order of 1-100nm. The pore size is also particularly difficult to obtain due to the liquid phase of gels. This makes the use of techniques like scanning electron microscopy or porosimetry which require vacuum, difficult as if the sample is dried it will affect the mesh size. Light scattering and inference from mechanical analysis are indirect methods which can be used to determine the mesh size[110]. Mechanical analysis is thus very useful as it allows for not only the mechanical behaviour to be obtained but also the physical properties to be inferred from the well-established structure-properties relations. When designing hydrogels for specific applications it is clear that the above mentioned structural considerations can be critical in getting gels fit for purpose. An overview of methods to design hydrogels for specific purposes will now be given, with a focus on the polysaccharides.

1.2.2. CMC and other Polysaccharide Gel Review

Polysaccharides, such as carboxyl methyl cellulose (CMC), are essentially polymers made by polymerisation of sugars into chains. They exhibit strong biocompatibility and are used widely in the pharmaceutical, food and cosmetic industries.

Cellulose is a naturally occurring material that is found in abundance and renewably. It can be synthesised into polymer gels and currently development of new

functional cellulose based gels is occurring for use in numerous different fields. The interest into cellulose based materials is driven by the growing demand for environmentally friendly and biocompatible polymers. Cellulose based gels can be made from pure cellulose, cellulose composites and cellulose derivatives. CMC is a hydrogel based on cellulose derivatives[105, 122, 123].

Water soluble cellulose derivatives are often biocompatible and as a result can be used for a vast range of applications including, thickeners, binding agents, film formers, lubricants and stabilisers, particularly for food, pharmaceutical and beauty products. CMC is a water soluble cellulose derivative that can be synthesised into a gel through either chemical or physical cross-linking[105, 122-124]. Other similar polysaccharides include gellan, alginate and xanthan.

Gel Preparation and Structure

CMC is a polysaccharide polymer gel that is made from native cellulose by replacing some of the OH groups to form cellulose esters. The structure of native cellulose compared with CMC is shown in figure 1.17, where for CMC the R represents CH_2COONa. The number of OH groups replaced, per repeat unit, is characterised by the degree of substitution and lies between 0 and 3. There are numerous different cellulose derivatives that can be each tailored to certain functions, however this report will only consider CMC[105, 125-129].

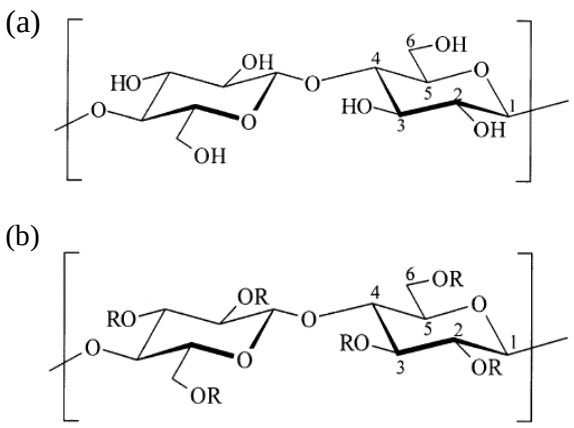

Figure 1.17 Chemistry of native cellulose (a) and water soluble cellulose derivatives (b) where for CMC R=CH_2COONa[125]

Once processed from native cellulose to CMC, gels can be made by dissolving into an aqueous solution. CMC can either be made into a physical or chemical gel depending upon the preparation. In physical gels secondary bonds from the methyl groups form to cross-link the gel network. The CMC chains will also form physical entanglements that will act as cross-links when under load. Adding ionic salts to the gel system can also assist the cross-linking of CMC by introducing ionic bonding. The use of ionic salts to cross-link a physical gel has also been used effectively with alginate gels[105, 125].

Using ionic cross-linkers in alginate has allowed for gels to be produced with tuneable stiffness making them useful for numerous different applications, like studies of substrate mechanics on cell behaviour[2, 33, 130]. The ionic cations form junctions across polymer chains forming complexes in what is known as the egg-box model[2, 125]. The rate of gelation when adding ionic cross-links is important as slowing the rate of gelation leads to more a controlled reaction occurring resulting in a more uniform gel with better mechanical properties. A frequently used ionic binder is calcium and this is typically added by dissolving calcium chloride into the gel solution. However

this results in rapid and poorly controlled gelation. One way of slowing the gelation process is to use a buffer containing phosphate which will result in the carboxyl and phosphate groups competing to react with the cations hence slowing the rate of gelation. Using less soluble calcium salts is also an effective way to slow the gelation process. Finally by lowering the temperature, the rate of reaction can be decreased as the reactivity of the ionic cross-linker is decreased[2, 131].

The use of multivalent cations can also result in the formation of coacervates rather than giving rigid cross-links. Coacervates result from the phase separation of polyelectrolyte complexes into a dense aqueous polymer aggregate phase within a more dilute phase. Coacervates can be split into two main types, complex coacervates and simple coacervates[132-137]. Simple coacervates involve a single macromolecule which complexes due to polymer-polymer interactions being promoted over polymer-solvent interactions, while a complex coacervate occurs due to complexing between two oppositely charged polyelectrolyte macromolecules[135, 136]. The formation of coacervates is strongly linked to the ionic strength of the solvent used. Increasing the ionic strength of the solvent reduces the distance over which opposite charges will act over, i.e. it reduces the Debye length, and hence reduces the potential for electrolytes to interact within the coacervate phase[136-138]. A major consideration when designing coacervates is how to ensure coacervation occurs, rather than polymer aggregates simply precipitating. If the polyelectrolytes are too strong it can cause precipitation, while increasing the solvent concentration can reduce the relative electrolyte strength, hence promoting coacervation[136].

The use of ionic cross-links to make polysaccharide gels has one major weakness associated with it; when left in conditions mimicking physiological conditions it has poor long-term stability due to the release of divalent cations into the surrounding

medium. Depending on the application the gel is being used for, the diffused ions can result in problems like haemostasis. In order to avoid these issues there has been a push towards using gels with covalent rather than ionic cross-links[2].

CMC has been successfully cross-linked using divinyl sulfone (DVS) as the covalent cross-linker as shown in figure 1.18. The swelling behaviour of these gels is highly sensitive to their environment both during and after gelation. The surrounding pH and temperature are particularly influential. As previously mentioned the swelling behaviour of a gel has a strong influence on its mechanics therefore the conditions in which these gels are produced as well as the working conditions must be carefully considered. Other materials, like PEG, have also been used to covalently cross-link gels. The swelling behaviour of these covalently cross-linked gels can also be altered by changing the molecular weight of the PEG or inserting spacers into the matrix when using DVS[105, 139]. The problem with using many of these materials is that they are toxic and hence cannot be used in CMC gels prepared for pharmaceutical, food or cosmetic purposes.

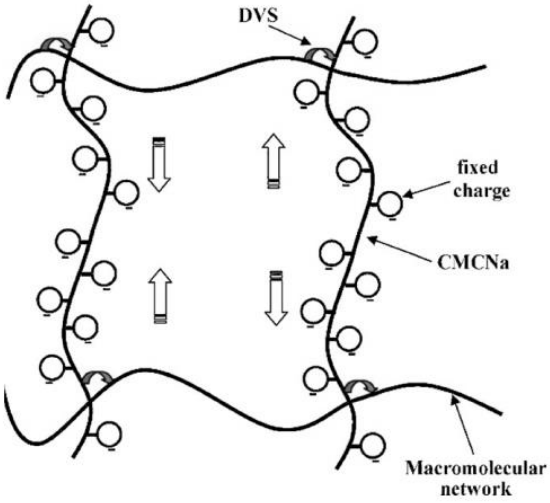

Figure 1.18 CMC macromolecular network with DVS cross-linkers and charged chains acting as contraction or expansion devices[139]

A significant difference between gels formed by ionic bonding rather than covalent bonding is the response to mechanical loading. In ionically bound gels, the stress can relax as bonds break and reform and water leaves the gel, resulting in plastic deformation. Whereas in covalently bound gels the bonds are permanent and cannot break resulting in a much more elastic response (there will still be a time dependant contribution due to the migration of water that can still occur)[2, 121]. The use of interpenetrating networks that combine a covalently bound network with an ionically bound network have resulted in gels being produced that exhibit extremely high toughness[140].

The covalent cross-linking of alginate has also been widely studied and it has been shown that numerous polymers can be used for this purpose depending upon the desired use of the gel. Alginate cross-linking was first investigated using poly(ethylene glycol)-diamines as the cross-linker. The mechanical properties of the alginate could be controlled by varying the cross-linking density and/or varying the weight fraction of the PEG in the gel. The elastic modulus of alginate increases with the weight fraction of PEG up until the point where the molecular weight between cross-links becomes less than the molecular weight of the PEG. The chemistry of the cross-linker also plays a role in the swelling and hence mechanics of the gel. Cross-linking typically results in a decrease in the hydrophilicity of the gel, but by using hydrophilic cross-linking molecules (like PEG) this can be compensated for[2, 130].

Recently the potential for using photo cross-linking for *in situ* covalent gelation has gained interest. Photo cross-linking could be conducted in mild reaction conditions, potentially even in contact with drugs and cells, provided appropriate chemical initiators are present. Photo cross-linked alginate gels have already been used *in vivo* to seal a corneal perforation. The alginate used was modified with methacrylate

and cross-linked via exposure to an argon ion laser for 30s in the presence of eosin and triethanol amine. This study suggests that photo cross-linked gels have potential for clinical use in sutureless surgery. One main issue associated with photo cross-linking is that it often requires the use of light sensitizers or the release of acid which are potentially harmful. Non-toxic methods of photo cross-linking are being researched, however, quite successfully[2, 141].

1.3 Interfacial Protein Adsorption and Mechanics

Interest in the mechanics of liquid-liquid interfaces stems from the study of emulsions. Emulsions are commonly used for processes in both the oil and gas and biochemical industries, such as two phase reactions and extraction separations. Understanding the stability of emulsion is key to utilising them for industrial processes. As thermodynamically unstable systems, emulsions should separate, however in the presence of surfactants many are shown to be stable and hence dynamically stable.

The destabilisation of emulsions occurs when the continuous phase between droplets drains, resulting in the droplets coalescing and hence phase separating. The Dejaguin Landau Verwey Overbeek (DVLO) theory is used to quantify the distribution of charges in ionic solutions and explain the stability of colloidal suspensions. It is thought that drop coalescence results from a combination of DVLO forces, like van der Waals and electric double layer forces, and non-DVLO forces, like steric hindrance and hydrodynamic forces[142].

Emulsions can be further stabilised with the addition of proteins which can bind and unfold at the interface. The unfolding of proteins at interfaces can greatly alter their mechanics and lead to far more mechanically stable interface forming. The im-

pact of surface active molecules deposited at interfaces depends on a number of factors, such as, their ability to lower the interfacial surface tension, the amount adsorbed, if they can desorb, whether they unfold upon binding, the thickness of the adsorbed layer and the ability of adsorbed molecules to interact (or cross-link) with one another[143].

The characterisation of the impact of the surface active molecules on interfacial mechanics along with understanding the interaction between colloids within emulsions is important to many industrial applications. Interfacial mechanics has also become of interest in the field of cell biology as it has been shown that cells can adhere and spread at liquid-liquid interfaces[144-146]. Within these cell experiments, the stabilisation of the interface was shown to be extremely important to cell adhesion. The importance of interfacial mechanics and protein deposition is clearly extremely important within numerous fields of research. As such an overview of the interfacial mechanical characterisation methods and the mechanisms of protein deposition and unfolding at interfaces will be given.

1.3.1 Interfacial Protein Adsorption and Emulsion Design

Proteins are biopolymers exhibiting high functional and structural variability. Proteins are important in numerous biological functions and processes including, substrate binders, structural components, and as transporters[147, 148]. Proteins are made up of sequences of amino acids, this structure and sequencing determines their function. Each protein repeat unit is made up of polypeptide chains which can assemble into two dimensional secondary structures which can in turn fold into three dimensional functional proteins. These three dimensional proteins can then complex into functional complexes[149].

The amino acid groups of proteins can interact through secondary bonding, such as hydrogen and ionic bonding and hydrophobic interactions[148-150]. These interactions give folded proteins their stability, however in the presence of heat and pressure or when deposited at interfaces the proteins can unfold, or denature, as these interactions are disturbed. Proteins can be defined as globular, like bovine serum albumin (BSA) or lysozyme, or non-globular, or random coil, like β-casein, although these classifications are seen to be something of an anachronism today.

The ability of a protein to bind and unfold at interfaces depends upon a number of factors, such as its thermodynamic stability, flexibility, amphipathicity, molecular size and charge[148, 149, 151, 152]. The adsorption of proteins at interfaces can be broken down into the following steps, diffusion of proteins to the interface from the solution followed by adsorption to the interface. The proteins then undergo some form of structural changes, such as unfolding, before spreading across the interface[148, 153, 154]. Structural changes to the protein upon adsorption are dependent on the nature of the interface (be it liquid-liquid, liquid-air or liquid-solid), the conditions of the protein solution, such as pH, ionic strength, protein concentration and temperature[143, 147, 155], and intrinsic properties of the protein. Once deposited many proteins show extremely strong and stable lateral interactions unfolding irreversibly[154].

Lateral interactions and bonding between deposited proteins are dependent on their three dimensional folding and structure, particularly their degree of hydrophobicity and/or amphipathicity. In general higher hydrophobicity leads to faster adsorption, greater decrease in surface tension and better emulsion formation. Once proteins are deposited the hydrophobic surfaces align onto the interface resulting in new sec-

ondary bonding between proteins. Ultimately this can result in proteins unfolding irreversibly[154, 156] and potentially forming close-packed, cross-linked structures[143, 155, 157].

The adsorption of proteins at interfaces depends upon a number of factors, such as the concentration of protein, the pH, temperature and the ionic strength of the buffer. The pH of the buffer has been shown to greatly impact the adsorption of protein films. If the buffer is at the isoelectric point, the pH at which proteins have a neutral charge, the proteins take their most compact shape. This reduces any steric hindrance between proteins and also prevents electrostatic repulsion, ultimately leading to faster and denser protein adsorption[156, 158].

The ionic strength of the buffer is also thought to influence interfacial protein adsorption. It has been shown in the case of lysozyme deposited at pH 7 that increasing the ionic strength of the buffer leads to a stronger film being formed[156]. The mechanism behind this is thought to result from higher ionic strength increasing the hydrophobicity of proteins as the charges are shielded, resulting in stronger interactions between proteins[156, 159].

Varying the concentration of protein has been widely shown to alter the adsorption of protein to interfaces. Generally speaking it has been shown that increasing the protein concentration increases the rate of adsorption[155, 156, 158, 160]. It is thought that the rate of deposition is proportional to the concentration and the square root of time[161].

Clearly there are many factors that influence the adsorption of proteins at interfaces and in order to properly control and design interfaces for applications they

must be taken into account, in reference to the intrinsic nature of the protein being deposited and the nature of the interface too.

1.3.2 Interfacial Mechanical Characterisation Methods

Interfacial Shear Rheology

One of the most commonly used techniques to probe the mechanics of proteins adsorbed at interfaces is interfacial rheology. Interfacial rheology can be divided into two categories, dilatational and shear. Dilatational interfacial rheology involves changing the interfacial surface area while recording the resulting change in interfacial tension. Interfacial shear rheology involves deforming the interface in the shear plane, without inducing any change to the surface area, and recording the force response. Each of these two techniques has specific issues associated with them. In the dilatational case, it is difficult to separate the shear deformation when measuring the dilatational elasticity and viscosity. In the case of interfacial shear rheology it can be difficult to separate any viscoelastic contribution from the bulk phase from the interface response[162].

In recent studies, novel methods of interfacial have been used to characterise interfacial mechanics. The use of parallel floating rods measuring the in-plane forces acting on them under compression has been shown to be a useful technique for measuring interfacial moduli, as shown in figure 1.19. This method is particularly useful as a wide range of strains can be applied as the film is compressed between the rods. Using this method it was able to show that the self-healing nature of globular proteins resulted from secondary bonding rather than covalent cross-links forming at the interface[163].

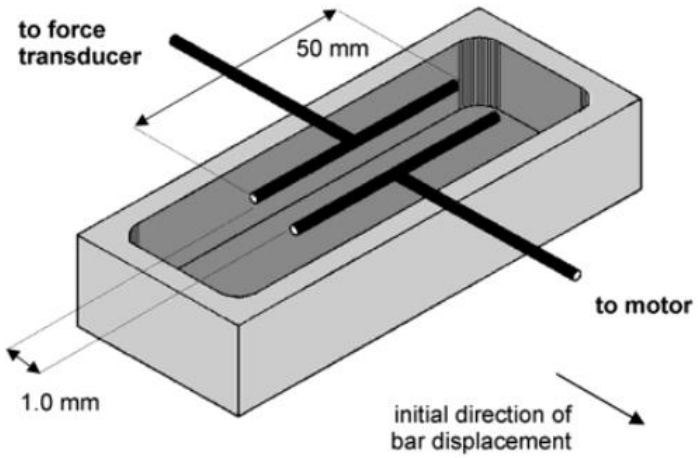

Figure 1.19 Schematic of interfacial rheometry set up used to measure shear forces between parallel floating rods[163]

Another interesting method gaining in significance, moves magnetised floating objects on the interface with magnetic fields. This has allowed for extremely sensitive rheological characterisation to be undertaken using highly sensitive magnetic interfacial needle rheology. However, here the influence of bulk phase drag on the floating objects is greater than in the normal case and hence great care must be taken to consider these effects on the interfacial moduli[164].

Finally developments in traditional interfacial oscillatory/rotational rheology, using geometry like a Du Noüy ring, have been greatly improved in recent years and can now measure interfacial forces with an extremely high resolution. This method allows for a large number of tests to be performed, dynamic mechanical analysis, creep and stress relaxation testing, and continuous flow experiments to name a few, mining many material properties and allowing for careful monitoring of film formation[152].

However these interfacial rheology techniques are limited in that they only probe in the shear plane and hence do not probe the contribution of surface tension forces to the mechanical response of protein adsorbed interfaces. The normal colloidal

interfacial forces between solid colloids and oil droplets has been studied extensively by AFM. Here an overview of the use of AFM to study interfacial mechanics will be given.

Interfacial Nanoindentation by AFM

DVLO theory describes the charge distribution in ionic solution and has been shown to provide an excellent theoretical underpinning of the stability of colloidal suspensions[165-167]. The DVLO theory is a stabilising theory to describe the overlap between the ionic spheres of two approaching particles. It fundamentally is a balance between the electrostatic double layer forces and the Van der Waals forces. The forces between droplets in suspension are also thought to predominantly consist of DVLO forces (van der Waals and electric double layer forces) combined with some non-DVLO forces such as steric hindrance and hydrodynamic forces. The thrust of much research into interfacial AFM is to be able to measure and quantify the forces acting between colloids in emulsions[168].

The direct measurement of forces between two colloids within an emulsion is however very difficult as they vary significantly on approach and retraction, and the forces can vary from attractive to repulsive depending upon the distance between the droplets[169]. Since the development of AFM, the direct recording of nano-Newton forces has been possible, allowing for more detailed understanding of interfacial mechanics between colloids[170]. Studies of interfacial mechanics by AFM have included studies between solid particles and liquid interfaces[171, 172], forces between two droplets[173] and even forces between two bubbles[174], as shown in figure 1.20. The forces between two colloids as described by DVLO theory is highly dependent on the distance between the two colloids, and as a result one of the greatest challenges with respect to interfacial AFM is that the exact film thickness (between the probe and the

oil phase) is not known[175]. Recent studies have been performed using laser scanning confocal fluorescence microscopy[176] and reflection interference contrast microscopy[177] in conjunction with AFM to quantitatively measure the film thickness during the AFM experiments.

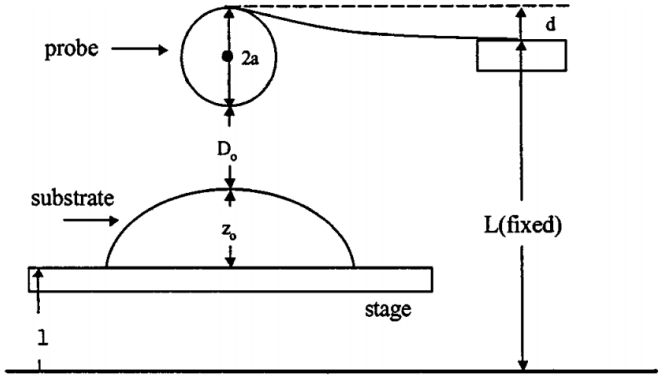

Figure 1.20 Schematic of the general geometry used for interfacial AFM measurements[171]

While interfacial AFM has been widely used to study interfacial forces between interfaces and colloids, these studies have not been used to study the influence of protein adsorption on the mechanical stability and strength of interfaces. The impact of adsorbed protein films across many applications, as discussed in section 1.3.1, makes it clear that a better understanding of the mechanical properties of protein layers adsorbed at liquid-liquid interfaces is of great interest across numerous fields.

1.4 Summary, Aims and Objectives

Within the field of bioengineering the mechanics of soft materials is clearly of utmost importance across numerous fields and in particular in the case of cell mechanics. However mechanical testing methods are developed for much stiffer engineering materials. Soft biomaterials also often have significant heterogeneity which lends to their functionality. As a result we aim to develop robust protocols to accurately characterise the mechanics of soft biomaterials across a range of length scales, form nm to bulk properties. Specifically, the sample – testing geometry interface is considered

and the impact of factors such as adhesion and heterogeneity on both the data analysis and acquisition are to be examined. The impact of adhesion and wetting on data acquisition and how it can be compensated for when extracting material properties is of particular interest. And how these factors vary in significance across different length scales and on materials with different structure and chemistry.

Polysaccharide hydrogels have been widely used across a range bioengineering applications. CMC has been used extensively as a physical gel for applications like denture adhesives. The ability to tune these gels is important to optimise them for applications. The use of multivalent ionic cross-linkers have been used to effectively tune the mechanics of other similar polysaccharides, either by forming rigid cross-links or by complex coacervation. Here we aim to study the impact of ionic cross-links on the rheological and adhesive properties of CMC gels. The aim here is to see how ionic crosslinks affect the structure of the CMC gels and how these structural changes impact the bulk mechanics and also the adhesive properties. The use of larger multivalent cationic crosslinkers is compared to the use of divalent cationic salts to probe whether different crosslinking mechanisms can be achieved by controlling the size and charge of the crosslinkers.

Finally the study of interfacial mechanics has become increasingly important in the study of cell biology. However the mechanics of proteins adsorbed at interfaces, to which cells have been shown to adhere, is not well understood, particularly under indentation testing. The contribution of surface tension forces compared with the protein film forces if of specific interest. Hence we aim to create a model to understand the relative contributions of surface tension and film forces on the overall mechanics of proteins adsorbed at liquid-liquid interfaces. The focus here is to understand the interplay between the interfacial forces, arising from surface tension and DVLO

forces, and the protein film forces when resisting deformation by indentation. As the interaction between the protein film and the interface is not trivial as a first approximation it will be assumed that this interplay results in the superposition of the resistance arising from these two phenomenon. The sensitivity of this model to varying the different variables that impact the force response to indentation is then done to probe the relative significance of these factors on the mechanics of these complex interfaces.

Chapter Two

Impact of surface adhesion and sample heterogeneity on the multiscale mechanical characterisation of soft biomaterials

This chapter is based on the following published paper,

Megone, W., N. Roohpour, and J. E. Gautrot. "Impact of surface adhesion and sample heterogeneity on the multiscale mechanical characterisation of soft biomaterials." *Scientific reports* 8 (2018).

2.1 Introduction

The mechanics of soft materials for use in biomedical applications has been widely studied, such as for use in tissue engineering [1, 2], drug delivery[2, 3], wound healing[2, 4, 5] , and cell culture substrates for *in vitro* studies[6-8]. In particular, the mechanics of biomaterials has been shown to be very important in determining cell response and for implant design. Levental et al. showed that collagen cross-linking within the ECM and ECM stiffening was present within tumour growth and breast malignancy [34]. Furthermore studies have shown how, for cardiac repair, the heart valve leaflet stiffness is a key design feature, again showing the importance of the mechanics of soft materials used in bioengineering [178, 179]

Despite the striking changes in cell phenotype observed on poly(acrylamide) (PAAm) gels with varying moduli (in the range of 1 kPa to 1 MPa), we previously reported the absence of apparent response of cells to Sylgard 184 poly(dimethyl siloxane) (PDMS) with moduli in the range of 0.1 kPa to 2 MPa [6]. However the origin

of this apparent lack of response remains unclear. It was proposed that, at the local (nano- to micro-) scale and for small strains, the modulus of weakly cross-linked Sylgard 184 PDMS is significantly higher (up to two orders of magnitude) than what is reported for elastic and shear moduli (Fig. 2.1 [58, 180-186]). However, the origin of such behaviour (material stiffening at the nanoscale) is not clear and not supported by molecular modelling of polymer samples deformation[187-191]. Similar discrepancies between mechanical characterisation at different scales have been reported by others, although systematic studies of materials prepared in identical conditions and characterised at different length scales are still lacking. In addition, multiple scale mechanical characterisation of PDMS and PAAm has highlighted a very wide range of moduli reported for these materials, particularly for very soft samples (Fig. 2.1)[58, 180-186]. However most mechanical testing techniques are optimised for traditional engineering materials which typically have high moduli (in the region of MPa – GPa), making characterisation of soft biomaterials particularly difficult[62]. Hence, understanding the origin of such discrepancies and determining which techniques are most appropriate to use at different length scales, but also at different ranges of compliance, needs to be urgently addressed in order to tackle important questions in the field of biomaterials design and mechano-biology.

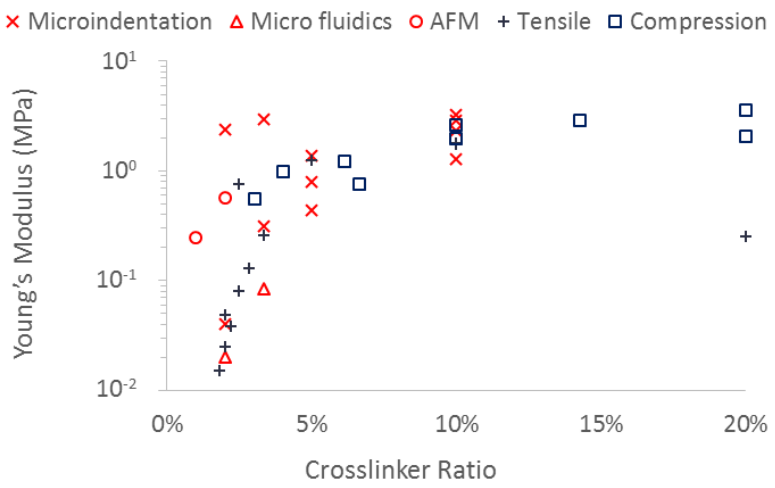

Figure 2.1 Young's modulus of Sylgard 184 PDMS samples with varying base/cross-linker ratios highlighting the discrepancies between different testing methods, particularly at low levels of cross-linking (softer samples)[58, 180-186].

A number of hypotheses have been proposed to account for differences between bulk and local mechanics, such as heterogeneity within the material [10, 11] and adhesion between the sample and testing geometry [104, 192]. Heterogeneity has been shown to lead to an increased modulus when using localised testing methods, such as nano indentation by AFM, however this is not reflected on the bulk mechanics [10].

This phenomenon occurs when the local deformations applied for mechanical testing occur on the same length scale as the heterogeneity. In contrast, impact of sample heterogeneity on bulk mechanics will only be significant in cases where the filler (or hard nanomaterial/phase) forms a percolated network, forming a connective path between the geometries used for mechanical testing[12].

Importantly, previous work has shown that the chemistry of the materials should be considered when determining a methodology for testing of a material at different length scales. Bush et al. introduced linear-harmonic interpolation of the Mooney-Rivlin and Boussinesq models, combined to compromise between nano and microindentation models allowing heterogeneity to be modelled using a finite, rather than small, strain model [10]. This method was designed to correct the contact model at

larger relative indentation depths, however this does not take into consideration any wetting of the tip and associated adhesion phenomena. Sirghi and Rossi proposed an altered version of the Oliver Pharr method in order to take into account adhesion between the testing geometry and sample, however this method assumes a Hertzian contact which is only valid when wetting can be ignored [104]. Therefore, it appears important to investigate and quantify heterogeneity and adhesion simultaneously when characterising soft biomaterials at different length scales.

In this study, we investigate the mechanical properties of soft biomaterials (Sylgard 184 PDMS hydrophobic elastomers, hydrophilic PAAm and carboxymethylcellulose (CMC) composite hydrogels) and quantify discrepancies observed between moduli determined at nano- to macro-length scales, via rheology, indentation and atomic force microscopy. In particular, we quantify the combined impacts of heterogeneity of the corresponding materials and adhesion and wetting between the materials tested and the geometries of the instruments used for characterisation.

2.2 Methods and Materials

Materials. Toluene extra dry**,** 3-(Trimethoxysilyl)propyl methacrylate, Acrylamide, Ammonium persulfate, NN'-Methylbis(acrylamide), NNN'N'-Tetramethylethylene diamine, Hexamethyldisilazane, Sylgard 184 PDMS, Alyl Bromide, PEG Di Thiol and all purchased from Sigma Aldrich. Aqualon Sodium CMC purchased from Ashland Chemicals.

PDMS Sample Preparation. PDMS samples were prepared using the Sylgard 184 elastomer kit. Samples with 1 wt%, 2 wt%, 3 wt% and 10 wt% cross-linker were mixed thoroughly using a spatula before being put under vacuum to remove the bubbles. The samples were then cured at 60^{o}C for 3hrs either in situ for use in rheology,

on 13mm glass coverslips for AFM indentation, and in 35mm petri dishes for microindentation.

PAAm Sample Preparation. Stock solutions were mixed according to the ratios shown in table 1.1. The AAm stock solutions were degassed for a minimum of 30 min before use. Samples were then mixed with the cross-linking agents according to the following ratios 500 μl stock solution with 2.5 μL APS and 0.75 μL TEMED. Samples were then either cured *in situ* for use with rheology or between a 13 mm methacrylate functionalised glass cover slip and a hydrophobised plate for testing by AFM.

Allyl CMC Hydrogel Preparation. Sodium CMC was dissolved in a 1:1 mixture of DMF and DI water, the DMF was used in order to protonate the CMC, at a concentration of 1mg/ml. Once the solution was homogenous Alyl Bromide was added at molar ratio of 30% alyl to CMC. The solution was heated to 70^{o}C and left overnight for the reaction to complete. The functionalised CMC was then precipitated in Acetone and dried. The final product was twice dissolved in DI water and precipitated in acetone to purify.

Functionalised CMC samples were then prepared by dissolving 100 mg/mL CMC in DI water and adding PEGDT and photoinitiator at the following alyl:PEGDT:PI ratio, 4:2:1. Samples tested by rheology were cured in situ and samples for AFM indentation were cured on 13 mm functionalised glass coverslips using UV light at 50 mW/cm^2 for 2 min.

Samples containing silicon microbeads were prepared using the same method, however the microbeads were dispersed in the DI water before adding the functionalised CMC.

Table 2.1 Polyacrylamide stock solution compositions

Gel	%AAm	%Bis	Ratio	40% AAm (mL)	2% Bis	H_2O (mL)	Total vol. (mL)
1	5	0.02	1/250	0.625	50 µL	4.325	5
2	8	0.15	3/160	1	375 µL	3.625	5
3	20	0.375	3/160	2.5	937.5 µL	1.563	5
4	20	1.5	3/40	2.5	75 mg	2.5	5

Bulk Mechanical Characterisation by Oscillatory Rheology. Oscillatory rheology was used to characterise the mechanics of the series of PDMS samples using a TA Discovery HR-3 hybrid rheometer. The samples were cured in situ at 80°C for 2 h and the gelation was monitored by an oscillating time sweep, with an oscillating frequency of 1 Hz and an oscillating displacement of 10^{-4} rad. Once cured the samples were then kept at room temperature for 5mins to cool and were then characterised using an oscillating frequency and stress sweep, and by transient stress relaxation. The frequency sweeps were performed from 0.1-100 Hz at an oscillating displacement of 10^{-4} rad and the stress sweeps were performed from 0.1-100 Pa at a frequency of 1 Hz. Finally stress relaxation was performed using a shear strain of 2 % and a hold time of 300 s.

For testing of the PAAm samples the same method was used however the temperature was kept at room temperature and the curing time was a maximum of 1.5 h. The PAAm samples were also tested with and without the use of functionalising the rheometer geometry. In order to functionalise the rheometer geometry methacrylate functionalised glass cover slips were attached to the top and bottom geometry. The cover slips were held in place using Loctite Super Glue Ultra Liquid Control® with a tensile shear strength of 10 to 20 MPa (product specification). This ensures that the shear properties of the materials tested (with moduli below MPa) are not affected, but also enabled simple detachment of functionalised coverslip by solvent immersion (the

glue is soluble in common organic solvents such as acetone). In order to minimise evaporation the rheometer geometry was enclosed in a solvent trap.

Bulk Mechanical Characterisation by Microindentation Testing. Indentation testing was performed using an MTS coil driven universal test frame with a 500 N load cell. The samples were indented using a 3 mm conical flat ended punch. Indentation was done by stress relaxation testing with an indentation depth of 10 % sample thickness at an indentation speed of 1 mm/s and a hold time of 300 s. The indentation retraction curves were fitted to the force-displacement model developed for the Oliver Pharr method [94].

Local Mechanical Characterisation by Nanoindentation by AFM. Nanoindentation was performed using an Ntegra AFM rig. Bruker 8-10 contact cantilever tips were used with a nominal tip diameter of 15 nm. The cantilever had a nominal stiffness of 0.05 N/m. The cantilevers were calibrated to obtain the conversion of nA to nm by doing initial indentations on Silicon wafer. Samples were tested by doing a 10X10 grid of indentation at three different location on three different samples of each formulation respectively.

Wet AFM was performed with samples submerged in DI water, ethanol and PBS for the PAAm, PDMS and CMC samples respectively.

The indentation curves were then analysed using a custom made MATLAB script using the Oliver Pharr [94], or Sirghi [104] method depending upon whether adhesion was present.

2.3 Results and Discussion

Macro-to nanoscale mechanical properties of PDMS hydrophobic elastomers

We characterised the bulk mechanical properties of PDMS samples cross-linked at different base to curing agent ratios via oscillatory rheology and microindentation first. The PDMS tested is a classical Sylgard 184 grade, commonly used in microfluidics, micro-contact printing and for cell culture [8, 44, 45, 193]. It was cross-linked at different ratios, from 1 to 10 wt% (curing agent to base), in order to control its mechanical properties. Oscillatory rheology was carried out over the full range of compositions tested, but microindentation was not possible for the softest PDMS sample due to a lack of sensitivity of the load cell used. Results of bulk mechanical testing performed on PDMS are gathered in Fig. 2.2 and 2.3.

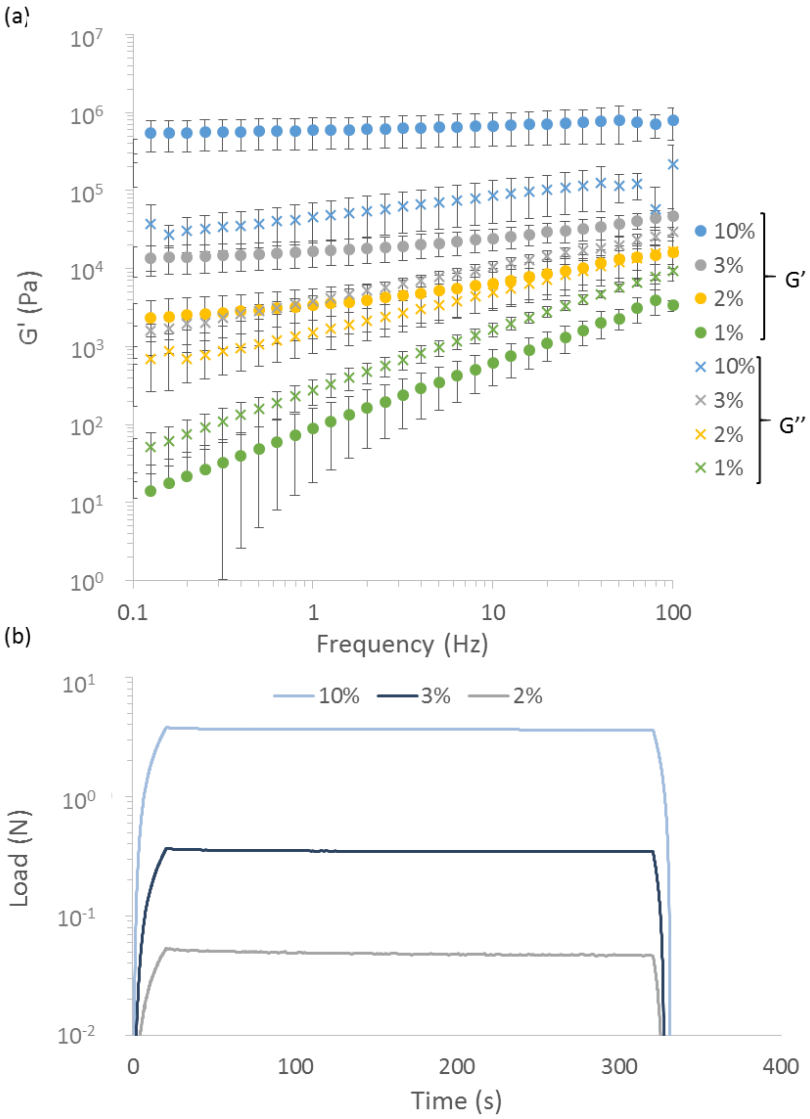

Figure 2.2 Bulk characterisation of PDMS by (a) Oscillatory rheology showing the frequency sweeps with frequencies from 0.1 – 100 Hz at an oscillating displacement of 10^{-4} rad for PDMS samples with % Cross-linker ranging from 1% – 10% a minimum of three repeats were conducted on each sample and (b) microindentation showing representative stress relaxation curves, of samples strained to 10% strain at a rate of 1%/s and a hold time of 5 min, each test was repeated three times. Error bars showing the standard deviation.

Oscillatory rheology clearly indicated a strong increase in shear modulus with increasing cross-linker (Fig. 2.2a). This trend is also clearly observed in microindentation results (Fig. 2.2b). Frequency modulated oscillatory rheology also clearly evidenced the viscoelastic character of weakly cross-linked Sylgard 184 PDMS (1% cross-linker), which displayed a quasi-linear log-log relationship between shear modulus and frequency, with the modulus increasing by more than three orders of magnitude, from 1 Pa at 0.1 Hz to 3 kPa at 100 Hz. Such viscoelastic response was much

weaker at higher cross-linker ratios and negligible at 10 % cross-linker. Hence our data is in very good agreement with previously published micro-indentation data for similar Sylgard 184 PDMS materials [6], confirming the bulk mechanical properties previously reported.

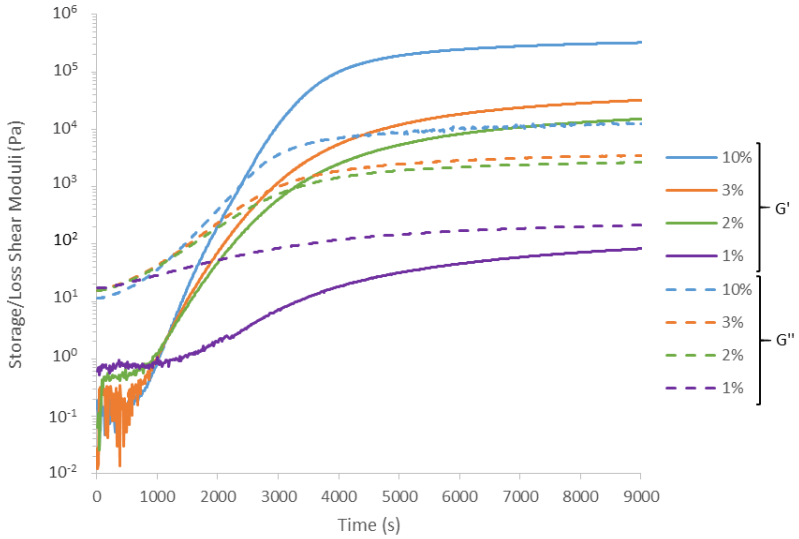

Figure 2.3. *Oscillatory rheology time sweeps monitoring the curing of PDMS at different base-cross-linker concentrations (indicated in the legend, the % referring to the weight % of cross-linker relative to the base). Time sweeps were conducted at a frequency of 1Hz and with a displacement of 10^{-4} rad.*

We next examined the nanoscale mechanical properties of PDMS via nanoindentation (Fig. 2.4a, b and 2.5). Whilst we measured elastic moduli in good agreement with bulk and shear moduli for the two stiffest PDMS formulations (elastic moduli of 0.41 MPa and 1.27 MPa for 3 and 10 % cross-linker PDMS formulations, respectively), strong adhesion prevented tip detachment for the softest two samples (1 and 2 %). This suggested important fouling of the cantilever surface by the soft PDMS formulation, a process that was clearly evidenced by *in situ* AFM-SEM imaging (Fig. 2.6a), hence, it is clear that Hertzian approximations cannot apply to weakly cross-linked Sylgard 184 PDMS materials.

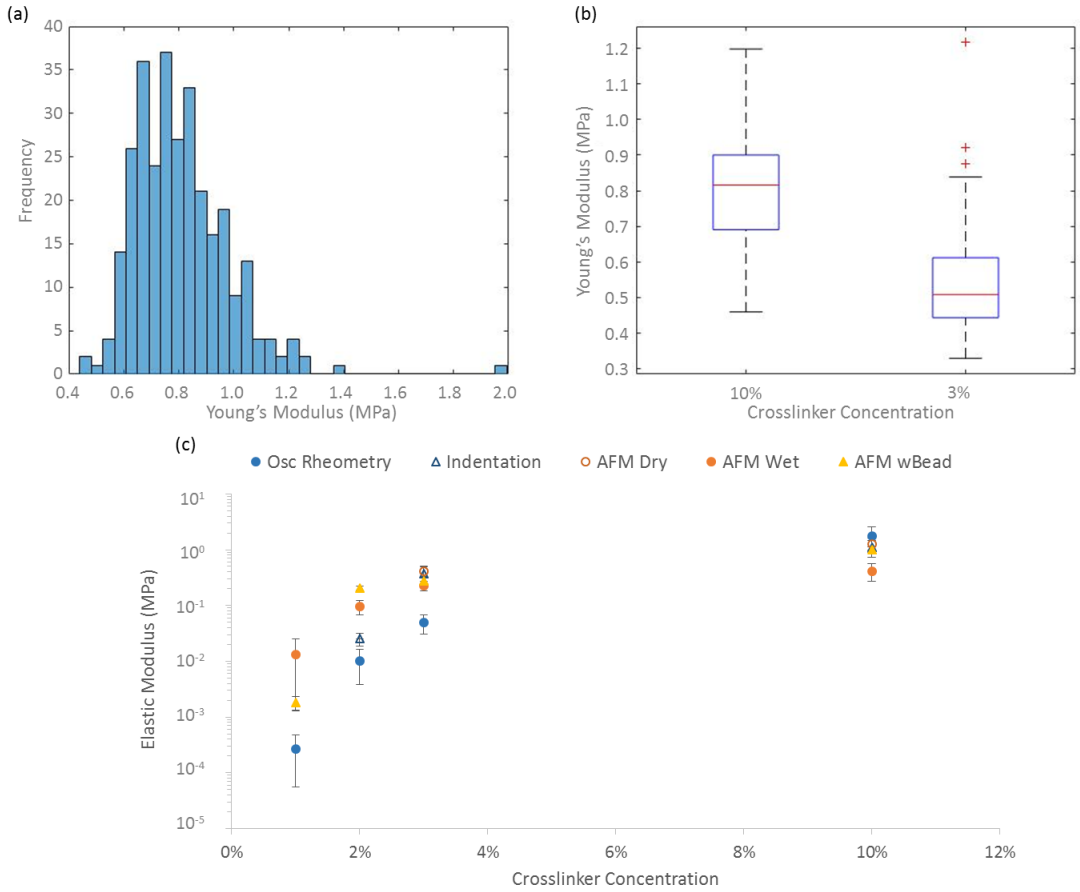

Figure 2.4 (a) Representative dry AFM histogram showing the spread in moduli value over three 5X5 □m locations with 100 indentations per location on a 10% cross-linker PDMS sample, (b) box and whisker plots showing the Young's moduli obtained across the range of PDMS samples tested by dry AFM and (c) comparison of the bulk and local mechanical characterisation of the PDMS samples tested. All AFM experiments were conducted with an indentation depth of between 500 and 1000 nm and each curve was done over 1 s. AFM experiments were conducted on three different samples for each formulation and each sample tested in three different location with 100 indentations done on a 5X5 mm square.

In order to reduce adhesion to cantilevers, AFM experiments were performed in ethanol solutions, which has been shown to reduce adhesion of silicone materials[194]. In these conditions, the adhesion component was reduced significantly, including for the softest PDMS materials tested and tip detachment occurred within the working distance of our instrument (Fig. 2.6b). These AFM results were again in good agreement with bulk measurements for the PDMS samples tested with the highest moduli, but displayed significantly higher moduli, for softer PDMS (in particular at 1% cross-linker, which displayed a local modulus of 13 kPa compared to the shear modulus of 270 Pa measured via rheology) as shown in Fig. 2.4c. Fig 2.6b indicates that there is

still significant adhesion between the sample and indenter tip for the softest PDMS samples during nanoindentation even in wet conditions.

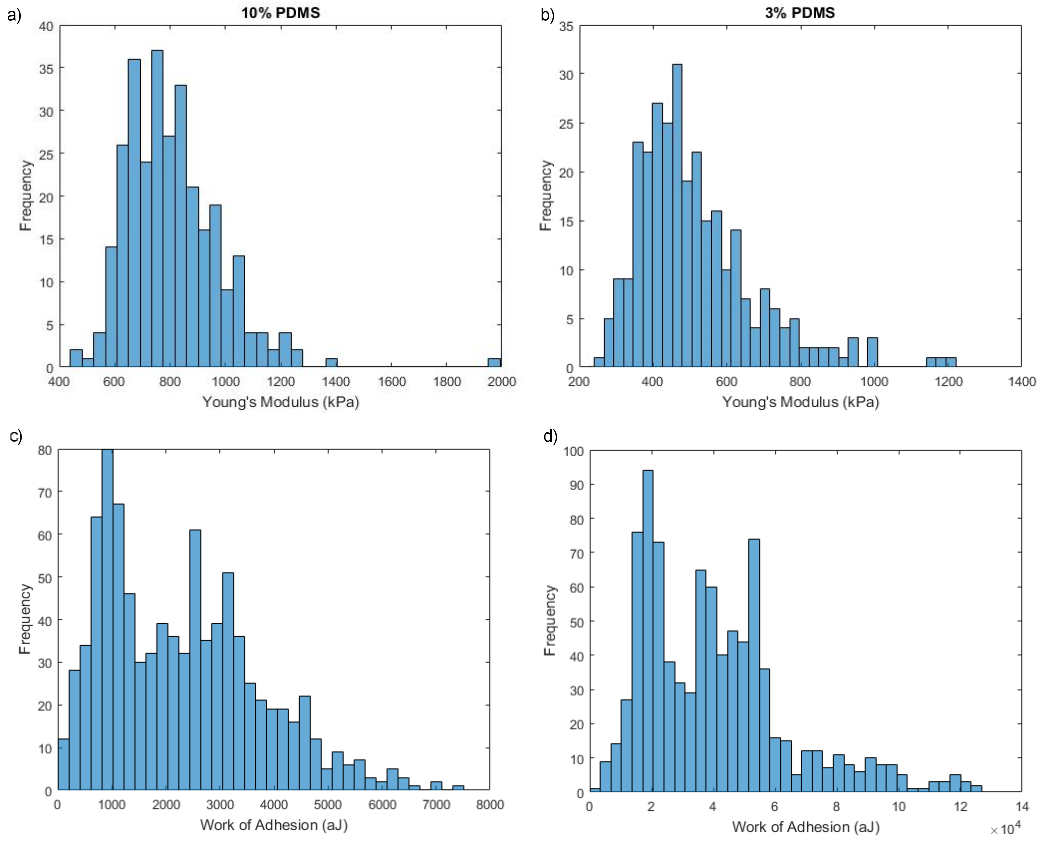

Figure 2.5. *Histograms showing the distributions in Young's moduli obtained by AFM on PDMS samples tested dry for PDMS samples with (a) 10% cross-linker by weight and (b) 3%. Each sample is tested in three 5X5um locations with 100 indentation tests spread evenly across each location and the spread in the work of adhesion for PDMS with (a) 10% and (b) 30% cross-linker*

The work of adhesion and maximum adhesive force were then characterised (Figure 2.6c and 2.7) to confirm that the level of adhesion between the sample and testing geometry was significantly higher for the softest PDMS sample (3,400 aJ for 1% cross-linker compared to 2.7 aJ for 10% cross-linker). Hence, the increase in the adhesion between the sample and AFM tip could explain the higher modulus obtained as the adhesion would change the wetting of the tip and hence the contact area between the sample and testing geometry. Furthermore, looking at the spread in Young's moduli by colloidal AFM it is clear that the spread in the data is similar across all the samples, this suggests that the higher modulus seen for the softest PDMS is not a result

of local heterogeneity. When looking at the Young's modulus as a function of work of adhesion shown in 2.7 it is also clear that the spread in Young's modulus coincides with increasing adhesion. Hence, our data suggest that, even in wet conditions, adhesion and wetting of soft PDMS substrates is causing significant deviation between local and bulk moduli.

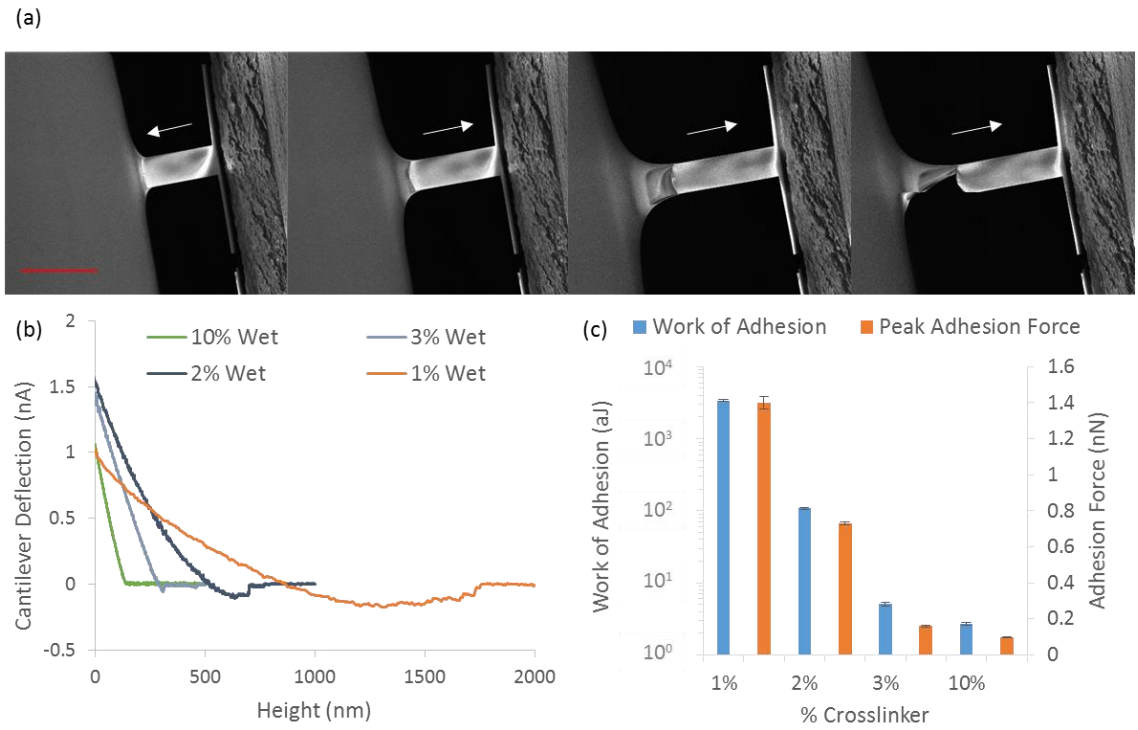

Figure 2.6 (a) SEM images, taken using an environmental SEM (Quanta 3D FEG, FEI), of AFM tip interaction with 2% PDMS highlighting the adhesion between PDMS and Silicon Nitride AFM Tip snapping into and coming out of contact as indicated by the arrow. Scale bar is 100um and (b) Nanoindentation by AFM retraction (lift) curves for PDMS samples tested wet in ethanol solution. All AFM experiments were conducted with an indentation depth of between 500 and 1000 nm and each curve was done over 1 s, each sample was tested in three different locations and 3 samples tested per formulation giving 900 data points per formulation (c) the average adhesion strength and peak adhesive force obtained by wet AFM

In order to correct the wetting contribution observed in PDMS materials, we proposed to take into account the contact area between the probe and substrate, by performing adhesion tack tests on the softest PDMS sample (1%) using a 30 mm diameter probe with a plasma treated glass cover slip as the contact surface (mimicking the surface of the cantilever). The work of adhesion from the AFM tests was then calculated as the negative area under the force-displacement curve (i.e. the attractive

force multiplied by distance)and the contact area assumed based on the following formula,

$$\frac{A_i}{W_{ad,i}} = \frac{A_{AFM}}{W_{ad,AFM}} \quad [2.1]$$

where A_i and A_{AFM} are the contact area for the 30 mm indenter probe and AFM tip respectively, and $W_{ad,\,i}$ and $W_{ad,\,AFM}$ are the work of adhesion for the indenter probe and AFM nanoindentation curves respectively. However this yielded contact areas for the AFM that were similar to that calculated using the assumptions present in the Oliver & Pharr method and the Sirghi method respectively. As a result nanoindentation by AFM was repeated across all the samples in ethanol solution however with a 4 μm colloidal bead attached as shown in Fig. 2.5. Here the results followed a similar trend as observed with the previous AFM experiments, however for the 1% PDMS the modulus was much closer to that obtained by oscillatory rheology (1.8 kPa for colloidal AFM, compared to 13.2 kPa and 0.27 kPa for pyramidal tip AFM and oscillatory rheology, respectively).

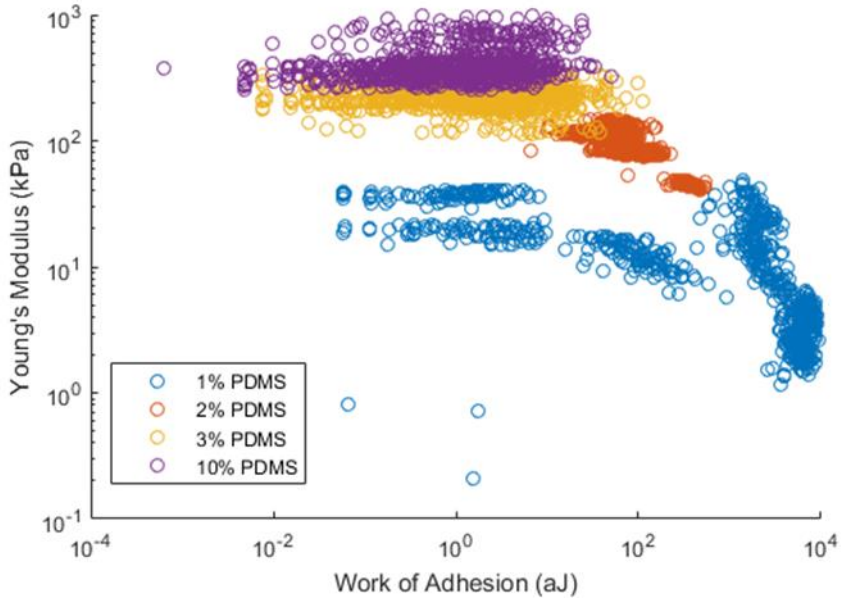

Figure 2.7. *AFM data showing the Young's modulus on PDMS samples with 1 – 10% cross-linker as a function of the work of adhesion. Three repeats on three samples per formulation giving 900 points per sample. Each individual sample is tested in three 5X5um locations with 100 indentation tests spread evenly across each location.*

The analysis of colloidal AFM indentation data was carried out using the Johnson[195] Force-Displacement relation, which best describes a colloidal indenter within the linear elastic region[92]. However due to the adhesion present for the 1 % PDMS the Sirghi method was adapted using the Johnson model with a colloidal indenter, rather than the Oliver Pharr, giving the following force displacement relation,

$$P = a(h - h_f)^{3/2} + b(h - h_f) \qquad [2.2]$$

where, P is force, h is displacement h_f is the point at which the lift curve crosses the x axis and b is a constant. The Young's modulus, E, is a function of the parameter a in equation 2, as follows:

$$a = \frac{4E\sqrt{R}}{3(1 - \upsilon^2)} \qquad [2.3]$$

where, R is the radius of the colloidal tip and υ is the Poisson's ratio. While the modulus obtained by this method does not exactly match that found by bulk testing methods it does offer a significant improvement. One reason for this is the significantly larger indenter geometry, a 4 μm diameter bead compared to an AFM tip with a nominal tip radius of 15 nm. Furthermore the change in shape of the probe is also likely to impact the results obtained and associated wetting and adhesion effects. Using high acuity probes (such a native Berkovich AFM tip) generates high shear and promotes plastic deformation, making them particularly suitable for elastoplastic deformation on materials such as ceramics, while for more viscous samples, such as soft PDMS, small acuity probes, such as spherical probes, are far better suited[92].

Hence our results do not suggest significant deviations between bulk and local mechanical properties of PDMS materials, especially at higher cross-linker ratios (5%

and 10%). We had previously reported that stem cell adhesion and fate decision was remarkably not affected by the mechanical properties of Sylgard PDMS substrates with an extremely wide range of mechanical properties (0.1 kPa to 2 MPa)[6]. This had raised the possibility that local and bulk mechanical properties of PDMS materials significantly differ, although no fundamental basis for such behaviour was proposed[181]. Hence, our results demonstrate that non-biofunctionalised PDMS materials display bulk and nanoscale mechanical properties that are in good agreement. Therefore, the lack of cell response to the bulk mechanical properties of PDMS must have an origin in other phenomena.

It was also previously proposed that the strain rates applied by cells were high enough to result in considerably stiffer perceived moduli, associated with the strong viscoelastic response observed for weakly cross-linked PDMS (1%, Fig. 2.2a)[181]. Cell sensing of their mechanical environment is proposed to be at velocities in the range of 20-200 nm/s [196] , limited by actin flow rates typically measured in the range of 100-200 nm/s[197]. In comparison, displacements achieved at the periphery of the rheology plate used (where viscoelastic effects should be maximised) are below 2 μm (displacement of the rheometry plate $1X10^{-4}$ rad which translates to 2 μm linear displacement at the edge), indicating that displacements exerted by cells should fall within a frequency range below that used in rheology measurements (< 0.1 Hz), a range for which the bulk moduli of PDMS materials still fall well below 1 kPa. Similarly, the indentation velocity used in our AFM measurements was 1 μm/s, a rate that remains significantly higher than those typically applied by cells and that correspond to shear moduli of 30 Pa. Therefore, the viscoelastic profile of weakly cross-linked PDMS materials does not account either for the observed cell spreading on these substrates. Instead, we recently proposed that additives contained in Sylgard 184 PDMS, or modifications

introduced during the tethering of extracellular matrix proteins to PDMS materials, are responsible for the increase in nanoscale mechanical properties, at the surface of these substrates, with which cells form adhesions. This behaviour explains, for example, our recent observation of high proliferation of adherent cells (HaCaT epidermal cell line) at the surface of low viscosity liquids, where bulk mechanical properties cannot account for cell adhesion and spreading[144]. In such cases, interfacial rheology measurements gave evidence for the formation of a stiff layer of proteins assembled at the interface between the cell culture medium and the oil used to support cell culture. Similar phenomena could occur at the surface of cross-linked Sylgard 184 PDMS substrates, after biofunctionalisation, therefore changing the nanoscale mechanical properties of the corresponding interfaces.

Mechanical properties of hydrophilic homogenous PAAm hydrogels

Given the importance of hydrogels for the study of cell adhesion and the development of degradable scaffolds for tissue engineering, multi-scale mechanical characterisation of hydrogels is essential to fully understand interactions between cells and these materials. For such applications, a full understanding of mechanical properties of hydrogels at multiple scales is essential, not only because of their importance to confer structural integrity to the corresponding materials, but also because local deformations and remodelling was shown to have an essential impact on cell phenotype[198, 199]. Poly(acrylamide) was used as a model substrate, given its importance for the study of mechanotransduction[6, 181, 200]. Previous characterisation of PAAm gels via microindentation had indicated that moduli ranged from 2 kPa to 231 kPa, depending on the level of cross-linking and the concentration of monomers used[6, 201-204]. However, in the case of PAAm too, a very broad range of moduli are reported for the softest hydrogels (between 1 and 5% cross-linker).

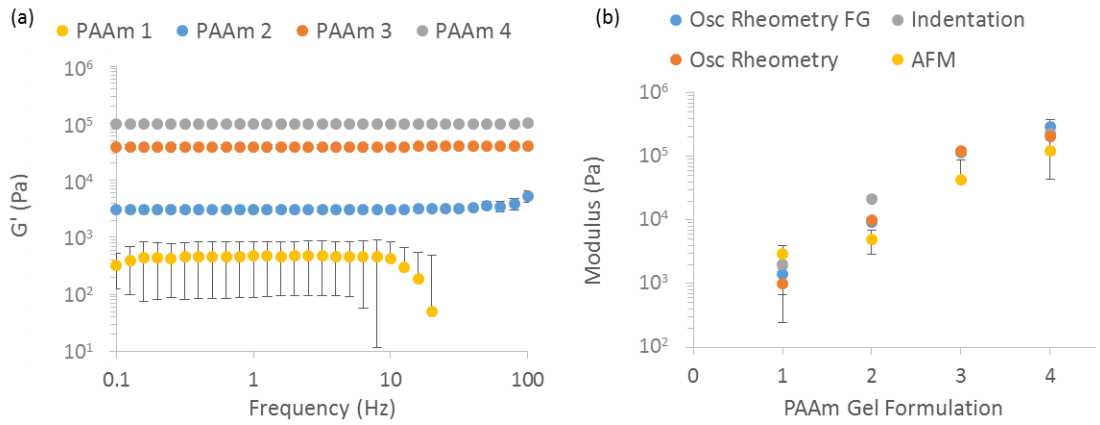

Figure 2.8 (a) Bulk mechanical characterisation of PAAm by oscillatory rheometry (frequency Sweeps) giving the shear moduli across a range of AAm and cross-linker concentrations (see Table 2.1 for details of compositions of PAAm 1-4, as indicated in the legend), frequencies tested were from 0.1 – 100 Hz at an oscillating displacement of 10^{-4} rad on a minimum of three repeats and (b) comparison of the Young's modulus of the softest PAAm sample measured moduli with and without functionalised geometry and between bulk (rheology and micro indentation) and local (nanoindentation by AFM) testing methods. Error bars showing the standard deviation.

We first investigated further the bulk mechanical properties of this full range of PAAm hydrogels (details of the compositions gathered in Table 1) via rheology (Fig. 2.8 and Fig. 2.9). Indentation data was in very good agreement with previous results reported, for the full range of compositions tested (Fig. 2.8b) [6]. In the case of rheology experiments, we generated PAAm hydrogels in situ between the two geometries of the rheometer.

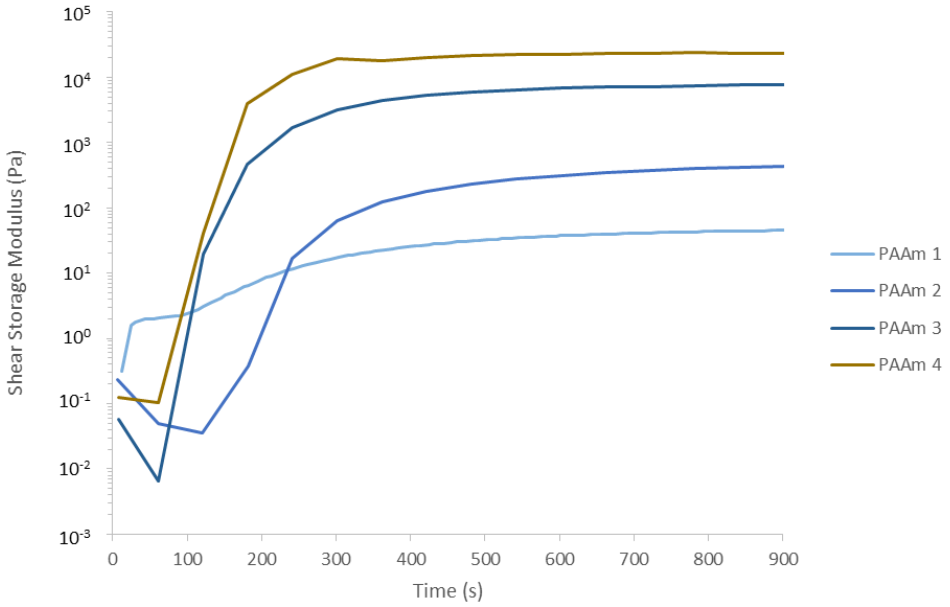

Figure 2.9. *Oscillatory rheology time sweeps monitoring the curing of PAAm gels with different compositions. The legend indicates which trace corresponds to gels 1-4 (see Table 2.1). Note that gelation of samples for analysis was allowed to continue without oscillation for 1.5 h time. Time sweeps were conducted at a frequency of 1Hz and with a displacement of 10^{-4} rad.*

Results of rheology measurements display the expected general trend of an increase in modulus with increasing cross-linking level and are in good agreement with the microindentation testing previously reported for stiffer samples (1.5 % cross-linker and 20 % AAm). The moduli of the PAAm samples also showed negligible frequency dependence, apart from the softest sample where there was a significant drop in modulus at frequencies above 10 Hz, this could be explained by the inertia of the testing geometry beginning to dominate the mechanics of the samples for soft PAAm. However at weaker cross-linking levels, the deviation between samples is significantly higher than for the stiffer samples when testing by rheology. Despite this larger spread the data is still in good agreement with the indentation previously measured (moduli of 1400 Pa, compared to 2000Pa measured before).

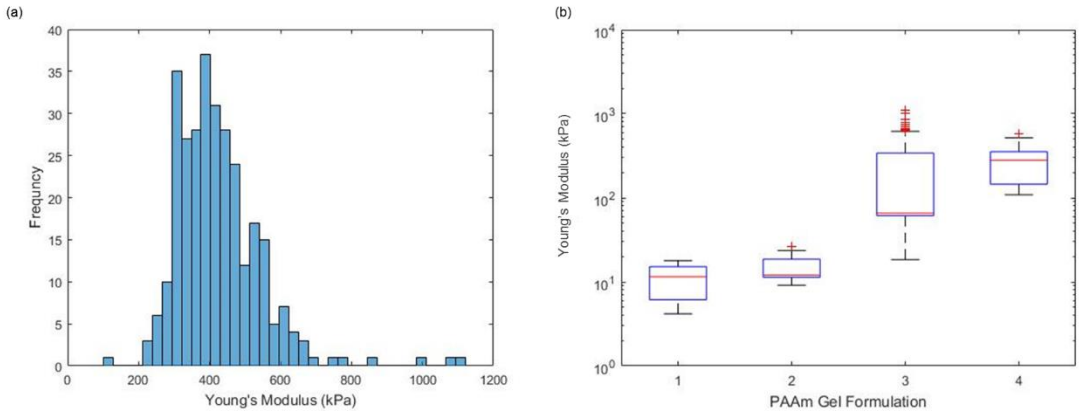

Figure 2.10 (a) Wet AFM data obtained on PAAm sample formulation 3 showing a histogram of the spread of moduli values for 3 repeats of 100 indentations on a 5x5 μm sampling area and (b) box and whisker plot showing the overall spread across the range of PAAm samples tested. All AFM experiments were conducted with an indentation depth of between 500 and 1000 nm and each curve was done over 1 s, 900 repeats per formulation were conducted with three samples per formulation.

We proposed that such discrepancy may originate from two main processes: 1. a lack of adhesion between the plate and the hydrogels generated, resulting in slippage, especially for weakly cross-linked and very hydrated gels; 2. differences in the polymerisation (and gelation) efficiency measured for gels formed in situ, compared to those formed for indentation and AFM measurements. The effect of adhesion between the rheometer geometries and the sample was investigated by intercalating two glass coverslips functionalised with methacrylate between the geometries and the samples being cross-linked. Rheological measurements carried out with such functionalised geometries displayed a modest increase in the shear moduli measured at low cross-linker ratio (from 990 Pa to 1400 Pa), indicating that slippage has an impact on shear moduli measured, but that it is not the dominating factor accounting for the discrepancies measured between indentation and rheology. The level of adhesion between the PAAm hydrogel formed and the testing geometries are however clearly enhanced, as was apparent when removing the samples as they clearly detached via cohesive failure, as shown in Fig. 2.11.

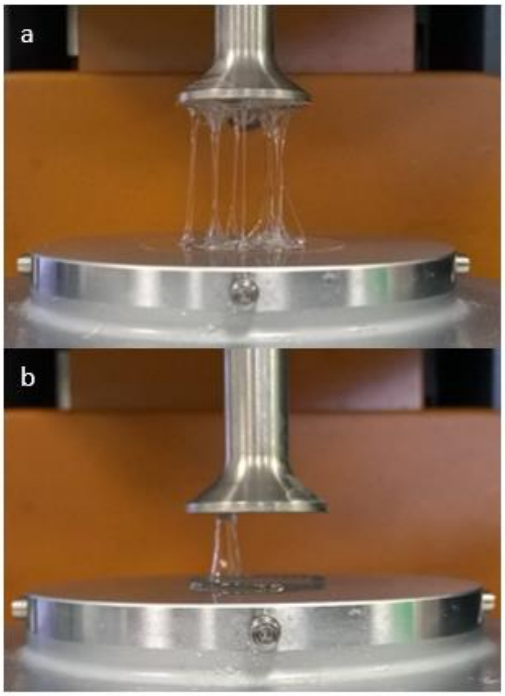

Figure 2.11. *Adhesion between PAAm samples (gel 1) to the rheometer geometry when coming out of contact with (a) and without (b) methacrylate-functionalised geometries.*

AFM indentation also confirmed the general trend observed between the cross-linker ratios used and the measured elastic modulus of the corresponding materials (Fig. 2.5b and 2.10). These measurements were in excellent agreement with macroscopic indentation, even in the low range of cross-linking investigated. For each samples tested, the spread of moduli measured was relatively low and gels were found to be relatively homogenous, although we observed a more pronounced variation between samples tested, reflected in the standard deviations. Hence the PAAm hydrogels tested were found to be relatively homogenous, in good agreement with previous results reported for PAAm and PEG methacrylate hydrogels[10]. Indeed heterogeneity and pore sizes for such gels were found to be at a lower scale than that of the cantilever tips used for our studies (nominal tip radius ~20 nm), based on analysis of stress relaxation profiles and the use of poroelasticity models of indentation[6, 10] (pores below 20 nm). Therefore heterogeneity is unlikely to be the origin of the discrepancies between rheology and indentation data. In addition, very little adhesion was observed in

AFM indentation traces at all PAAm moduli (Fig. 2.12).This is perhaps expected as PAAm is only very weakly adhesive and a neutral gel resulting in little sample-tip interaction. Hence discrepancies between rheology and indentation testing is most likely explained by the different methods of sample preparation where the quality of the gel network is heavily influenced by any contact with oxygen during gelation.

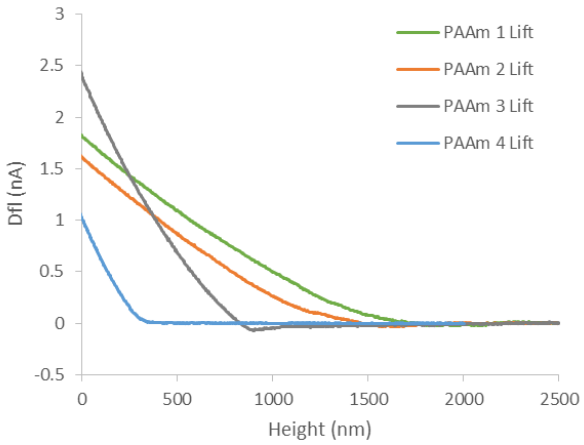

Figure 2.12 *Raw AFM retraction curves for the series of PAAm samples tested (see Table 1) with a 4 μm bead attached to the AFM tip. The indentation depth was between 300 and 1000 nm was and the curves were completed over 1s.*

Mechanical properties of cross-linked carboxymethyl cellulose hydrogels

In contrast to poly(acrylamide) hydrogels that do not show significant levels of heterogeneity and do not lead to significant adhesion with the surfaces of probing geometries, other charged hydrogels and composite structures are often associated with significant discrepancies between local and bulk moduli [10, 12]. We used a carboxymethyl cellulose (CMC) hydrogel as a case study, for comparison to PAAm hydrogels previously discussed. Since CMC is not covalently cross-linked, we introduced additional cross-links via allyl pendant chains that react with poly(ethylene) glycol dithiol cross-linkers via thiol-ene coupling [205]. This type of reactions was of particular interest because of its relevance for *in situ* cell encapsulation within 3D hydrogels [206], under mild conditions and its good tolerance of moderate oxygen concentrations [207,

[208]. Two allyl CMC hydrogel samples were tested, both at 100 mg/mL CMC concentrations, with and without the addition of 5 wt% silica beads (displaying a composite morphology with local heterogeneity). The two samples were characterised via oscillatory rheology and nanoindentation (Fig. 2.13 and Fig. 2.14).

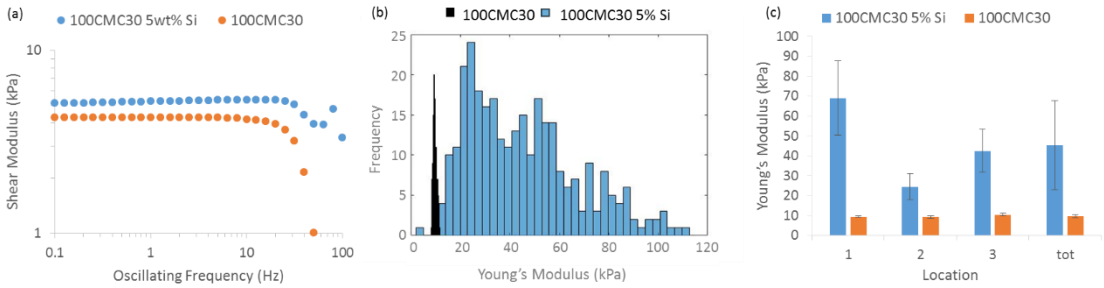

Figure 2.13 (a) Representative oscillatory frequency sweeps on 100CMC30 with and without Si beads, frequencies of oscillation were from 0.1 – 100 Hz at an oscillating displacement of 10^{-4} rad showing no frequency dependence (at the highest frequencies the inertia of the testing geometry dominates over the mechanics of the gel resulting in the decrease in measured modulus) and (b) Histogram comparing the moduli of 100 CMC30 with and without Si beads, the large spread of data with Si beads illustrating the impact heterogeneity has on local mechanical testing. All AFM experiments were conducted with an indentation depth of between 500 and 1000 nm and each curve was done over 1 s. (c) Summary of AFM tests performed on 100CMC30 with and without Si beads highlighting the difference resulting from heterogeneity on mechanical testing with a black line representing the moduli of CMC samples obtained by oscillatory rheology.

Oscillatory rheology displayed classical frequency independent elastic profiles (up to 30-40 Hz) for both CMC samples, with and without silica beads, with very similar bulk moduli (16.5 and 13.5 kPa, respectively). Above 40 Hz we see a significant drop in the shear storage modulus, this could be explained by the inertia of the testing geometry dominating the mechanics of the sample itself, as stated for the softest PAAm, however as these samples are significantly stiffer than the softest PAAm it is likely to be a combination of this with some shear thinning or perhaps the contact between the sample and testing geometry breaking down.

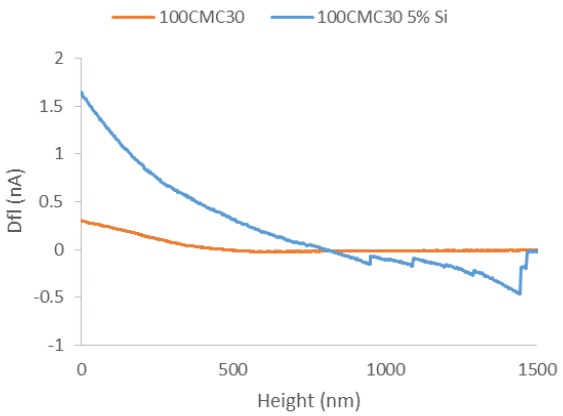

Figure 2.14 *Representative AFM lift curves for CMC gels with and without Si beads mixed into the sample. The indentation depth were kept between 500 and 1000 nm and each indentation was carried out over 1s.*

Despite the rheology data on the two CMC gels being in good agreement, when characterised by AFM indentation, they displayed significantly different behaviours as shown in Fig. 2.13. The CMC gel incorporating silica beads displayed a significantly higher modulus (45 kPa) compared to that of the same gel without any added beads (10 kPa). In addition, the spread in the modulus within one sample was significantly broader for the composite hydrogel, clearly indicating a high level of heterogeneity (Fig. 2.13). Therefore, rheology and AFM data are in excellent agreement for the CMC gel investigated, but display significant discrepancy for the composite hydrogel. This is thought to arise at low loading levels of fillers, for which a percolated network has not been achieved yet, hence resulting in a negligible impact on bulk mechanical properties whilst the local modulus of the sample at or close to silica beads will appear significantly higher than that of the surrounding soft material.

2.4 Conclusions

When comparing the mechanical characterisation data obtained across the three systems studied, we clearly observe very good agreement between bulk and local mechanical testing methods for the stiffest samples. However this agreement breaks down when testing soft materials (moduli of the order of kPa), in particular for the

soft PDMS samples. Our results clearly identify potential origins for the discrepancy between local and bulk mechanics. Wetting and adhesion cause fouling of the local testing geometry when performing nanoindentation. This results in an increase of the contact area and therefore a decrease of the true stress applied to the sample. We propose that this phenomenon explains the apparently stiffer modulus measured for 1% cross-linked Sylgard 184 PDMS when tested by AFM indentation. Despite reducing the amount of adhesion between the AFM tip and the PDMS sample by performing the tests in ethanol solution, adhesion between the geometry and the sample could not be totally eliminated. This phenomenon was not as prevalent in the case of hydrogels such as PAAm, owing to the hydrophilicity and neutral charge of these materials. It is therefore important to consider the tip sample interaction when deciding the best method for mechanical testing.

Heterogeneity was also found to have a significant effect on the mechanical properties obtained when using local testing methods. This phenomenon was highlighted within the allyl CMC loaded with silica nanoparticles, where local stiffening was observed by AFM. However the dimensions of phases required to have an effect on the measured modulus should be comparable to the probe size. This contrast with the impact of heterogeneity on viscoelastic and poroelastic profiles, which can be sensed by AFM indentation even in the case of features orders of magnitude smaller than the probe diameter[14].

In conclusion, the characterisation of soft materials at multiple scale can be influenced by a number of factors that should be examined in order to validate the methodology used for such comparisons. Adhesion and heterogeneity in particular, alongside potential differences between sample preparations, have been highlighted as possible causes of discrepancies between bulk and local mechanical testing. These

phenomena are, however, not universal and the characterisation of soft biomaterials should involve the analysis of the impact of such factors to validate the methodology selected.

2.5 Appendix

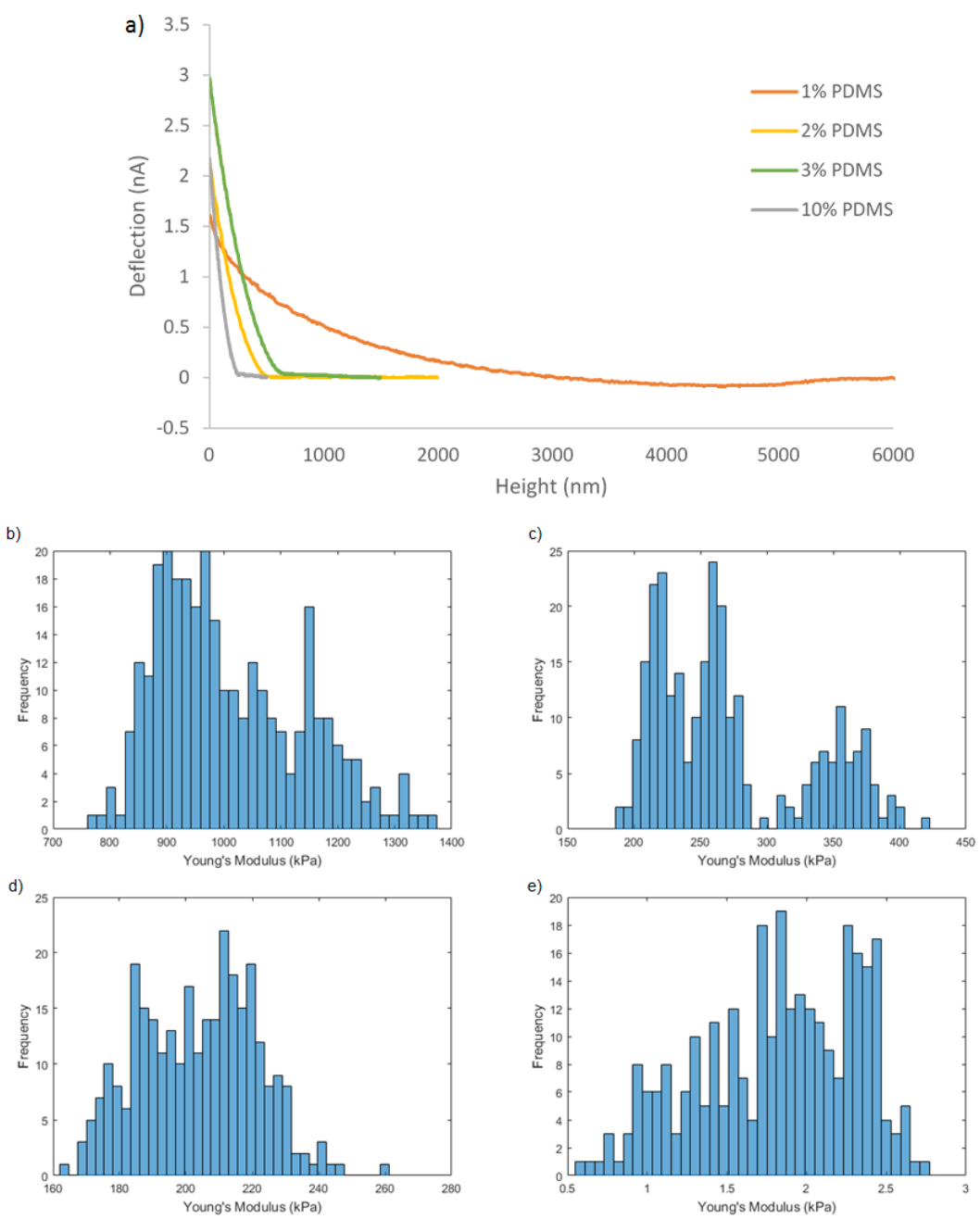

Figure A2.1. (a) Raw AFM retraction curves for PDMS at varying cross-linker concentrations tested in ethanol solution with a 4 μm bead attached to the AFM tip. The

indentation depth was around 500 nm and each curve was done over 1s. For the softest sample adhesion is still observed. (b), (c), (d) and (e) histograms of the Young's moduli obtained for the PDMS samples with 1%, 2%, 3% and 10% cross-linker respectively. Each sample is tested in three 5X5um locations with 100 indentation tests spread evenly across each location.

Chapter Three

Impact of non-covalent cross-linking chemistry on the rheological behaviour of CMC Hydrogels

3.1 Introduction

Carboxymethyl cellulose (CMC) is a polysaccharide synthesised from native cellulose by replacing OH groups on the cellulose ester with CH_2COONa as shown in figure 3.1. As cellulose is an abundantly found naturally occurring material it is a very appealing material due to the drive for environmentally friendly, biocompatible polymers[105, 125, 129]. CMC is currently used for numerous applications such as thickeners, binding agents, film formers, lubricants and stabilisers, particularly for food, pharmaceutical and beauty products[105, 125, 129]. CMC can be utilised in gels with either physical or chemical cross-links and has similar properties to other polysaccharides such as gellan, alginate and xanthan[4, 125, 209].

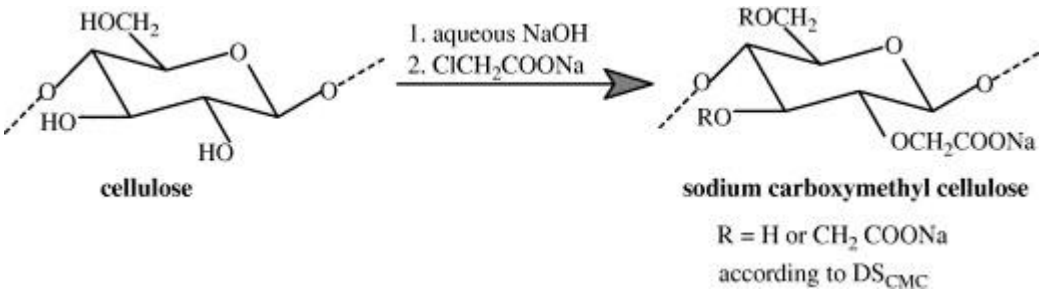

Figure 3.1 Chemical reaction to generate CMC from cellulose where R = H or CH_2COONa and the degree of separation is determined by the number of R groups that are replaced by CH_2COONa per repeat unit[210].

CMC gels are also used extensively as denture adhesives[83, 211, 212]. For this application it is necessary that they have suitable mechanical properties, both in terms of the bulk mechanics and also adhesive strength. In practice dentures must withstand

complex loading as during mastication they will be loaded cyclically in both shear and normal directions. However dentures are also removable so the adhesive should not cause discomfort to the customer when being removed. Clearly there is something of a balancing act here to make gels that have the requisite mechanical and adhesive strength but are also temporary and easy to remove and clean away. Furthermore there is the issue of comfort for the user, which is a by-product of the mechanics, micro-structure and composition of the gels[213-215].

The solution properties (hydrodynamic diameter, viscosity) of CMC, its chemistry and the structure and mechanics of CMC-based gels have been well characterised [105, 125, 128, 216, 217]. It has also been shown that the use of ionic cross-linkers can strengthen the polymer network of CMC solutions increasing the viscosity[125]. Similarly it has been shown that other similar polysaccharides can be strengthened with the addition of cationic binders forming gels with ionic cross-links, for example alginate has been shown to have tuneable properties with the addition of ionic binders[4, 131], as have xanthan[218] and gellan[219]. It is thought that the addition of cationic binders to CMC gels has a similar effect and allow for careful tuning of the mechanics of CMC gels for use as denture adhesives. As CMC polymer chains have negatively charged hydroxyl and carboxylate groups it is thought the addition of cationic binders may form cross-links between chains in an 'egg box' model as shown in figure 3.2. Although this is well accepted for alginate-based gels, cationic cross-linking of CMC gels seems less efficient, presumably as the distribution of carboxylate moieties is randomly distributed along the polymer backbone, unlike the chemical structure of alginate[2, 130, 220].

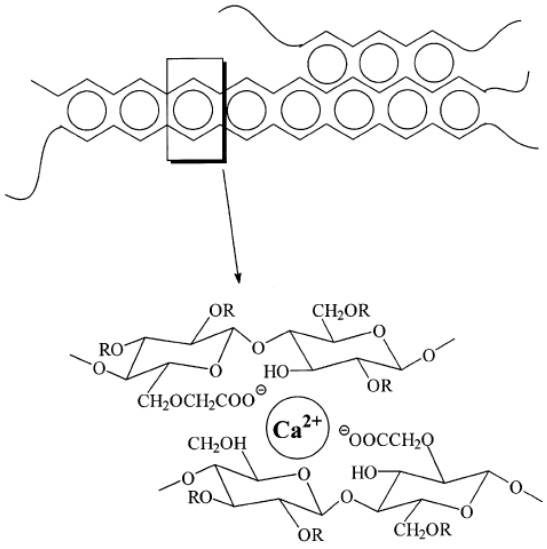

Figure 3.2 Schematic showing the association of divalent calcium ions with the negatively charged carboxylate and hydroxyl groups of a CMC chain according to the egg box model[125].

Carboxylated polysaccharides cross-linked by multivalent cations typically lead to rigid local cross-links, with some level of heterogeneity, at the molecular scale[132, 221]. However systems relying on soft cross-links, as in coacervates, have also been proposed. For example Hawker et al. have shown that by combining PEG based bloc copolymers with oppositely charged end caps it is possible to obtain a coacervate system with clusters of entangled polymer chains within a larger loosely cross-linked system, as shown in figure 3.3[11].

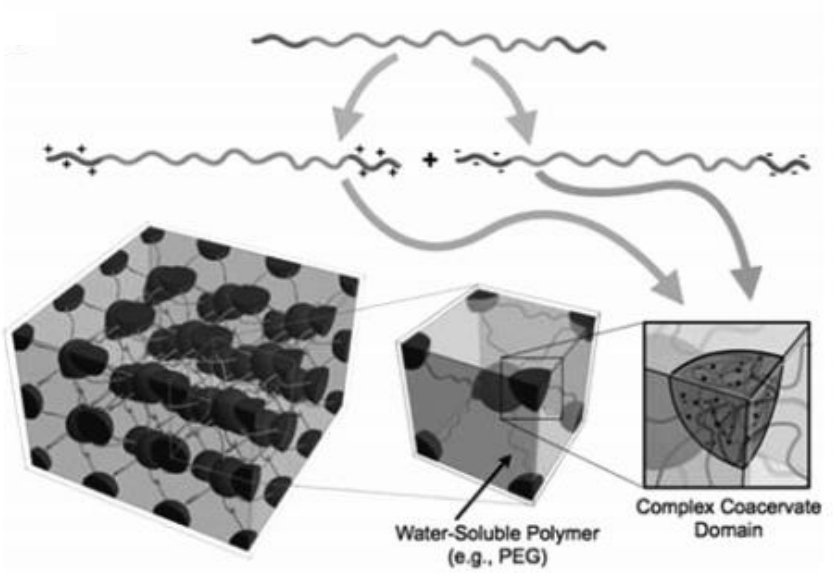

Figure 3.3 Schematic showing the formation of a coacervate hydrogel resulting from the combination of two block copolymer solutions with oppositely charged end caps. The coacervate domains then act as physical cross-links within the hydrogel system[138].

CMC is made of a rigid glucose repeat units and as a derivative of cellulose has inherited many of its structural characteristics. CMC has an extended conformation coming from the structural rigidity of the C-O-C bonds. The large OCH_2COO^- side groups prevents CMC from forming parallel associations, like those in native cellulose, due to steric hindrance and electrostatic repulsion. However, intramolecular and intermolecular hydrogen bonding is still possible between OH groups[222]. The degree of substitution of CMC is defined as the number of CH_2COOH groups attached to the hydroxyl groups on each repeat unit, hence a theoretical maximum of three, although in practice it seldom exceeds two[125, 222]. The CH_2COO^- are accepted to be randomly distributed across the CMC backbone[126, 222, 223]. The structure of CMC makes it a very interesting biomaterial for a plethora applications.

The numerous carboxyl groups on CMCs backbone make it a negatively charged polyelectrolyte which can form hydrogel complexes in the presence of positively charged polyelectrolytes[105, 222, 224, 225]. It has been reported that CMC forms ho-

mogenous polyelectrolyte polymer complex membranes when combined with chitosan in the presence of a cationic solution[225]. When being used as films CMC has been shown to ionically cross-link with polyvinylamine maintaining film integrity in the presence of water, however does not improve the dry modulus of the films[226]. In these films the CMC chains cross-link primarily through hydrogen bonding while the electrolyte solution promotes CMC to complex[225].

The polyelectrolyte structure of CMC has been utilised to form interpenetrating gels when mixed with chitosan, another polyelectrolyte polysaccharide, as shown in figure 3.4. These gels have been weakened in the presence of ionic salt solutions as the salts interfere with the ionic bonding between chains weakening the overall gel network[224]. It is evident that CMC can be utilised for many applications and can be tuned for specific purposes with careful design.

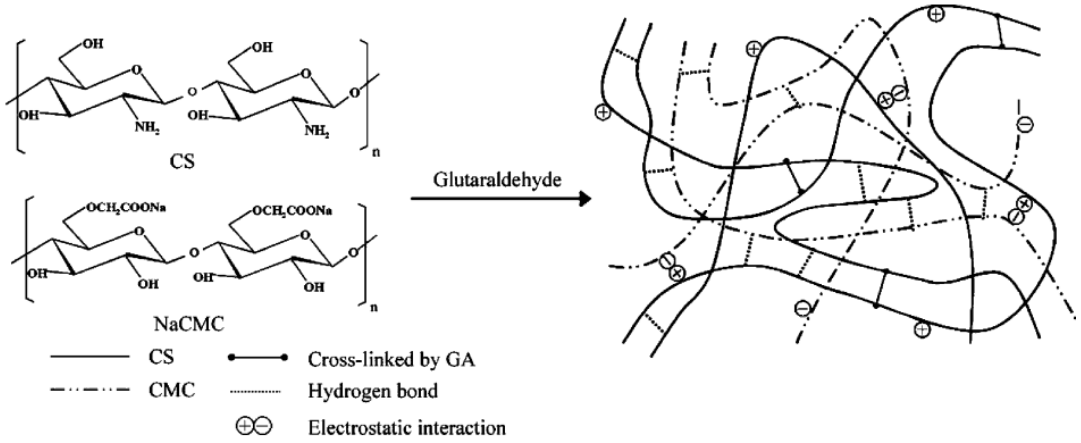

Figure 3.4 Schematic showing the formation of Chitosan/CMC interpenetrating network hydrogels[224].

Polysaccharide complexes occur typically as a result of electrostatic interactions between oppositely charged macromolecules. Soluble complexes can continue to aggregate until insoluble in order to reduce the free energy of the system. A coacervate then forms as a result of a liquid-liquid phase separation giving discrete liquid

coacervate droplets coexisting within a more dilute phase. The end product is a two phase system consisting of a coacervate phase within a solvent rich sub-phase[132-137].

The phenomenon of coacervation can be split into two types; complex coacervation and simple coacervation. A simple coacervate consists of a single macromolecule where polymer-polymer interactions are promoted over polymer-solvent interactions, by something like a dehydrating agent. A complex coacervate results from oppositely charged macromolecules complexing[135, 136]. Coacervation is an entropy driven occurrence allowed by low translational entropy of the polyelectrolyte, gain in entropy from the release of counter-ions and the restructuring of water molecules around the charged electrolyte during the complexation of the macromolecules[136, 137]. The formation of coacervates is strongly affected by the salt concentration of the solution as increasing the salt concentration reduces the Debye length, or the distance two opposite charges will interact over, hence reducing the interactions between electrolyte blocks within the coacervate[136-138]. The reduction in interaction strength allows the polyelectrolyte blocks to remain suspended in the non-coacervate phase. Furthermore the increase in ionic strength of the solution reduces the entropic gain of releasing counter –ions into the solution, which results in higher water content within the coacervate, a decrease in the interfacial energy and hence a reduction in the amount of coacervate phase formed[136, 137].

One of the main design considerations when making coacervates is how to promote polyelectrolyte phases to form dynamic coacervates rather than solid static precipitates[227, 228]. If the polyelectrolyte solutions are too strong it restricts the polymer chain movement resulting in precipitation. Increasing the salt concentration in the solvent can reduce the electrolyte strength promoting coacervation[136].

Similarly, it has been shown that the addition of ionic cross-links to charged hydrogels can result in chain collapse and/or the formation of micelles which reduce the interactions between polymer chains within the gel system. In this study, we explore how altering the chemical structure of cationic cross-linkers alters the mechanical performance of CMC hydrogels. The use of inorganic divalent cations, as well as multivalent organic cations and block copolymers with charged endcaps will be examined. The aim here is to correlate molecular structure and changes in shear modulus and adhesive strength of the CMC gels, as shown in figure 3.5.

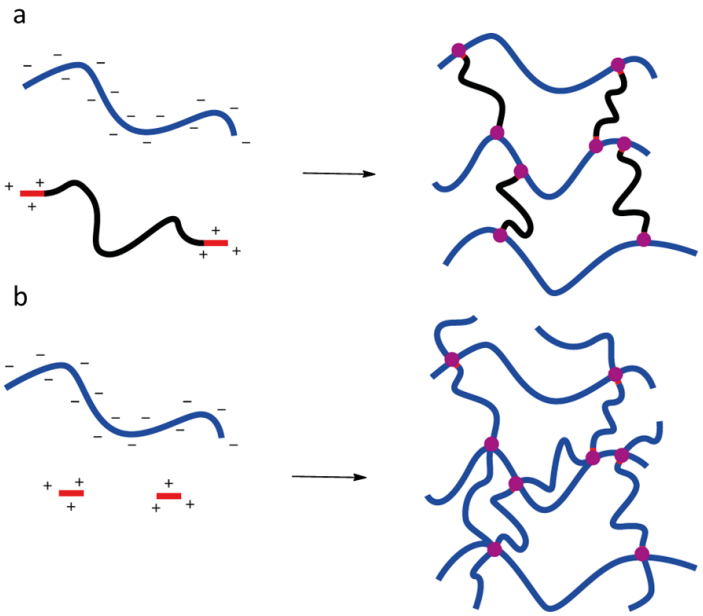

Figure 3.5 Schematic showing the cross-linking of CMC in the presence of a) block copolymer with cationic charged end caps and b) cationic inorganic salt solution.

3.2 Methods and Materials

Materials

Calcium Chloride, Strontium Chloride, Diethyl Triamine (DETA), Pentaethylenehexamine (PEHA), PEG-di-p-tosylate (average Mn 3,500), 2-ethyl-2-oxazoline and Hydrochloric Acid (HCl) were all purchased from Sigma Aldrich. Sodium Carboxymethyl Cellulose (CMC) (250,000 Mw) was purchased from Ashland Chemicals. The

end capped PEG – Polyoxazoline block copolymer was synthesised by Dr Pei Tang as outlined in the sample preparation. Sample Preparation

Sodium CMC was mixed in the ratios shown in table 3.1, 3.2 and 3.3 with deionised water and the desired salt solution. The CMC and the salt solutions were prepared separately and once both were completely homogenous, they were mixed together. If the salts were added as a powder to the dissolved CMC, they resulted[221] in localised precipitation and a relatively heterogeneous mixture, so ensuring the CMC and salt solutions were completely homogenous prior to combining the two proved essential. In the cases where HCL was used these were prepared with the salt solutions before being added to the CMC solutions.

Initial tests were carried out on PEG – CMC samples with varying amounts of salt. In these initial tests the wt% of CMC and PEG were 3% and 1.5% respectively and were characterised by oscillatory rheology. As these samples were still very fluid later experiments were done on 12.5 wt% CMC gels allowing for adhesion testing to be performed.

Once the CMC and salt solutions had been mixed and appeared homogenous they were centrifuged at 4000 rpm for 2 min to remove bubbles. If the bubbles were not removed after the first centrifuging this was repeated until a clear homogenous sample was obtained.

Where PEG and CMC were used together the solid PEG and CMC were mixed before being dissolved in deionised water and then mixed with the appropriate salt solution. The PEG and CMC powders were mixed in this way as the PEG and CMC solutions, both relatively viscous, were relatively difficult to mix otherwise. Hence, in

order to achieve homogenous samples, it was decided to mix these materials dry prior to their hydration.

Samples prepared for light scattering measurements were significantly more dilute, however were mixed according to the same protocol as for the preparation of hydrogels, for improve comparison of results. The hydrodynamic diameters of materials were characterised at the same ratio of CMC to cross-linker as for hydrogels (see tables 3.2 and 3.3), however the concentration of CMC was only 0.05 wt%.

The polyoxazoline end capped PEG block copolymers were synthesised by Dr Pei Tang for these experiments. Two variations of the block copolymers were produced, one with 10 PEtOx repeat units on each end and one with 35 PEtOx repeat units, referred to as bloc 10 and bloc 35 respectively. The PEtOx-PEG-PEtOx (10:1:10) was produced with the following procedure, 0.205 g PEG-di-p-tosylate (0.07mmol), 0.142 g 2-ethyl-2-oxazoline (1.42 mmol) and 2 mL anhydrous acetonitrile were added to a pre-dried microwave vial. The vessels were then and placed in a microwave synthesizer. The reaction solution was then heated to 160 °C over 30s and held for 10 min at this temperature. The vessels were then cooled to room temperature under gas flow. The reaction solution was next heated to 80 °C for 12 h. After the acetonitrile was evaporated the polymer was dissolved in chloroform. The solution was washed three time in an aqueous saturated sodium bicarbonate solution three times followed by being washed three times in brine. Finally the solution was dried with potassium sulfate and filtered before evaporating any leftover solvent under vacuum. The PEtOx-PEG-PEtOx (35:1:35) was synthesised using the same protocol, however 0.497 g of 2-ethyl-2-oxazoline was used.

The PEtOx-PEG-PEtOx block co polymers were then hydrolysed by dissolving 0.1 mmol in 12 mL 0.5 M HCl in a one neck flask under reflux and kept at 120 °C overnight degassed in nitrogen. Finally the acid solution was removed under reduced pressure.

Oscillatory Rheology

Oscillatory rheology was performed using a Discovery Hybrid Rheometer 3 (DHR3) from TA Instruments. The tests were performed using a steel 20 mm parallel plate top geometry and a steel Peltier plate as the bottom geometry. Samples were tested using the following protocol, first, a frequency sweep was conducted with an oscillating displacement of 10^{-4} rad from 0.1 – 100 Hz. This was followed by an amplitude sweep at an oscillating frequency of 1 Hz from 10^{-5} to 10^{-3} rad. All tests were performed at room temperature and a 30 s dwell time was allowed between tests. A minimum of three repeats on each sample was carried out.

Lap Shear Testing

Lap shear testing was performed using an Instron 5943 Universal Testing System with a 500 N load cell. The following protocol was used to test the samples: 2 g of material was placed at one end of a PMMA slide. The gel was then covered by an overlapping slide, with an overlapping area of 25 by 25 mm. The sample is then compressed between the two slides with a force of 90 N force for 5 s. The load is then removed and the sample is left to relax for 5 min before being loaded with 90 N force again for 5 s. The sample is then mounted and the test started as quickly as possible. The sample is deformed at a rate of 50 mm/min until failure. A minimum of 5 repeats per sample were performed.

Zetasizing

Light scattering measurements of hydrodynamic diameters were carried out using a Malvern Instruments Nano-ZS Zetasizer. 1 mL of sample was added to a 2.5 mL VWR Cuvette and measurements were carried out using the following protocol: first, a 1 min dwell time was allowed once the sample was loaded. Next scans were repeated 3 times per sample with 13 scans per repeat with a wavelength of 632.8 nm and a back scattering angle of 173 °. A minimum of three samples were tested for each set of conditions. Data analysis was performed by the equipment software and the hydrodynamic particle size determined using the Stokes-Einstein equation[229],

$$D_H = \frac{kT}{f} = \frac{kT}{3\pi\eta D}$$

Where k is the Boltzmann constant, f is the particle frictional coefficient, η is the solvent viscosity, T is the absolute temperature, and D is the translational diffusion coefficient. The nanoparticles were assumed to be spherical, monodisperse, non-interacting.

3.3 Results and Discussion

3.3.1. Impact of Inorganic Cross-linkers on PEG-CMC Gels

We initially set out to examine the impact of combining inorganic divalent cations with PEG-CMC gels. It was thought that this would result in the formation of ionic cross-linking and hence strengthen the gel network. The gels mechanics were characterised by oscillatory rheology to investigate the impact cations had. PEG-CMC was chosen initially as they are commonly used together in commercial denture adhesives. The composition of the PEG-CMC gels used are shown in table 3.1. Figure 3.6 collects the results obtained in these experiments.

Table 3.1 PEG-CMC and ionic salt ratios for initial experiments

Sample Name	CMC Concentration /wt%	PEG Concentration /wt%	Ionic Salt	Molar Ratio (CMC:Salt)
NaCl-5000	3	1.5	NaCl	5000:1
NaCl-500	3	1.5	NaCl	500:1
NaCl-50	3	1.5	NaCl	50:1
NaCl-5	3	1.5	NaCl	5:1
$CaCl_2$-5000	3	1.5	$CaCl_2$	5000:1
$CaCl_2$-500	3	1.5	$CaCl_2$	500:1
$CaCl_2$-50	3	1.5	$CaCl_2$	50:1
$CaCl_2$-5	3	1.5	$CaCl_2$	5:1
$SrCl_2$-5000	3	1.5	$SrCl_2$	5000:1
$SrCl_2$-500	3	1.5	$SrCl_2$	500:1
$SrCl_2$-50	3	1.5	$SrCl_2$	50:1
$SrCl_2$-5	3	1.5	$SrCl_2$	5:1
HCL-10000	3	1.5	HCL	10000:1
HCL-1000	3	1.5	HCL	1000:1
HCL-100	3	1.5	HCL	100:1
HCL-10	3	1.5	HCL	10:1
HCL-1	3	1.5	HCL	1:1

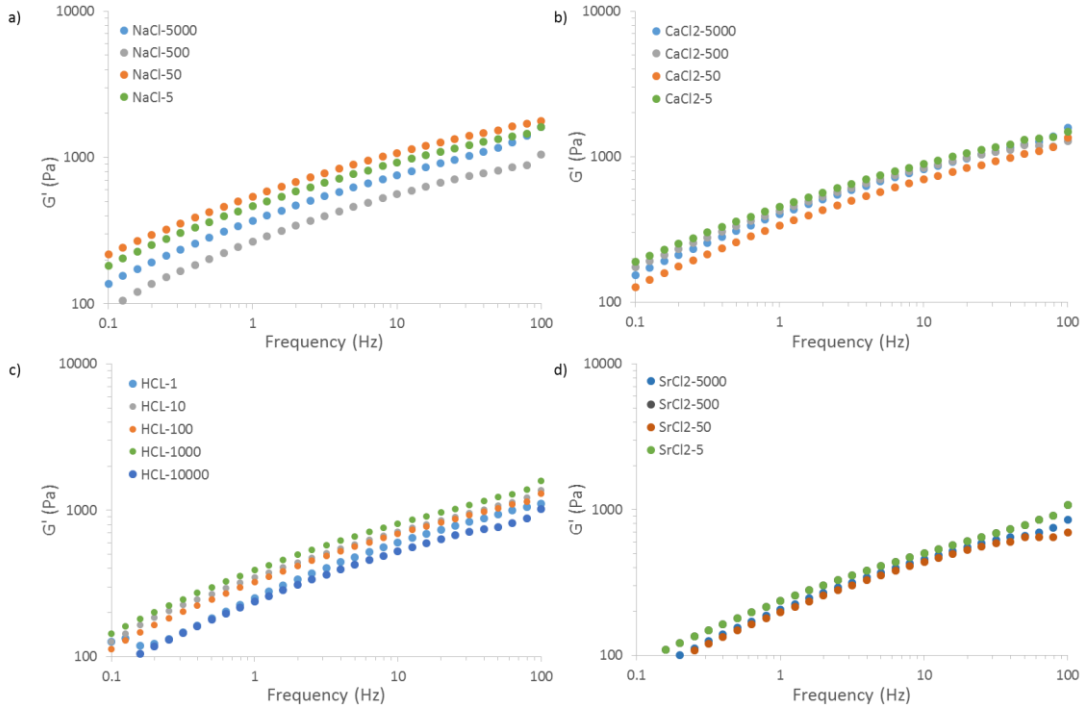

Figure 3.6 Representative Frequency Sweeps carried out via oscillatory rheology on PEG-CMC gels with 3 wt% CMC and 1.5 wt% PEG and varying (a) NaCl, (b) CaCl2, (c) HCL and (d) SrCl2, at concentrations as shown in table 1. Frequency sweeps were carried out at room temperature with an oscillating displacement of 10^{-4} rad from 0.1 – 100 Hz.

From figure 3.6 we can see that all the PEG-CMC gels, with and without inorganic cross-linkers, behave similarly with moduli strongly frequency dependent. This is expected from physical gels with large water contents, leading to viscoelastic and poro-viscoelastic mechanical properties[209, 230, 231]. The observation of frequency dependent moduli is common to physical gels as the gel stability comes from the physical entanglement of polymer chains which when strained at high frequency will lock together giving a stronger network, while when strained at lower frequency the chains will have more time slide past one another and hence behave as a weaker network. This has been shown to be the case for CMC gels[209] and chitosan/poly(vinyl alcohol) gels[230].

However, from these initial experiments it is clear that the shear modulus of the corresponding PEG-CMC gels is not sensitive to the concentration of the inorganic cross-linkers selected. While this was expected with the addition of NaCl[218] as this is a monovalent ion and so would only be able to interact with a single chain at a time it was expected that the divalent cations would have had a strengthening effect as in the case of alginate[2, 130, 220, 232] and gellan[219, 233]. This implies that the ionic interactions between the negative pendant charges on the CMC backbone and the divalent salts are not resulting in efficient cross-linking between chains. Alternatively, it may also be proposed that local sample cross-linking results in some heterogeneity, and the formation of isolated "hard" hydrogel pockets that do not contribute to strengthening of the mechanical properties of the corresponding hydrogels. The dual PEG network may also be influencing the efficacy of the ionic cross-linking by chelating and hence competing with cationic binding[234]. The chelation may also give rise to localised complexes forming contributing to sample heterogeneity. CMC with a high degree of substitution (< 1.2) has also been shown to aggregate in dual polymer networks as a result

of hydrogen bonding, hence the cationic electrolyte solution may be contributing to the formation of complexes rather than forming cross-links[226].

The impact of PEG on CMC gel mechanics was also characterised, with the mechanics of native PEG gels also investigated, as shown in figure 3.7. Native PEG gels with wt% from 0.13% to 6.25% were studied and PEG – CMC gels across the same range of PEG concentrations combined with 12.5 wt% CMC to see what impact the PEG was having on the CMC gel network. The influence of Pluronic on the mechanics of CMC gels was also investigated to compare with the results for PEG.

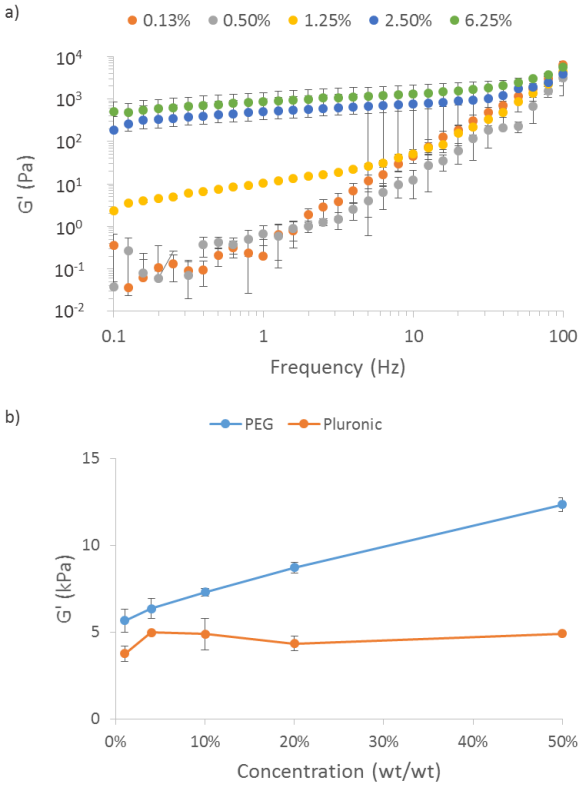

Figure 3.7 a) Frequency sweeps on PEG gels with weight concentrations from 0.13% to 6.25% and b) comparison of the impact of PEG and Pluronic on the shear moduli of CMC gels, measured by oscillatory rheology, with wt/wt concentration of PEG/Pluronic ranging from 1% - 50% compared to the wt concentration of CMC. The concentration of CMC was kept at 12.5 wt%. All error bars are standard deviations.

From figure 3.7a it can be seen that as the concentration of PEG increases the moduli of the gel increases. The frequency sweeps also show a strong frequency dependence of PEG gels particularly at low PEG concentrations. From figure 3.7b we

can see that the addition of PEG to CMC gels increases the moduli of the gel, however this is not seen in the case of Pluronic. This suggests that the PEG is forming an interpenetrating network with the CMC resulting in an increased modulus while the Pluronic is more acting as a surfactant. The formation of an interpenetrating network between PEG and CMC may increase the likelihood of competition between the PEG and CMC when cationic salts are added as cross-linkers[234].

3.3.2. Impact of Inorganic Cross-linkers on Hydrodynamic Diameter of CMC Gels

To gain further insight on the impact of inorganic cations on the molecular structure of CMC hydrogels, we next examined the effect of these analytes on changes in hydrodynamic diameter of dilute CMC solutions (therefore focusing on individual polymer chains). It was thought that the addition of inorganic cationic crosslinkers would result in cross chain crosslinking, however, as will be shown it in fact seemed to result in a coacervate like structure with the chains crosslinking with themselves and collapsing, as shown in figure 3.8. We first examined the evolution of hydrodynamic diameter and viscosity as a function of CMC concentration (Figure 3.9). Varying the concentration of CMC solutions from 0.001 to 0.1 wt%, it was observed that the hydrodynamic diameters measured initially increased steadily (below 0.01 wt%), before reaching a plateau[235] at higher concentrations. In parallel, the viscosity of solutions increased monotonically as the polymer concentration increased, even after the hydrodynamic diameter plateau was reached. As the pH of these solutions was kept constant, this indicates that CMC chains gradually assemble into small aggregates, reaching stable sizes above 0.01 wt%. However, it should be noted that the light scattering set up used, and the 632.8 nm wavelength of the light source, are not as adapted

for particles/polymers with hydrodynamic diameters above 500 nm, as secondary scattering events are potentially occurring and are ignored by the data processing protocol[235, 236].

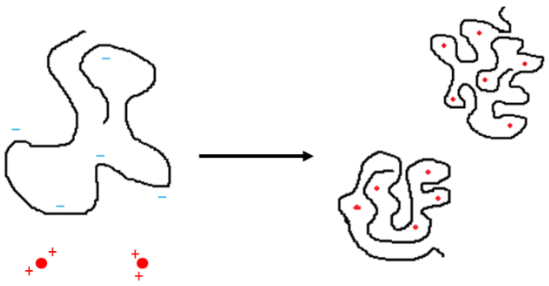

Figure 3.8 Schematic showing the result of the addition of inorganic divalent cationic crosslinks on CMC gels.

Varying the concentration of two inorganic cations, $CaCl_2$ and $SrCl_2$, had a strong impact on the conformation of polymer chains in dilute solutions. Hence hydrodynamic diameters decreased rapidly as the concentration of these two cations increased. This occurred faster in the case of Ca^{2+}. Such trend implies that CMC chains (and aggregates) are complexed by divalent cations and partially collapse, as a result of intramolecular cross-linking. It could also be argued that divalent cations dissociate aggregates seen at higher concentrations, perhaps as they compete with carboxylic moieties and associated hydrogen bonding. It has been shown that polyelectrolytes in the presence of oppositely charged nanocolloids form micelles, where polyelectrolyte chain collapses due to ionic interactions with the oppositely charged nanocolloids[237]. Similarly increased ionic strength has also been shown to result in a decrease in the hydrodynamic diameter of sodium hyaluronate[238] a worm like charged polysaccharide. Hence our results confirm the strong impact of divalent inorganic cations on CMC chain conformation and molecular bonding. This implies that the lack of change

in rheological profiles observed in PEG-CMC hydrogels results from the lack of mechanical coupling between densely cross-linked and collapsed nodes, rather than the absence of interactions between divalent cations and CMC molecules.

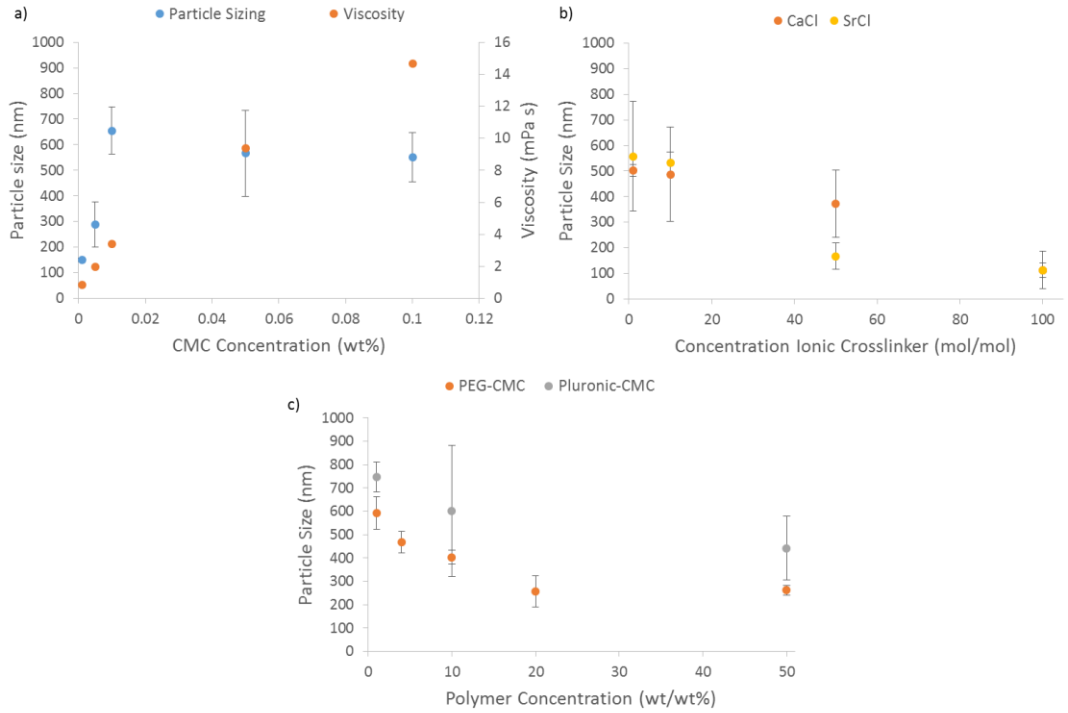

Figure 3.9 a) Particle sizing and viscosity measurements of CMC solution from 0.001 – 0.1 wt% CMC, b) particle sizing of 0.05 wt% CMC gels with 1% to 100% mol/mol inorganic cationic cross-linkers relative to the molar concentration of CMC and c) particle sizing of 0.05 wt% CMC gels with 1 to 50 wt/wt% PEG or Pluronic relative to the weight concentration of CMC. All error bars are standard deviations.

The influence of PEG and Pluronic on the particle sizes of PEG-CMC gels was also investigated. Here the results show that increasing the PEG concentration causes a decrease in the particle size, from 590 nm at 1% PEG to 260nm at 20%, plateauing at PEG concentrations above 20 wt/wt%. This shows that the PEG chains are interacting with the CMC network forming aggregates, similar to what is seen with polysaccharide/protein coacervates. The interpenetrating network formed by the PEG does however interact across aggregates as shown by the increase in the moduli of PEG-CMC gels with increasing PEG. The Pluronic shows a less significant trend which

corresponds well with the rheological data where the Pluronic has negligible effect on the mechanics of the Pluronic-CMC gels.

As a result of this data, it was decided that the experiments would be repeated in the absence of PEG and at higher CMC concentrations (more relevant for denture adhesive applications and in an effort to increase chain density and cross-linking). In addition, as gels were stiffer, they also proved adapted for adhesive testing by lap shear assay, as the gel would not significantly flow under the weight of the slides alone.

3.3.3. Impact of Inorganic Cationic Cross-linkers on CMC Gels

The CMC concentration and molar ratios of inorganic cations used are shown in table 3.2. Results from the oscillatory rheometry, lap shear testing for these conditions are shown in figure 3.11a-c.

Table 3.2 CMC gel and ionic salt concentrations tested

Sample Name	CMC Concentration /wt%	Ionic Salt	Molar Ratio (CMC:Salt)
$CaCl_2$-20	12.5	$CaCl_2$	20:1
$CaCl_2$-5	12.5	$CaCl_2$	5:1
CaCl2-2	12.5	$CaCl_2$	2:1
$CaCl_2$-1	12.5	$CaCl_2$	1:1
$SrCl_2$-20	12.5	$SrCl_2$	20:1
$SrCl_2$-5	12.5	$SrCl_2$	5:1
SrCl2-2	12.5	$SrCl_2$	2:1
$SrCl_2$-1	12.5	$SrCl_2$	1:1

We found that, at the highest concentrations of ionic salt added, we began to see slight precipitation, as shown in figure 310. This was assumed to be the result of the CMC chains collapsing in the presence of the inorganic divalent cations, resulting

in the formation of denser complexes and increasing the heterogeneity of the corresponding hydrogels.

Figure 3.10 Image of CMC gels with a low (20:1 CMC: CaCl2) salt concentration added on the left and a high (1:1) salt concentration on the right. It is clear that at high salt concentration the CMC begins to precipitate out and becomes heterogeneous, hence the cloudy appearance of the gel.

Precipitation at high salt concentration is also observable in the lap shear profiles, particularly for the CMC-$CaCl_2$ samples, for which we observed an initial increase in the adhesive shear strength as the salt concentration increased, before a drop at the highest concentration as shown in figure 3.11b.

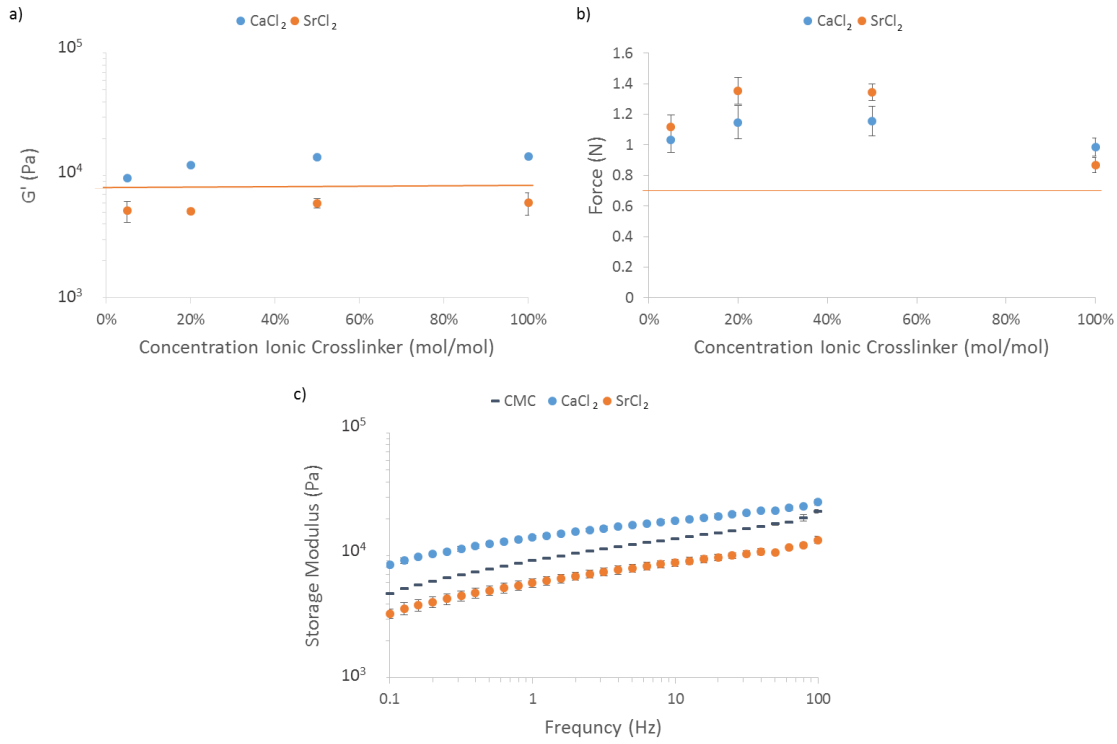

Figure 3.11 Characterisation of CMC gels with varying concentration of inorganic divalent cations by a) and c) oscillatory rheology showing a summary of the moduli at the different salt concentrations at 1Hz (the orange line showing the modulus of native CMC) and representative frequency sweeps at a salt concentration of 20% respectively, b) summary of the lap shear data showing the peak adhesive force for CMC gels as a function of cation molar concentrations (with respect to the carboxylic acid moiety molar concentration); orange line showing the average peak of native CMC gel), and A minimum of three samples per experiment were tested. All error bars are standard deviations.

Figure 3.11 gathers results from the oscillatory rheology and lap shear testing carried out on CMC gels in the presence of divalent cations Ca^{2+} and Sr^{2+}, as shown in table 3.2. From the frequency sweeps, in oscillatory rheology, it is clear that the shear moduli of CMC gels with and without ionic salts have a strong frequency dependence, this is again expected due to the microstructure of the CMC gels, being physical gels with high water content, leading to strong viscoelastic or poro-viscoelastic properties[14, 121]. Furthermore, the increase in moduli with increasing ionic salt concentration seen with the addition of $CaCl_2$ implies that ionic bonds between CMC chains are being formed which are strengthening the gel network. This phenomenon has been shown in other similar polyelectrolyte polysaccharides such as alginate[232] and xanthan[218]. Furthermore ionic cross-links in CMC solutions have been shown to

increase the viscosity implying some degree of bridging between CMC chains[239]. Furthermore the strong frequency dependence of soft physical gels is expected in the presence of ionic cross-links[14, 239].

The increase in shear moduli with increasing $CaCl_2$ ions is in good agreement with the lap shear data, with increasing peak force at increasing ionic strength. However in the lap shear data the peak force begins to decrease again at the highest salt concentrations (1:1 molar ratio) whereas shear moduli remain stable at these concentrations. Furthermore, the trend in the rheology data as a function of $CaCl_2$ concentration was not reproduced with the addition of $SrCl_2$, although the lap shear data is in good agreement between these two samples. The addition of ionic cross-links to gellan gum has been shown to result in a significant increase in the ultimate tensile strength despite not increasing the Young's modulus[240], similar to what has been found in our study where the peak adhesive force is increased by ionic cross-links while the shear moduli is unaffected. This could imply that the ionic cross-links add an energy dissipation method which increases the ultimate tensile strength of the gel, however does not significantly influence the Young's moduli.

To gain further insight in the behaviour of the gels at increasing ionic strength, we analysed light scattering data for CMC solutions in the presence of these two cations (figure 3.9b). As noted above, we had observed that, as the salt concentration increased, the hydrodynamic diameter of polymer chains decreased. This implies that, in the presence of divalent cations, CMC chains are collapsing rather than forming bridges between chains, as would be expected at such high dilutions. Increases in shear moduli observed at higher Ca^{2+} concentrations may indicate that these ions, at such higher CMC concentrations (and in the absence of PEG chains) are able to bridge

macromolecules and clusters of macromolecules, contributing to the mechanical properties of the macroscopy network. However, Sr2+, displaying weaker interactions with CMC molecules (Figure 3.11) and associated changes in hydrodynamic diameters, do not lead to such strengthening, and in fact may shield interactions between carboxylic groups, resulting in a slight decrease. Hence, as clusters of polymer within the soft matrix arise, in lap shear tests, Sr^{2+} ions may limit the propagation of dislocations and fractures, and allow to delay sample failure.

The idea that the CMC chains are collapsing in on themselves is also suggested by the visible precipitation that occurs at high concentration of electrolytes. It is therefore believed that the addition of divalent cations does not only generate cross-links between chains, but also result in chain collapse and the formation of isolated "hard" clusters that do not contribute mechanically to the macroscopic mechanical properties of the materials. Hence, two opposing effects impact on CMC hydrogels macroscale mechanics. Therefore, we proposed that polymeric cross-linkers that display terminal cationic "handles" would allow simultaneous complexation of CMC chains, as well as acting as tethers between the resulting hard cores, to strengthen hydrogel mechanics.

3.3.4. Impact of Organic Cationic Cross-linkers on CMC Gelation

Given the results obtained for the addition of divalent cationic salts on CMC gel mechanics, appearing to cause chain collapse, the impact of longer chain length organic cationic cross-linkers was investigated. Using longer chain length crosslinks it was thought could promote interchain crosslinking, however again the results suggest something different. As will be shown in this case while the multivalent organic crosslinkers result in some inter-chain crosslinking there is also still chain collapse as shown in figure 3.12.

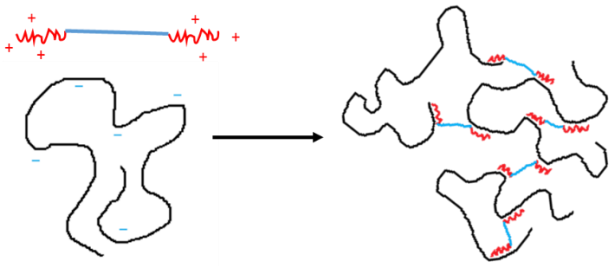

Figure 3.12 schematic showing the impact of multivalent cationic organic crosslinkers on CMC gels, promoting chain collapse alongside some inter-chain crosslinking.

Here the cross-linkers studied were DETA, PEHA and two end capped poly-oxazoline block copolymers, shown in figure 3.13, therefore displaying cationic "handles" with different chain lengths. The cross-linkers used and their concentrations are shown in table 3.3. The DETA and PEHA are not charged at neutral pH, so HCL was added to the corresponding solutions, at ratios of 3:1 and 6:1 respectively (HCL: DETA/PEHA) molar ratio. DETA and PEHA were also used without HCL as a control.

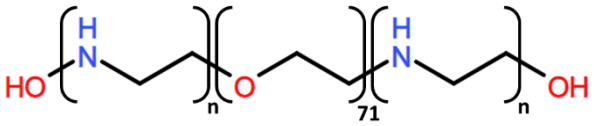

Figure 3.13 Chemical structure of the PEtOx-PEG-PEtOx block copolymers, where n = 10, for bloc 10, and n = 35 for bloc 35, with cationic tertiary amine groups on the end caps

The synthesised PEtOx-PEG-PEtOx block copolymer consists of positively charged end caps on a PEG backbone. Two variants of the block copolymer have been used, bloc 10 and bloc 35, where n = 10 and 35 respectively for the number of repeat units of each end cap. These two block copolymers were chosen to investigate the impact of oppositely charged polyelectrolytes, with varying molecular weights, on the hydrodynamic diameter and mechanics of CMC gels.

Table 3.3 CMC gels and organic cross-linker concentrations tested

Sample Name	CMC Concentration /wt%	Ionic Salt	Molar Ratio (CMC: X-Linker: HCL)
bloc 10 - 20	12.5	bloc 10	20:1:0
bloc 10 - 5	12.5	bloc 10	5:1:0
bloc 10 - 2	12.5	bloc 10	2:1:0
bloc 10 - 1	12.5	bloc 10	1:1:0
bloc 35 - 20	12.5	bloc 35	20:1:0
bloc 35 - 5	12.5	bloc 35	5:1:0
bloc 35 - 2	12.5	bloc 35	2:1:0
bloc 35 - 1	12.5	bloc 35	1:1:0
DETA - 20	12.5	DETA	20:1:0
DETA - 5	12.5	DETA	5:1:0
DETA - 2	12.5	DETA	2:1:0
DETA - 1	12.5	DETA	1:1:0
PEHA - 20	12.5	PEHA	20:1:0
PEHA - 5	12.5	PEHA	5:1:0
PEHA - 2	12.5	PEHA	2:1:0
PEHA - 1	12.5	PEHA	1:1:0
DETA HCL - 20	12.5	DETA	20:1:3
DETA HCL - 5	12.5	DETA	5:1:3
DETA HCL - 2	12.5	DETA	2:1:3
DETA HCL - 1	12.5	DETA	1:1:3
PEHA HCL - 20	12.5	PEHA	20:1:6
PEHA HCL - 5	12.5	PEHA	5:1:6
PEHA HCL - 2	12.5	PEHA	2:1:6
PEHA HCL - 1	12.5	PEHA	1:1:6

The CMC gels with varying organic cross-linker concentrations, shown in table 3.3, were tested using the same protocols used to study the inorganic ionic cross-linkers, namely oscillatory rheology, lap shear testing and dynamic light scattering. The results obtained for the CMC gels with organics cross-linkers are shown in figure 3.14.

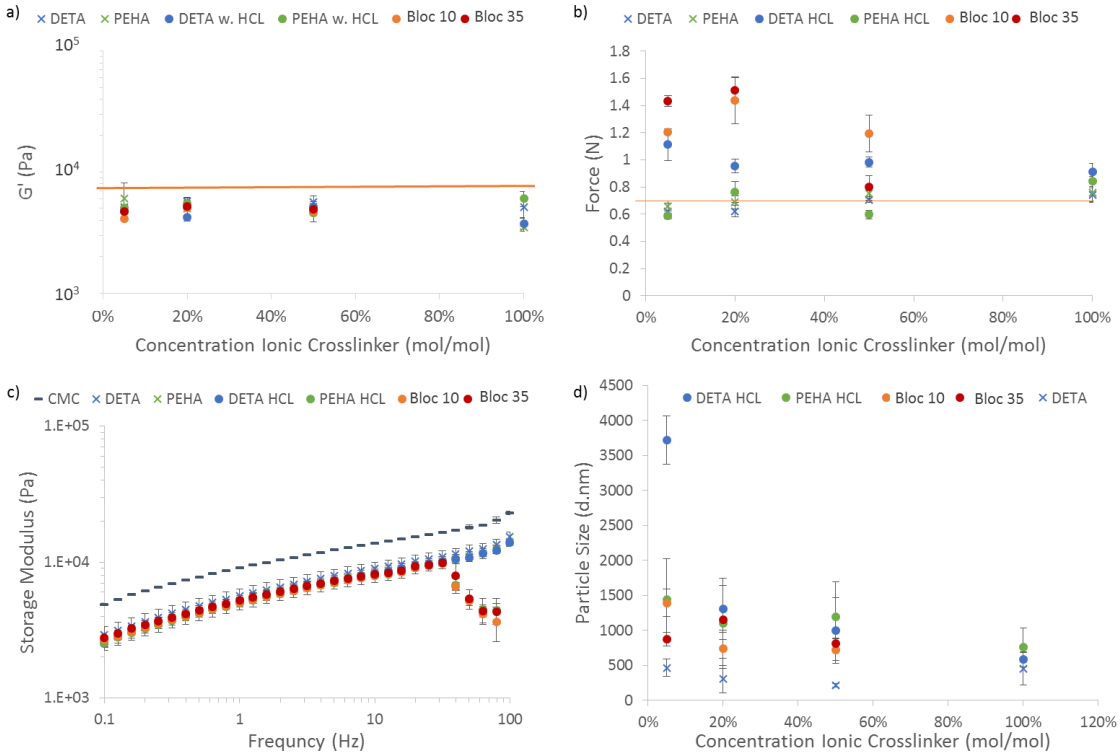

Figure 3.14 Characterisation of CMC gels with varying mol/mol concentrations of organic cations (where the mol/mol ratio is the ratio of amines per mole of carboxylic acid) by a) and c) oscillatory rheology showing a summary of the moduli at the different salt concentrations at 1Hz (the orange line showing the modulus of native CMC) and representative frequency sweeps at an organic binder concentration of 20% respectively, b) summary of the lap shear data showing the peak adhesive force for CMC gels varying the organic binders molar concentrations (orange line showing the average peak of native CMC gel), and d) light scattering data for CMC with varying organic cation concentrations with a CMC weight concentration of 0.05%, keeping the ratios of CMC: organic cations the same as those used for the rheology and lap shear experiments. A minimum of three samples per experiment were tested. All error bars are standard deviations.

From figure 3.14 we can see that our results for the CMC gels with varying concentrations of organic cations are similar to those we obtained for inorganic cationic salts. Again, the shear moduli of the CMC with and without the organic cross-linkers show a strong frequency dependency, as shown in figure 3.14c, as we would expect for a physical gel with high water content. The high frequency dependence resulting from the viscoelastic nature of the CMC being a physical gel with high water content. Here however there is no increase in shear moduli with any of the organic binders studied. Similar polysaccharide based coacervates like BSA/pectin[241], BSA/k-carrageen[242], gelatin/sodium montmorillonite[243] and O-carboxymethyl chitosan/gum Arabic[244] show similar strongly frequency dependent rheological properties arising

from the purely physical nature of the gel. Furthermore increasing the ionic strength of the solution results in a modest decrease in the shear moduli of many of these gels[241, 242], as opposed to any matrix strengthening.

However, we observed a clear increase in the peak adhesive strength of 1.6 N in lap shear tests (Figure 3.14B). This is particularly clear for the block copolymers, for which a sharp increase is seen at very low concentrations. The PEHA and DETA without HCL, however show little to no impact on the adhesive shear strength. This is as expected as without HCL the PEHA and DETA samples are not charged and hence no cross-linking is expected to result from adding these to the CMC gel, whereas with DETA and HCL we do see a noticeable increase in the adhesive shear strength. As was the case for the inorganic cross-linkers, all the samples tested by lap shear failed cohesively with clear samples residues still covering both sides of the lap shear testing geometry.

Dynamic light scattering was carried out next, to explore molecular interactions between the different organic cations and CMC chains. Significantly larger particle sizes resulted from the addition of the bloc copolymers when compared to the inorganic salts (apart from the addition of unprotonated DETA), with particle sizes in the range of 3000 to 550 nm in the presence of organic cations, compared to 550 to 100 nm with the inorganic salts. While μm sized particles cannot be reliably quantified by dynamic light scattering, this still suggests significant bridging between CMC chains with the addition of such multivalent organic salts. However, at higher cation concentrations, the hydrodynamic diameters of CMC complexes decreased in size, as was observed for inorganic cations. Therefore, our results indicate that, although organic cations are bridging across several CMC chains and bringing them together to former larger complexes at low mole ratios, they result in the collapse of CMC chains

at high mole ratios, as shown in figure 3.14. This phenomenon is seen in other coacervate systems where if the ionic strength of the solution is not carefully tuned the electrolytes will complex and precipitate rather than forming a two phase coacervate gel[136, 227, 228]. In contrast, unprotonated DETA did not display initial increase in complex size and did not result in CMC chain collapse, in line with its neutral structure and the absence of any significant hydrogen bonding between the components of this system. Therefore, the bridging of CMC chains by organic cations results in very little change in the bulk mechanics of CMC gels due to the local collapse of CMC chains. It could be proposed that longer PEG tethers could help alleviating such local collapse and provide improved long range cross-linking of CMC chains. In contrast, the adhesive shear strength of the corresponding gels was significantly improved at low binder concentration, presumably due to stronger fracture healing properties of the associated networks.

3.4 Conclusion

The impact of inorganic divalent cationic cross-linkers and organic cationic polyelectolyte cross-linkers on CMC gel rheology and adhesive strength was studied. It was thought that the inorganic cationic cross-linkers would form rigid cross-links between CMC chains. However it was found that there was no significant impact on the bulk mechanics characterised by oscillatory rheology. It was also found that when the ionic cross-linker concentration was high the gels became cloudy and hence some precipitation was occurring. The particle size was characterised using dynamic light scattering showing the addition of inorganic divalent cations was resulting in a decrease in the particle size. It was therefore shown that the addition of inorganic cationic cross-linkers was resulting in the CMC chains complexing rather than cross-linking across chains. The inorganic cross-linkers did however result in an increase in the

adhesive strength characterised by lap shear testing. This suggests that the complexes formed and ionic cross-links did result in as energy dissipation method giving the gels a greater adhesive strength.

In the case of adding organic cationic cross-links the results were similar with no significant increase in the bulk mechanics resulting from the addition of the cross-linkers. When studying the particle sizing it was found that the particle sizes in the presence of the organic cross-links were significantly larger, ranging from 3000 nm – 550nm compared to 500 – 100 nm in the case where inorganics cross-links were used. This showed that some cross-linking was occurring between the CMC chains. However it was again seen that at high concentrations of ionic crosslinks precipitation was occurring. The interactions between the organic cationic polyelectrolyte cross-linkers and the CMC chains appears to result in complex coacervation where complexes of CMC chains are loosely bound within a more dilute bulk network. Interestingly the formation of the CMC coacervates also resulted in an increase in the adhesive strength, suggesting that the coacervates offer an energy dissipation method resulting in an increased adhesive strength.

Chapter Four

Analytical Modelling of Interfacial Mechanics of Liquid-Liquid Interfaces

4.1 Introduction

The use of emulsions in processing is a common occurrence in the oil and gas and chemical industries[143, 168, 245-247]. Understanding the properties of emulsions and parameters stabilising oil-water interfaces is of the utmost importance for processes such as, emulsification, and two-phase reactions and extractions that yield products such as bulk and fine chemicals, pharmaceuticals and nanoparticles[168, 246]. The stability of emulsions is one of the major concerns for industrial applications. Emulsions are dispersed systems and, as a result are thermodynamically unstable, however in the presence of surfactants can remain stable for long periods of time and can hence be considered dynamically stable[245].

An important mechanism for the destabilisation of emulsions consists of the drainage of the continuous fluid phase between droplets, leading to their coalescence[246, 247]. This lead to research into the forces between oil droplets within emulsions and the development of DVLO theory[165-167]. The DVLO theory describes the distribution of charges in ionic solutions and can be used to describe forces between colloids and provides some of the fundamental understanding of the stability of emulsions. This theory has been extended to understand forces between a colloidal AFM indenter and oil droplets in solution[171, 172, 248] and shows that van der Waals and electric double layer forces are key factors influencing interfacial mechanics.

Another method to study interfacial mechanics is the use of interfacial rheology. Here the factors dominating the mechanical response can be broken down into the physical properties of the fluids and the properties relating to surface-active species across the fluid interface. The former is a function of the viscosity, density, purity and polarity of the two phases, and the pH and ionic strength of the continuous phase. For the later the capability of the surface active molecules to lower the interfacial surface tension, the amount they adsorb, their ability to desorb and unfold upon adsorption, the thickness of the absorbed layer, interactions between molecules and their mobility will define the mechanical properties of the interface/emulsion[143, 249].

Interfacial rheology focuses on the relationship between the shear deformation of an interface and the force applied both as a function of time. The understanding of this relationship is utilised in many industrial applications for example modelling of foam drainage and Ostwald ripening in emulsions[250, 251]. Furthermore the study of interfacial mechanics is becoming increasingly relevant to bioengineering, particularly the study of cell adhesions and cell fate[144-146].

Recently, the importance of interfacial mechanics was also highlighted in the field of cell biology and stem cell culture. Indeed, adherent cells are typically thought to require solid, elastic or viscoelastic, substrates in order to proliferate. Studies have shown that substrate bulk mechanics and cell adhesion do not directly correlate with cells being shown to adhere to liquid PDMS[6], viscoelastic hydrogels[33] and soft nanofibers[198]. Cell adhesion to liquid interfaces is particularly surprising in light of the speed at which they relax (typical relaxation times < ms) which is thought to prohibit stabilisation of focal adhesions. This implies either a very different cell adhesion mechanism, or the formation of a mechanically stable elastic interface to which the cells can form stable adhesions[145]. Hence understanding the interfacial mechanics in

shear and normal to the interface are essential to understanding the mechanism by which cells adhere at liquid interfaces.

An important aspect of cell adhesions at liquid interfaces is stabilisation of the interface. Similar to stabilising emulsions, a protein film is deposited at the interface in this case allowing for cells to adhere. Protein have been widely studied and are important in many biological functions, such as acting as catalysts, substrate binders, as structural components and as transporters[147, 148]. The function of proteins is defined by their amino acid sequences. Proteins chains can assemble forming two dimensional secondary structures, which in turn can fold into three dimensional, tertiary, fully functional proteins. The tertiary proteins can then assemble into larger functional complexes. Protein complexes remain stable and folded through amino acids interacting by hydrogen bonding, ionic and hydrophobic interactions[143, 147].

The surface activity of proteins depends upon numerous factors, including, their thermodynamic stability, flexibility, molecular size and charge[148, 151, 152]. The adsorption of proteins at interfaces is a multistep process which follows the following general steps [148, 153, 154], first, diffusion of proteins from the aqueous phase to the interface, followed by adsorption of the proteins. The proteins can then change their molecular structure, finally spreading across the interface. Protein unfolding after deposition is dependent on the nature of the interface, if it is air/liquid, liquid/liquid or liquid/solid, the bulk phase conditions, such as the pH, temperature, ionic strength and protein concentration[143, 147, 155], and on the intrinsic properties of the protein itself. Protein adsorption leads to a decrease in the interfacial surface tension, the change in surface tension changes over time and can take minutes to hours to plateau depending on the conditions[147]. Upon deposition the proteins can interact laterally often resulting in irreversible binding[154]. The mechanics of adsorbed protein films at interfaces is

determined by the by the bonding of the protein to the interface and the nature of the bonding between protein chains. Adsorbed proteins have been shown to form close packed, cross-linked gel like structures[143, 155, 157].

The interfacial mechanical response of proteins films by shear rheology is predominantly a function of the structure formed between the adsorbed proteins, as there is no change in the surface area under shear loading. However when tested by nanoindentation the mechanical response is more complex as you have a combination of the interfacial surface tension forces and the response owing to the deformation of the protein film. On the μm scale, or below the capillary length, the interfacial surface tension response to indentation is shown to be a complex problem with the mechanics resulting from a combination of numerous phenomenon, including, the electrostatic double layer forces between the probe and the droplet, hydrophobic interactions, van der Waals forces and surface tension forces[171, 172, 252-256]. When protein layers are introduced as well this clearly becomes an even more involved problem. The interactions between interfaces and colloidal indenters is described by DVLO theory[165-167, 171, 172], however these models do not include any contribution from the deformation of the protein film.

The aim of this chapter is to characterise and model the interfacial mechanics of protein films adsorbed on liquid/liquid interfaces. The characterisation of the interfaces was performed by interfacial oscillatory rheology and nanoindentation by AFM. The relative mechanical contribution of the interfacial surface tension forces and the adsorbed protein films to indentation was modelled in order to better understand the mechanics of adsorbed protein films at liquid/liquid interfaces.

4.2 Methods and Materials

Materials

Pentafluorobenzoyl chloride (PFBC), benzoyl chloride, lysozyme, bovine serum albumin (BSA), poly-l-lysine (PLL) and 20 μm diameter silicon particles were all purchased from Sigma Aldrich. Blandol® White Mineral Oil was purchased from Sonneborn. 3M™ Novec™ 7500 Engineered Fluid was purchased from fluorochem. Bruker ORC 8 – 10 AFM tips were purchased from Bruker.

Sample Preparation

Interfaces were prepared following comparable protocols, with small variations depending on how they were to be tested, in order to accommodate for the equipment being used. The different compositions used are shown in table 4.1. The oils with pro-surfactant (acyl chloride) were always mixed separately before the aqueous phase was added. In cases, where proteins were used these were added after the aqueous and oil phases were mixed and allowed to deposit over time. The PLL and BSA films on fluorinated oil were allowed to assemble for at least 2 h to form a protein film, while films on the mineral oil were left overnight. For samples characterised by AFM and Zetasizing the excess protein was washed away by removing as much of the aqueous phase as possible and refilling it with PBS, this was repeated 6 times to ensure the solution was adequately rinsed.

Table 4.1 Composition of oil – PBS interfaces characterised by rheology, nanoindentation and pendent droplet testing

Oil Phase	Aqueous Phase	Surfactant	Surfactant Concentration (mg/mL)	Protein	Protein Concentration (mg/mL)
Fluorinated Oil	PBS pH 7.4	-	-	-	-
Fluorinated Oil	PBS pH 7.4	Pentafluorobenzyl Chloride	0.01	-	-
Fluorinated Oil	PBS pH 7.4	-	-	Bovine Serum Albumin	1
Fluorinated Oil	PBS pH 7.4	Pentafluorobenzyl Chloride	0.01	Bovine Serum Albumin	1
Fluorinated Oil	PBS pH 7.4	Pentafluorobenzyl Chloride	0.01	Poly-L-Lysine	0.1
Fluorinated Oil	PBS pH 10.5	Pentafluorobenzyl Chloride	0.01	Poly-L-Lysine	0.1
Mineral Oil	PBS pH 7.4	-	-	-	-
Mineral Oil	PBS pH 7.4	Benzoyl Chloride	0.1	-	-
Mineral Oil	PBS pH 7.4	Benzoyl Chloride	0.1	Lyso-zyme	10

For pendent droplet experiments, using mineral oil, the protein had to be added to the aqueous solution before being introduced to the oil as the oil was less dense than PBS and hence the droplet was the aqueous phase and so the protein couldn't be added sequentially.

Finally for electrophoretic light scattering, samples were prepared as emulsions by vortexing the samples after adding the protein. Once vortexed the samples

were left for two hours for the protein to fully absorb before being washed using the same method outlined in the paragraph above.

Interfacial Rheology

Interfacial rheology was carried out using a Discovery Hybrid Rheometer 3 from TA Instruments. The following protocol was used to characterise the interfaces shown in table 4.1. First, the denser of the two phases was added to the PTFE trough (19 mL) and the height of the liquid zeroed by measuring the normal force whilst lowering the De Nouy ring until the 'pull in' force is observed. The ring is then lowered to position the first liquid-air interface at the ring equatorial plane, before the second phase, either oil or aqueous depending on the density of the oil used, is added (20 mL). For samples without any protein the interfacial modulus is then directly measured using an oscillatory frequency sweep, from 0.001 – 0.1 Hz with a displacement of 10^{-4} rad. The relaxation profile is also recorded using a peak strain of 1% at a rate of 1 %/s, the strain is then held for 120 s. Where a protein film was studied the first step is a time sweep initially without any protein. The protein is then added after 30 min and the time sweep is left to run for 3 h and 12 h, for the films on the fluorinated and mineral oil respectively, these times correspond to the time it took for the interfacial shear moduli to plateau and hence for the film to fully form. After the time sweeps the frequency sweep and stress relaxation tests are performed as before. Finally an amplitude sweep is performed from 10^{-6} – 10^{-1} rad at 0.1 Hz.

Interfacial rheology experiments on the fluorinated oil – PBS system with BSA and PLL were performed by Dexu Kong and Lihui Peng of Queen Mary University of London. The interfacial characterisation of BSA[144] and PLL[146] films have both been published. All interfacial rheology on the mineral oil – PBS system with lysozyme were performed independently.

Interfacial AFM

Interfacial AFM was performed using an NT-MDT Ntegra Atomic Force Microscope with Bruker ORC 8 – 10 Contact AFM Tips with spring constants of ~0.05 N/m, the spring constant for each tip used was measured using the Sader method[257]. The tips were plasma oxidised before each experiment. Before testing the interfaces the tips were calibrated by indenting a silicon wafer in order to be able to convert the deflection in nA into nm. Each interface was indented on three separate 1 μm X 1μm areas over which 100 indents were performed. The curve time for each curve was 1 s. The indentation depth was kept between 500 – 1000 nm depending on the sample. A minimum of three samples for each condition were tested.

Zeta Potential

The surface charge of the nanoparticles were determined by electrophoretic light scattering using a Malvern Zetasizer Nano ZS fitted with a 633 nm red laser. The zeta potential (ξ) of the particles was estimated from the electrophoretic mobility (u) as according to the Helmholtz-Smoluchowski equation:

$$u = \epsilon \frac{\xi}{\eta} \qquad [4.1]$$

Where η is the viscosity, and ϵ is the dielectric constant. 0.5 mL of each emulsion was used in DTS1070 Folded Capillary Zeta Cells.

Pendant Droplet

The measurement of surface tension using the pendent droplet assay was performed using a Kruss DSA 100 to capture images, which were then analysed using Image J. The droplets were always from the denser of the two fluids and as large a drop as possible (whilst recording the corresponding volumes) were suspended before images were taken. Images were taken as soon as the droplet was suspended and after

10 min for the interfaces in the absence of any protein. Where the protein was added, images were captured as soon as the protein was added and up to 10 min after, then the samples were left over night to ensure the film was fully formed and then further images were captured.

4.3 Results and Discussion

4.3.1. Mechanical Characterisation of Fluorinated Oil Interfaces with BSA and PLL Protein Films

The study of the mechanics of fluid – fluid interfaces was prompted to better understand the mechanical behaviour of these interfaces and identify important parameters regulating cell adhesion and growth at fluid interfaces. It has been shown that cells can grow on liquid-liquid interfaces (fluorinated oil-PBS) at which protein nanosheets were deposited (both PLL and BSA). It was observed, *via* interfacial rheology, that the interfacial shear moduli of the corresponding interfaces increased by several orders of magnitude upon addition of the protein solution, depending on the concentration of pro-surfactant and pH of the aqueous phase[144-146]. To confirm these observations, the mechanics of the corresponding fluorinated oil – PBS interfaces, with and without protein, were initially characterised by AFM nanoindentation and compared to the previously recorded results. Oscillatory rheology and nanoindentation were selected in order to probe both the bulk, or macroscale, mechanics and the local, or nano-scale, mechanical properties. However interfacial rheology probes the shear "in-plane" properties of interfaces, whilst AFM nanoindentation probes transverse mechanical deformations, which are thought to result from a complex combination of surface tension and nanosheets mechanics, amongst other parameters (see

model and discussion in section 4.3.4). The local mechanics were particularly interesting from the perspective of cell adhesion and mechano-transduction. Initial AFM experiments were conducted using a plain pyramidal AFM tip.

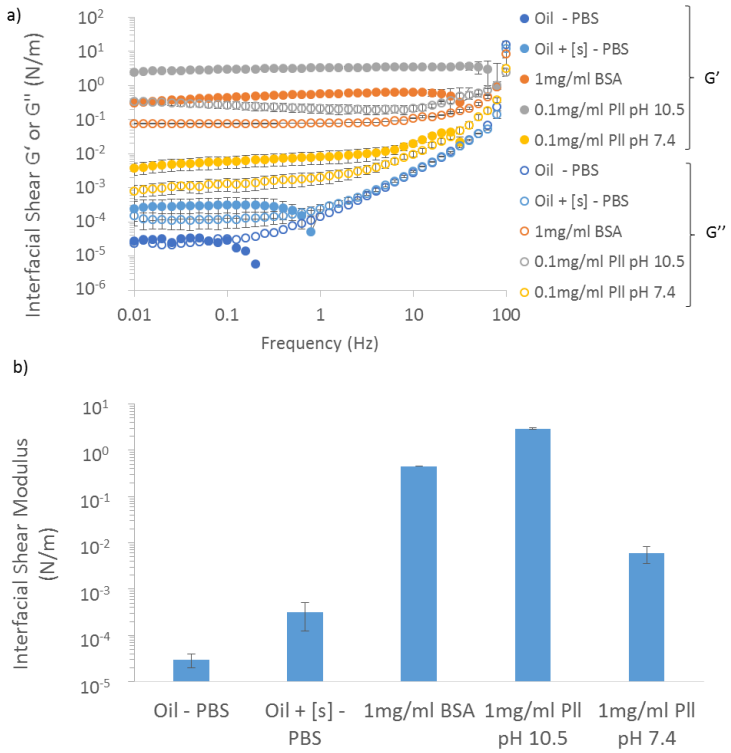

Figure 4.1 Mechanical characterisation of fluorinated oil – PBS interfaces, done by Dr Dexu Kong, with and without protein films by oscillatory rheology[144, 146], showing a) the frequency sweeps performed on the different interfaces with an oscillating displacement of 10^{-4} rad, from 0.01 – 100 Hz, and b) a summary comparing the storage moduli for the different conditions tested. All error bars are standard deviations. The surfactant used was PFBC at 0.01 mg/mL and the PLL and BSA concentrations were 1 mg/mL and 0.1 mg/mL respectively.

The collected results of the frequency sweeps by interfacial rheology on the fluorinated oil – PBS interfaces, shown in figure 4.1 and 4.2, are in good agreement previous data obtained after the addition of BSA (0.45 N/m here compared to 20 N/m reported by Keese and Giaever in similar conditions[258]) and PLL proteins resulting in a dramatic (3-4 orders of magnitude) increase in the shear moduli. In particular, PLL assembled at pH 10.5 gives a much more significant increase in moduli compared to the PLL assembled at pH 7.4. This is expected as, at neutral pH, PLL is protonated and cannot form amide bonds that are responsible to tether this polymer to the pro-surfactant and pin it to the interface[259]. At pH 10.5, PLL forms a stronger film than

the BSA on the fluorinated oil, implying better cross-linking or network formation, although the detailed mechanism regulating such mechanical properties remains unclear.

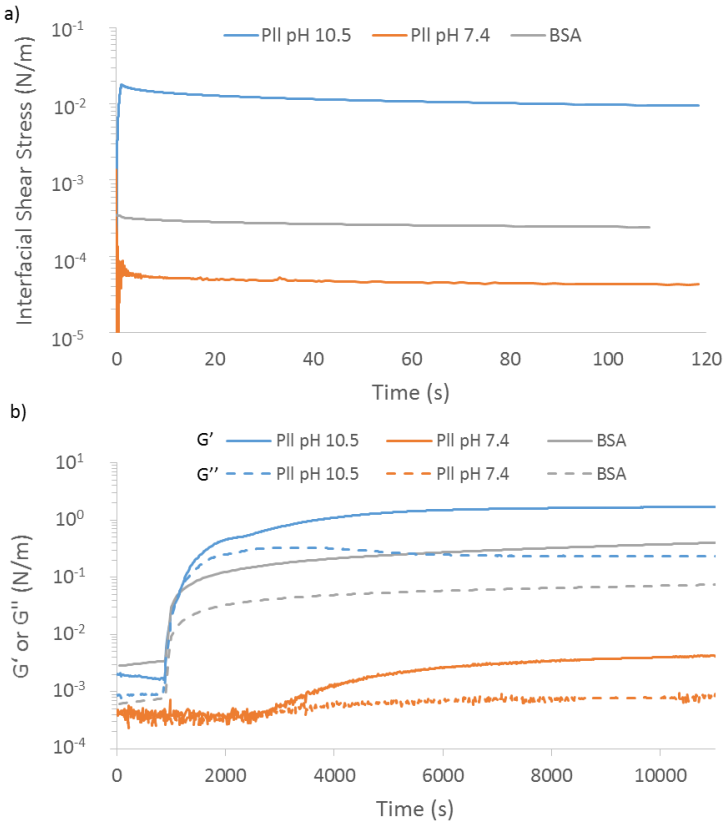

Figure 4.2 Mechanical characterisation of fluorinated oil – PBS interfaces, done by Dr Dexu Kong, with and without protein films by oscillatory rheology[144, 146], showing, a) representative stress relaxation data on fluorinated oil + [s] – PBS + PLL interfaces with the PLL deposited at pH 10.5 and 7.4 and c) comparison of protein film adsorption at fluorinated oil + [s] – PBS interfaces for BSA, PLL at pH 7.4 and PLL at pH 10.5.

PLL nanosheets assembled at pH 10.5 also showed the least frequency dependent profiles, with evidence of failure only above 60 Hz, hence indicating the least viscous response. PLL nanosheets assembled at pH 7.4 displayed the most frequency dependent profiles, which implies that while some of the PLL was deposited at the corresponding interface, it didn't form a strong network with interlock or physically cross-linked chains, in a similar sense to a physical gel forming in 3D. In the absence of protein, films were extremely weak and appeared to destabilise at high frequencies (0.1-0.25 Hz). The interfaces were then characterised by nanoindentation by AFM to

compare the local normal mechanical response to the interfacial shear properties found *via* oscillatory rheology, as shown in figure 4.3.

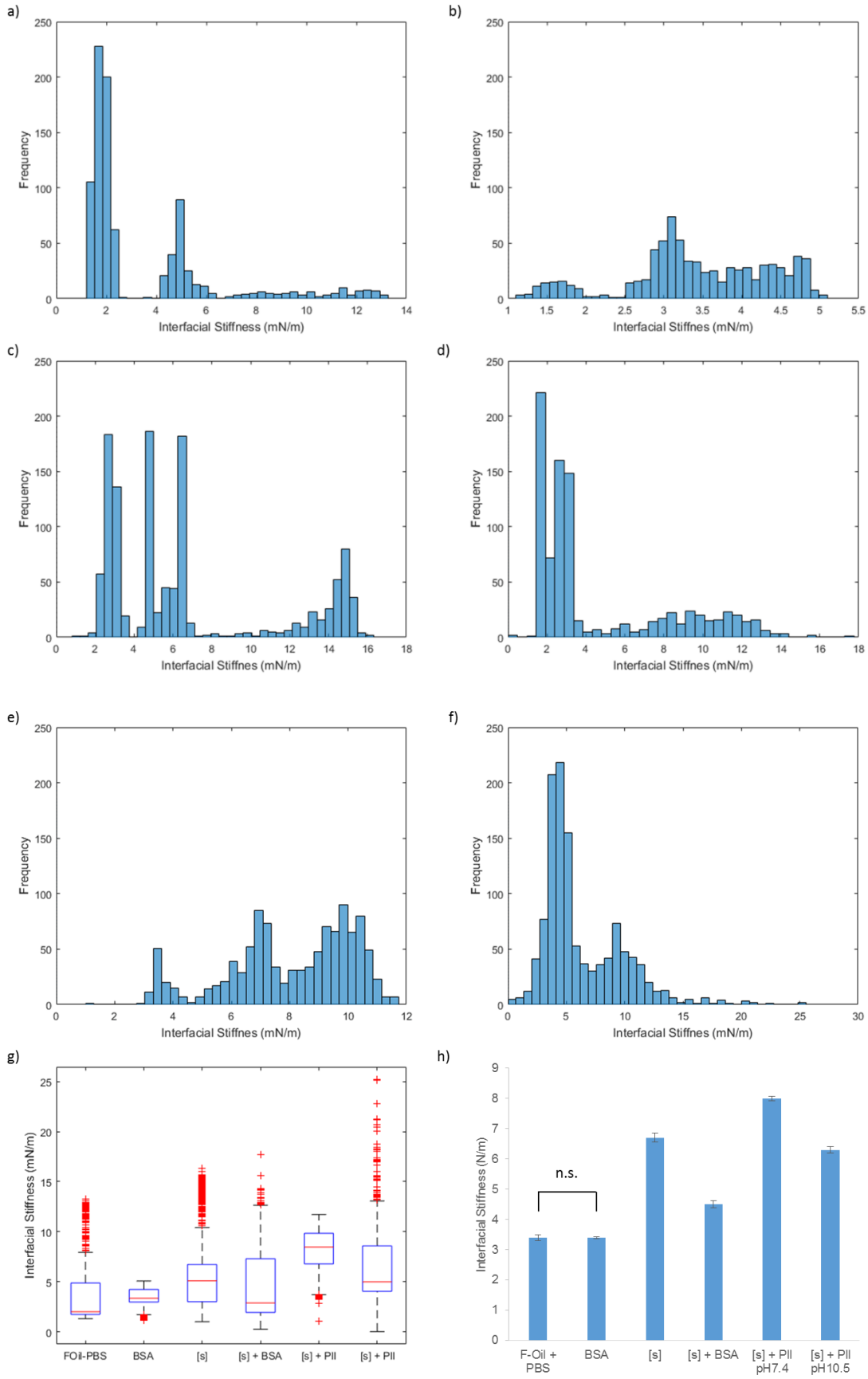

Figure 4.3 Nanoindentation by AFM on fluorinated oil – PBS interfaces with and without protein using a plain pyramidal AFM tip showing a) – f) histograms of the interfacial stiffness for fluorinated oil – PBS only, fluorinated

oil – PBS + BSA, fluorinated oil + [s] – PBS, fluorinated oil + [s] – PBS + BSA, fluorinated oil + [s] – PBS + PLL at pH 7.4 and fluorinated oil + [s] – PBS + PLL at pH 10.5 respectively, g) box plot summarising the distribution of the moduli for the fore mentioned conditioned and h) summary of the interfacial stiffness obtained for the different interfaces. PFBC was used as the surfactant with a concentration of 0.01 mg/mL and the BSA and PLL concentrations were 1 mg/mL and 0.1 mg/mL respectively. AFM experiments were conducted on a minimum of three samples with each sample being tested in three 1 μm X 1 μm squares performing 100 indents in each area. All error bars are standard errors and all values are significantly different apart from those labelled n.s. with $p < 0.01$

The AFM results with a plain AFM tip as the indenter, shown in figure 4.3, gave some quite surprising results, especially compared to the interfacial rheology profiles previously discussed. As the figure 4.3h shows the summary of the interfacial stiffness of the fluorinated oil – PBS interfaces, with and without any protein. Comparing these results to the rheology it is striking that the addition of PLL results in only a modest increase, from 3.4 N/m to 6.3 N/m, in the transverse indentation stiffness, when tested by AFM, while when tested by rheology we get a significant increase in the interfacial shear modulus, from 4 to 5 orders of magnitude. It was also striking to see that PLL gave a greater interfacial stiffness when deposited at pH 7.4 compared to pH 10.5, the opposite to what was shown in the oscillatory rheology. Similarly, the addition of BSA to interfaces led to a slight decrease in the indentation stiffness of associated interfaces, instead of the increase in interfacial shear modulus observed by rheology. This is presumably the result of conflicting effects of interfacial shear mechanics, surface tension and tip-interface adhesions on the indentation profile measured by AFM.

The fact that the addition of proteins gave such unexpected results led to the investigation of the spread in the moduli of the interfaces across the sample sets tested, shown in figure 4.3a – f. The spread in indentation stiffness was large, with a large number of outliers, as shown in figure 4.3g. It was reasoned that this could be a result of complex variation in local tip-interface interactions and indentation contact geometry (the droplets indented have a finite radius of curvature). In addition, considering the softness of the interfaces characterised and the relatively noisy traces obtained, it

is also likely that we are working at the limits of resolution of the tip being used. As such it was decided to investigate the local mechanics using an AFM tip with a colloidal bead attached. This would increase the contact area and hence the magnitude of the forces being measured. Using a colloidal tip would also change the nature of the contact area, as a sphere has a much lower aspect ratio than a pyramid tip, hence giving a more uniform contact with less shear forces. The results of the nanoindentation using a colloidal tip are shown in figure 4.4.

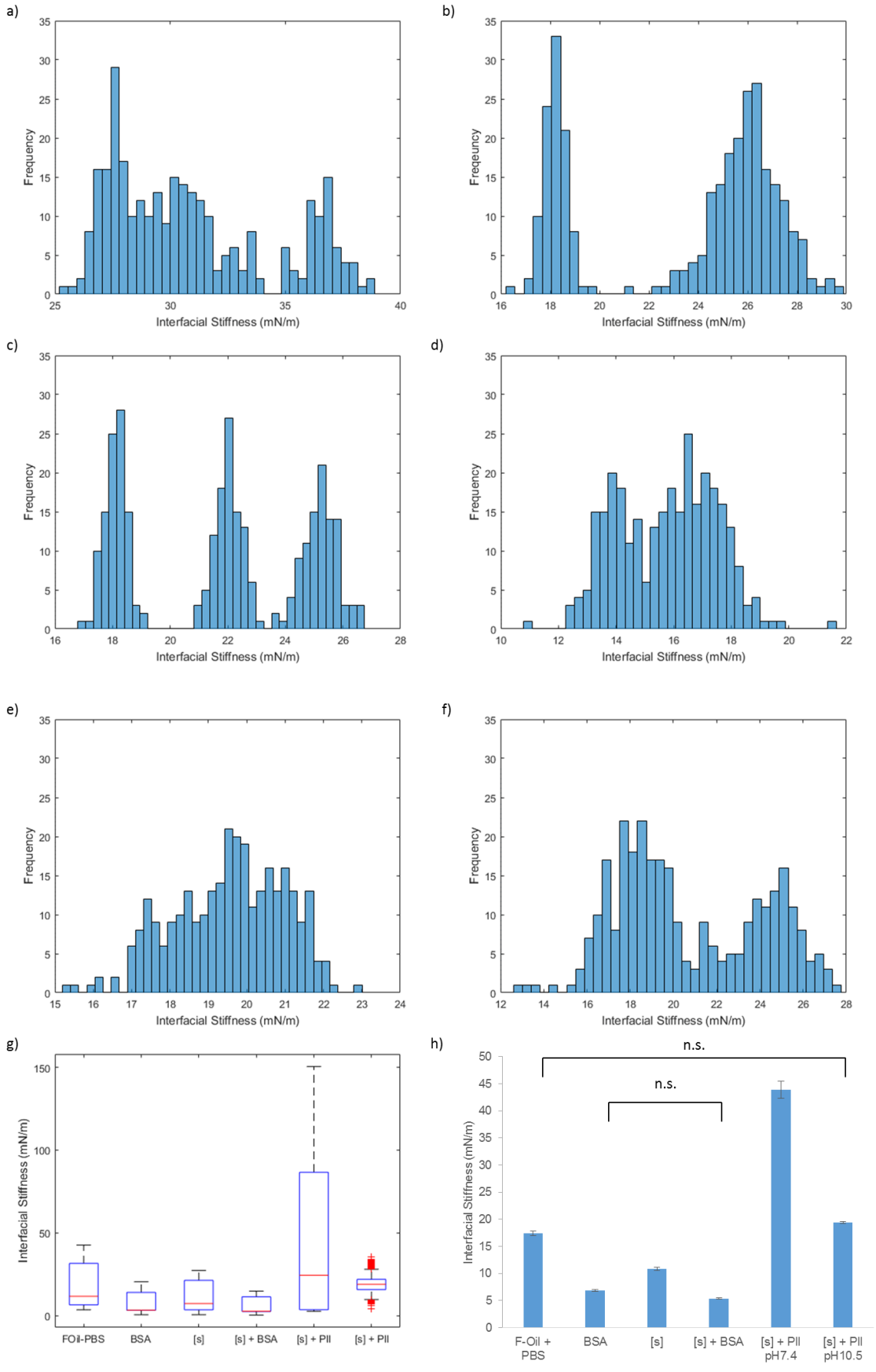

Figure 4.4 Nanoindentation by AFM with a 20 μm diameter colloidal tip on fluorinated oil – PBS interfaces with and without protein using a plain pyramid AFM tip showing a) – f) histograms of the interfacial stiffness for

fluorinated oil – PBS only, fluorinated oil – PBS + BSA, fluorinated oil + [s] – PBS, fluorinated oil + [s] – PBS + BSA, fluorinated oil + [s] – PBS + PLL at pH 7.4 and fluorinated oil + [s] – PBS + PLL at pH 10.5 respectively, g) box plot summarising the distribution of the moduli for the fore mentioned conditioned and h) summary of the interfacial stiffness obtained for the different interfaces. The surfactant used was PFBC at a concentration of 0.01 mg/mL and the proteins used were BSA and PLL at concentrations of 1 mg/mL and n0.1 mg/mL respectively. AFM experiments were conducted on a minimum of three samples with each sample being tested in three 1 μm X 1 μm squares performing 100 indents in each area. All error bars are standard errors and all values are significantly different, apart from those labelled n.s. with $p < 0.01$

The results for the colloidal nanoindentation by AFM on the fluorinated oil – PBS interfaces, figure 4.4, showed very different trends to both the pyramid tip and the oscillatory rheology. First, both the fluorinated oil + surfactant – PBS, and fluorinated oil + surfactant – PBS + BSA interfaces resulted in a significant drop in interfacial stiffness compared to the fluorinated oil – PBS interface, rather than an increase in stiffness as seen using a pyramid tip and by rheology. The increase in stiffness from adding PLL at pH 10.5 was also insignificant for the colloidal AFM compared with using the plain pyramidal tip. Despite these differences the addition of PLL at pH 7.4 again resulted in the most significant increase in the interfacial modulus. Interestingly across all the AFM experiments performed, with and without a colloid, the histograms of the spread in interfacial stiffness gives bi, or trimodel distributions. The fact that we have numerous peaks shows that across samples we are measuring different mechanical properties. What is driving these differences is not clear, however as will be shown in 4.3.4 small changes to the surface chemistry can result in significant changes in the mechanics of the interfaces and this may be what is being seen here. The differences between the colloidal and pyramid tip nanoindentation are highlighted in figure 4.6 where the normalised interfacial stiffness is compared.

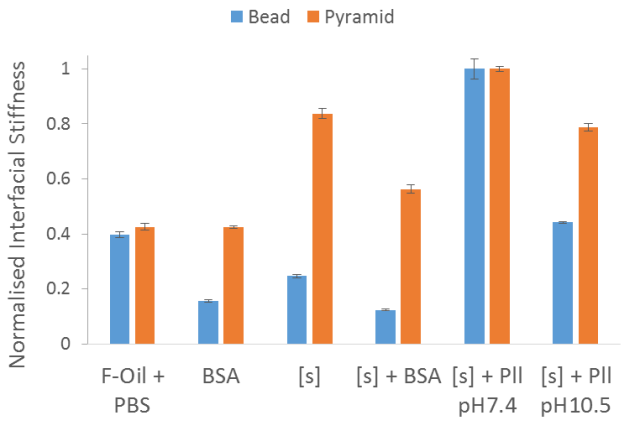

Figure 4.5 Comparison of the normalised interfacial stiffness of fluorinated oil – PBS interfaces, with and without protein, when tested using a colloidal AFM tip against a plain pyramid tip. All error bars are standard errors.

Despite showing a very different trend to the results obtained by oscillatory rheology the colloidal AFM data may make sense as the nature of the loading by indentation is very different to the shear forces exerted by rheology. As such the contribution to the interfacial stiffness by surface tension, as well as other tip-interface interactions, should be considered for the nanoindentation, whereas these factors can be neglected in the case of rheology, as the contact areas between the different geometry are essential constant. Hence, the decrease in stiffness from the addition of surfactant, observed in Figure 4.5, may be a result in the surface tension being reduced. The reduction in surface tension from the additional surfactant may also explain why the BSA does not have the same strengthening effect as seen in oscillatory rheology, as the modest increase in interfacial stiffness resulting from the BSA is negligible compared to the decrease in the surface tension resulting from this protein surfactant (BSA can denature at hydrophobic interfaces). Indeed, when BSA is added in the absence of any surfactant, we observed a significant decrease in indentation stiffness, compared to the plain oil – PBS interface.

In contrast, PLL nanosheets assembled at pH 10.5 formed a stiffer film by interfacial rheology which would also explain why these interfaces were associated

with greater interfacial stiffness compared to the BSA films, albeit modest compared to the large increase observed by interfacial rheology. What still remained unclear was why the PLL interfaces assembled at pH 7.4 still resulted in such a significant increase in interfacial stiffness.

The results from the colloidal AFM also show a much lower spread in the moduli as shown by the histograms in figure 4.4a – f. The decrease in the spread and lower number of outliers is further highlighted in figure 4.5g, where the box plot shows the scatter of this data. Apart from for the PLL at pH 7.4 where the spread in data is far greater than for all other conditions. To better understand this phenomena the impact of surfactants and proteins on the surface tension was investigated, discussed in section 4.3.3.

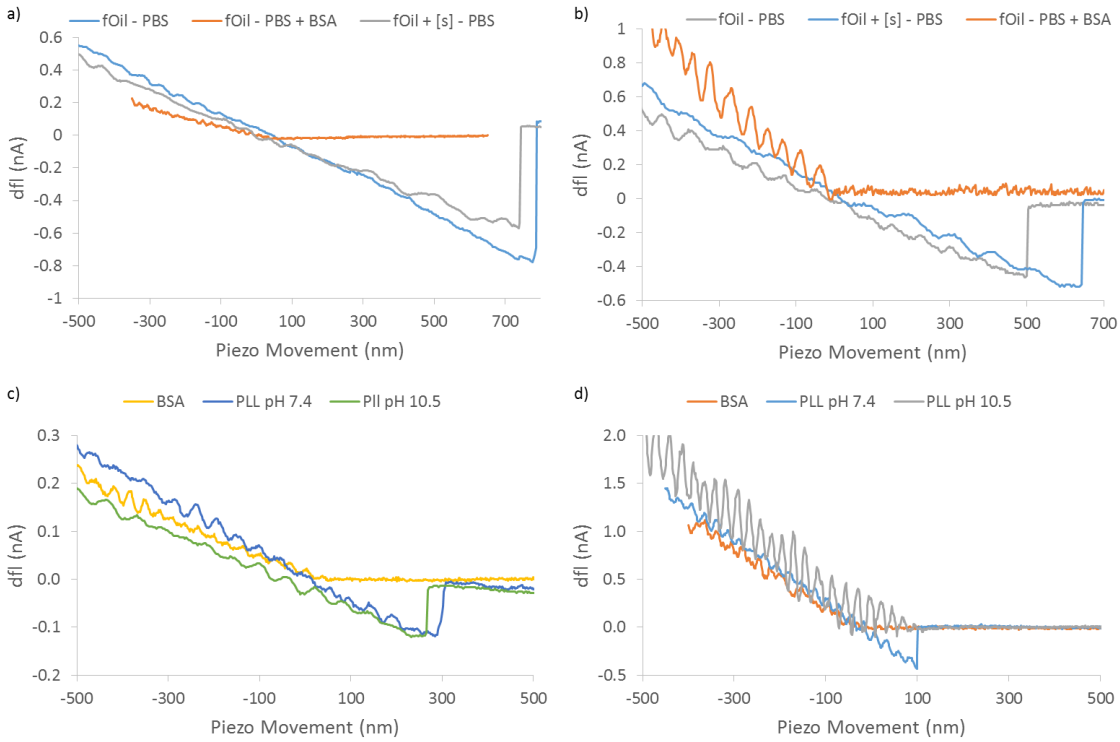

Figure 4.6 Representative raw AFM nanoindentation curves on fluorinated oil – PBS, fluorinated oil + [s] – PBS and fluorinated oil – PBS + BSA interfaces using a) a plain pyramid tip and b) a colloidal tip and raw AFM curves on fluorinated oil + [s] – PBS + BSA/PLL at pH 7.4/PLL at pH 10.5 using c) a plain pyramid tip and d) a colloidal tip). The surfactant used was PFBC at a concentration of 0.01 mg/mL and the BSA and PLL concentration were 1 mg/ml and 0.1 mg/mL respectively.

The raw AFM curves, shown in figure 4.6, also indicate some interesting adhesion profiles which may account for the differences between the results obtained by nanoindentation and interfacial rheology. Figure 4.6a and 4.6b show the raw nanoindentation curves for fluorinated oil – PBS, fluorinated oil + [s] – PBS and fluorinated oil – PBS + BSA using a plain pyramid tip and colloidal tip respectively. Interestingly here the presence of BSA prevents adhesion which is at a similar level for both the other conditions. From figure 4.6c and 4.6d showing representative nanoindentation curves with fluorinated oil + [s] – PBS + BSA/PLL at pH 10.5/PLL at pH 7.4 using a plain pyramid and colloidal tip respectively again we that the presence of BSA prevents sample tip adhesion. Furthermore comparing the adhesion between the samples with PLL and the samples without any protein the level of adhesion is far reduced in the presence of PLL. It is also clear that AFM testing using a plain tip exhibits far more noise than using a colloid. This is expected as the use of a colloidal tip greatly increases the contact area, with the plain tip having a nominal radius of 50 nm compared to the 20 μm colloid.

4.3.2 Mechanical Characterisation of Mineral Oil Interfaces and the Impact of Lysozyme and Benzoyl Chloride on Interfacial Mechanics

In addition to the systems studied above, we next examined the adsorption of Lysozyme to mineral oil. Indeed lysozyme adsorption to hydrophobic liquids has been studied in some detail, including via interfacial rheology. Lysozyme is an enzyme which is known to promote hydrolosis at the cell wall[156]. It is a globular protein with 129 residues, 9 acidic and 18 basic. It has been widely studied for its interfacial properties and has been shown to cause a decrease in surface tension upon film formation[156, 260, 261]. At interfaces, globular proteins like lysozyme have been shown to form strong intermolecular bonds by both physical and covalent bonds[156]. Many have

shown that globular proteins like lysozyme can unfold to form rigid films at interfaces[262, 263]. As mineral oil is a classic hydrophobic oil (not fluorophilic), we changed the pro-surfactant from pentafluorobenzoyl chloride to benzoyl chloride. A preliminary experiment was carried out to test what pro-surfactant would allow the formation of stable emulsions, as shown on figure 4.7. Lysozyme with benzoyl chloride was chosen as the system to study as it formed the most stable emulsion of those tested.

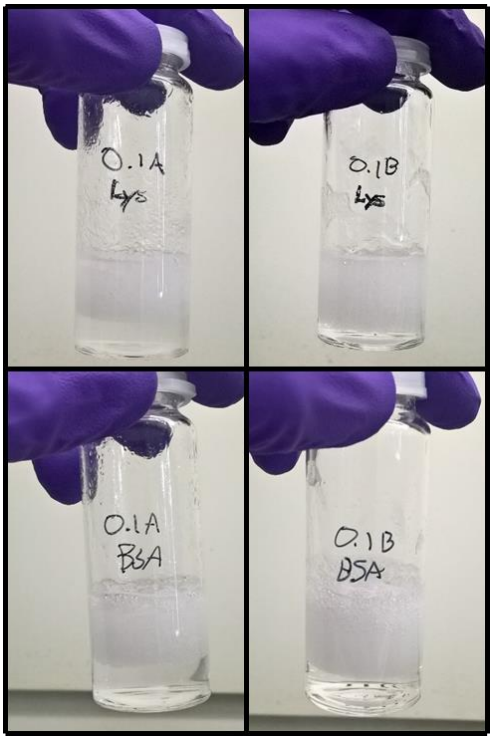

Figure 4.7 Image showing emulsions made using mineral oil and PBS with BSA and Lysozyme as the proteins and benzoyl chloride (marked A) or sebacoyl chloride (marked B) as the surfactant. The surfactant was always used at a concentration of 0.1 mg/ml and the protein concentration was kept at 10 mg/ml

Following these experiments, it was decided to focus on interfaces of lysozyme with benzoyl chloride as the pro-surfactant. The results of the oscillatory rheology experiments performed on the mineral oil interfaces are shown in figure 4.8.

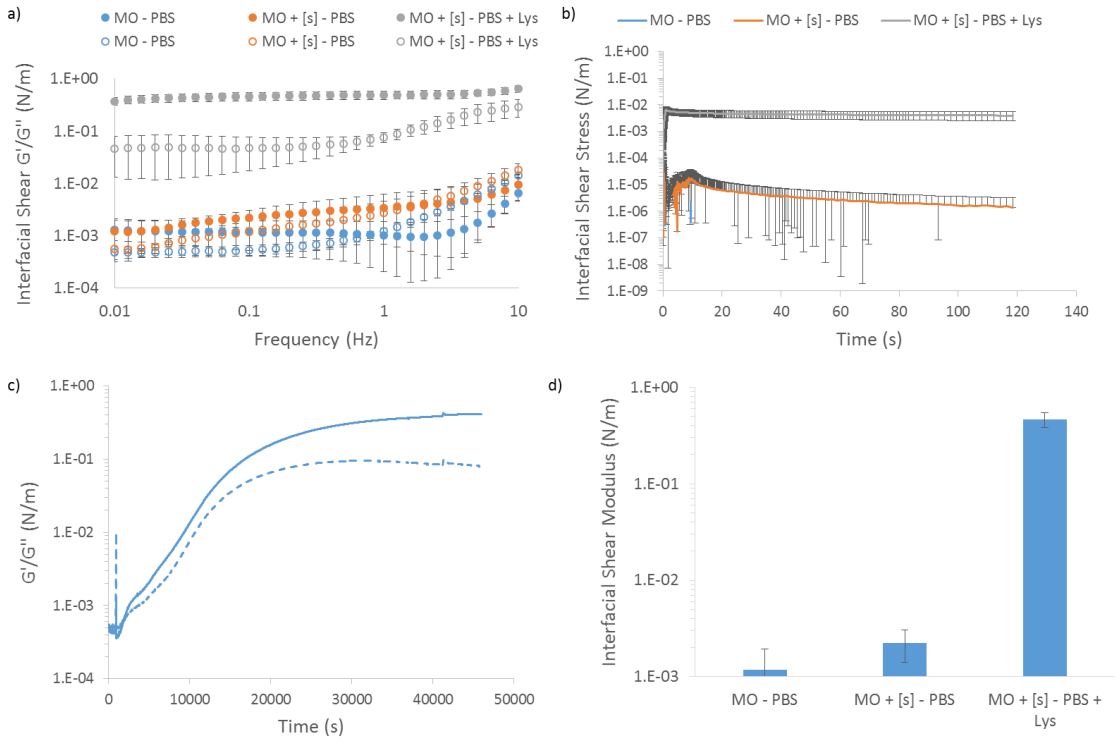

Figure 4.8 Oscillatory rheology characterisation of mineral oil – PBS interfaces by a) Oscillating frequency sweep with a oscillating displacement of 10^{-4} rad from 0.01 – 10 Hz on mineral oil – PBS interfaces with and without lysozyme (used at a concentration of 10 mg/mL) and benzoyl chloride (used at a concentration of 0.1 mg/mL)respectively, where the solid dots are G' and hollow dots are G'', b) stress relaxation data on interfaces showing the impact of protein on the relaxation profile, c) representative time sweep showing the formation of a lysozyme protein film on a mineral oil – PBS interface (solid line showing G' and the dotted line G''), d) summary of the interfacial mechanics of mineral oil – PBS interfaces comparing films with and without surfactant and lysozyme respectively. A minimum of three samples was tested per test. All error bars are standard deviations.

The interfacial oscillatory rheology data for the mineral oil – PBS interfaces with and without pro-surfactant and or protein was in good agreement with the results obtained for the fluorinated oil system, with the oil – PBS having the lowest moduli, and the addition of surfactant resulting in a marginal increase, whilst the introduction of the protein increasing the moduli by several orders of magnitude to 0.5 N/m. The frequency sweeps, in figure 4.8a, also indicates that the elastic moduli of lysozyme protein films have very little frequency dependence similar to the BSA and PLL films on fluorinated oil. Interestingly the interfacial G' of the mineral oil + [s] – PBS interface showed a linear log – log frequency dependence, while in the fluorinated system there was negligible impact from the frequency on G'. Furthermore, in the fluorinated system the interfaces without protein broke down at a frequency of around 1 Hz while

for the mineral oil they are stable up to 10 Hz. The stress relaxation curves on the mineral oil system, figure 4.8b, are in good agreement with the frequency sweeps with the protein film resulting in a very elastic film exhibiting negligible relaxation, while the oil + [s] – PBS film shows some relaxation and finally the oil – PBS interface carrying almost no load. The lysozyme films tested showed similar stress relaxation profiles to the BSA films, with 40% and 30% relaxation respectively while the PLL showed significantly greater relaxation at 70%. Stiff films with significant have been widely recorded in the literature for stiff globular proteins like BSA and lysozyme[148, 149, 160] while non-globular random coil proteins, like PLL, are typically soft hence the significantly greater relaxation seen in PLL.

Looking at the time sweeps for the deposition and unfolding of lysozyme on the mineral oil – PBS interface shows a similar steady adsorption with time to the adsorption of PLL and BSA to fluorinated oil interfaces, however the kinetics of this system are very different. For lysozyme, it takes around 12 h for the film to start to plateau whereas for both BSA and PLL the film will be fully formed in around 2 h. From figure 4.8 we see that the bulk interfacial properties of the mineral oil system are similar to those observed for fluorinated oil, with lysozyme, PLL (at pH 10.5) and BSA films having an interfacial moduli of 0.5, 2.5 and 0.6 N/m respectively. The local interfacial mechanics were then studied using the same protocol as used on the fluorinated system, as shown in figure 4.9.

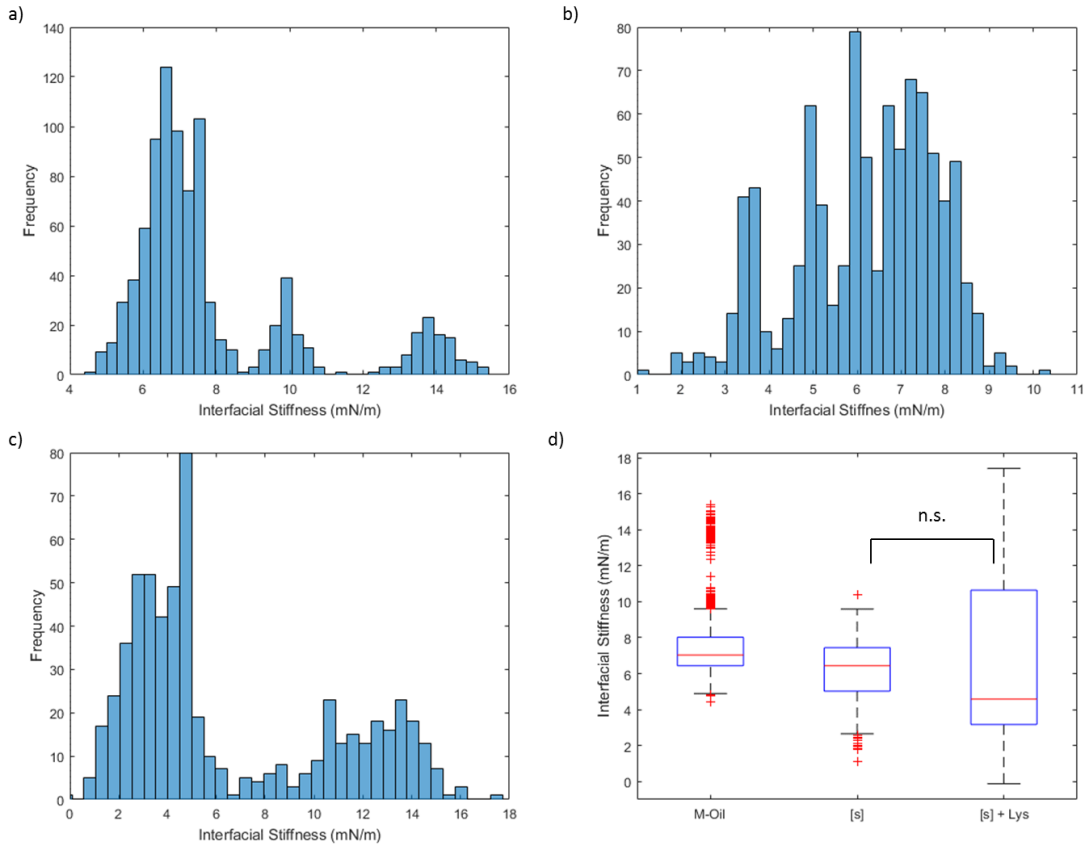

Figure 4.9 a) – c) Histograms showing the distribution of interfacial stiffness obtained by interfacial nanoindentation by AFM using a colloidal probe on mineral oil – PBS, mineral oil + [s] – PBS, and mineral oil + PBS – PBS + lysozyme interfaces respectively, formed at pH 7.4 with benzoyl chloride and lysozyme concentrations of 0.1 and 10 mg/ml respectively and d) boxplot summarising the distribution of the interfacial stiffness of the mineral oil systems, showing the spread in data for the plain mineral oil – PBS interface, mineral oil + [s] – PBS and mineral oil + [s] – PBS + lysozyme interfaces. A minimum of three samples for each condition were tested, three 1μm X 1μm areas on each sample were tested with 100 indentation curves taken at each location. The colloidal AFM tip used had a diameter of 20μm. All the data is significantly different with $p < 0.01$ unless labelled not significant (n.s.).

Results of the interfacial AFM nanoindentation on mineral oil – PBS interfaces with and without protein and or pro-surfactant are shown in figure 4.9. Figure 4.9a – c show histograms of the distribution of interfacial stiffness for mineral oil – PBS, mineral oil + [s] – PBS, and mineral oil + [s] – PBS + lysozyme interfaces respectively. While there is some variation in these results the distribution of data between scans is largely in good agreement. The addition of protein greatly increases the spread of interfacial stiffness values recorded in both the fluorinated and mineral oil systems. The reason for this is unclear, however it could be a result of the protein film deposited not being homogenous. Alternatively it could be due to the protein altering the nature

of interactions between the colloidal tip and the interface and again if the films are not homogenous the changes to the interfacial forces may vary resulting in a greater spread in the apparent stiffness.

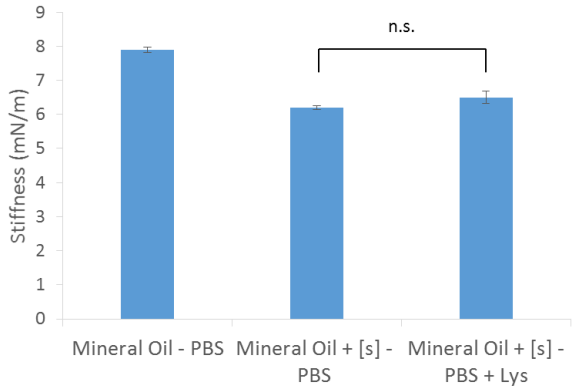

Figure 4.10 Summary of the interfacial stiffness of the mineral oil systems, showing the average stiffness of the plain mineral oil – PBS interface, mineral oil + [s] – PBS and mineral oil + [s] – PBS + lysozyme interfaces. A minimum of three samples for each condition were tested, three 1 μm X 1 μm areas on each sample were tested with 100 indentation curves taken at each location. The colloidal AFM tip used had a diameter of 20 μm.All error bars are standard errors and all the data is significantly different with $p < 0.01$ unless labelled not significant (n.s.).

A summary of the nanoindentation on the mineral oil interfaces with and without surfactant and lysozyme is shown in figure 4.10, showing that the addition of pro-surfactant to the mineral oil – PBS resulted in a significant decrease in the interfacial stiffness, as did the addition of the lysozyme compared to the plain mineral oil – PBS interface. The reduction in stiffness resulting from the addition of pro-surfactant is similar to what was seen with the fluorinated system, however the further addition of PLL resulted in an increase in the interfacial stiffness. Within the fluorinated system the addition of BSA to the oil + [s] – PBS interface still gave a weaker interface than the plain oil – PBS. The addition of PLL however gave a stronger interface, although this was more pronounced at low pH, unlike what is observed by interfacial rheology. Based on interfacial rheology results, PLL gave the stiffest interface, followed by BSA and lysozyme respectively, from this it may suggest that while the addition of surfactant reduces the surface tension and hence reduces the interfacial stiffness, recorded

by AFM, the addition of proteins increases the observed transverse stiffness of the corresponding oil droplets, and in the case of PLL, makes it significantly greater than in the absence of any protein but with surfactant. The fact that lysozyme further reduces the interfacial stiffness suggests that it may be stronger surfactant than benzoyl chloride and/or the corresponding hydrolysed benzoic acid, therefore further reducing the surface tension of the corresponding interface. Alternatively it could be due to the changes in the surface chemistry resulting in changes of interactions between the probe and interface. It has been shown that the mechanical response to interfacial colloidal nanoindentation by AFM is governed by a complex combination of electrostatic, van der Waals and surface tension forces[171, 172], in the absence of any protein film. As such to better understand what is occurring in the presence of protein films the changes to surface tension and electrostatic surface potential were investigated.

4.3.3. Characterisation of the Impact of Surfactants and Protein Deposition on Surface Tension of Liquid-Liquid Interfaces

The surface tension was next investigated given the importance it plays in interfacial mechanics. Understanding how the surface tension is changing in different conditions would potentially help lead to a better understanding of the mechanical response of the oil – PBS interfaces. The influence of the surfactants on the surface tension of the oil – PBS interfaces was then studied by doing pendent droplet experiments, as shown in figure 4.12. We observed that the drop profile clearly changed after addition of pro-surfactant. For the mineral oil samples it is a PBS droplet in mineral oil, as the PBS is denser than the oil, while for the fluorinated oil it is an oil droplet in PBS.

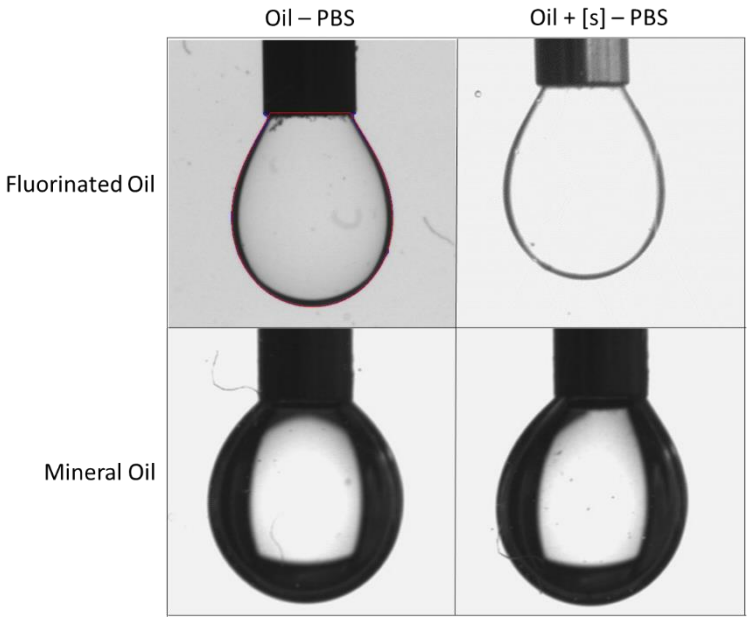

Figure 4.11 Representative pendent droplet images of fluorinated oil droplets in PBS and PBS in mineral oil with and without surfactant. The surfactant used for the fluorinated and mineral oil were PFBC and benzoyl chloride respectively at concentrations of 0.01 mg/mL and 0.1 mg/mL respectively. The image of the fluorinated oil – PBS droplet has a representative fit (red line) used to characterise the surface tension.

Figure 4.11 shows the influence of adding PLL and lysozyme to mineral oil + [s] – PBS and fluorinated oil + [s] – PBS interfaces, respectively, initially and after 2 h and 14 h for the mineral oil and fluorinated oil, respectively. The mineral oil – lysozyme was given longer for the protein film to form based on the results from the oscillatory rheology on this system. The lysozyme film on the PBS droplet in mineral oil is clearly visible after being left overnight. Furthermore there is a clear difference in the drop profile as a result of the protein being added in the case of the mineral oil droplet.

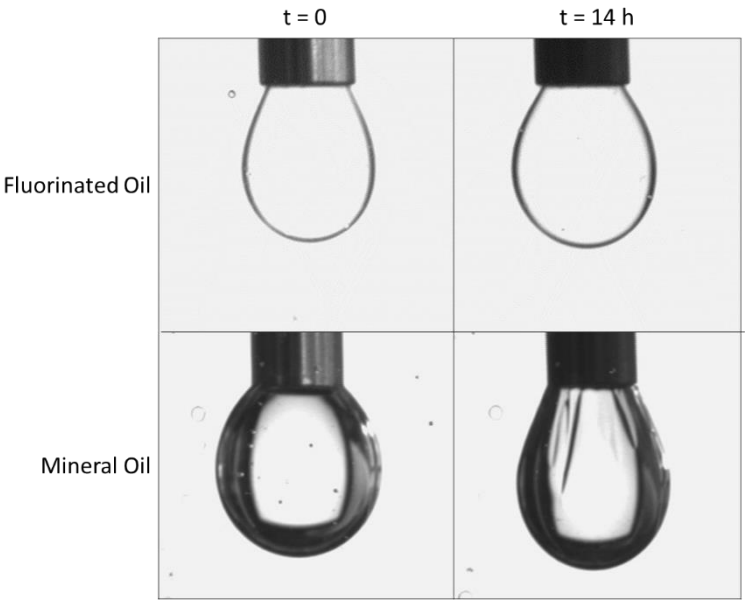

Figure 4.12 Representative pendent droplet images showing the impact of protein absorption on the drop profile initially, t = 0, and after 14 h allowing for the films to fully deposit. For the fluorinated oil PFBC and PLL were used as the surfactant and protein respectively at concentrations of .0.01 mg/mL and 0.1 mg/mL respectively. For the mineral oil 0.1 mg/mL benzoyl chloride was used as the surfactant and 10 mg/mL lysozyme was used as the protein.

A summary of the surface tension measured by pendent droplet analysis are shown in figure 4.12. It is clear that the lysozyme protein film formation is causing a significant decrease in the surface tension of the mineral oil – PBS interface, while the PLL is causing an initial slight decrease, the surface tension is recovered with time once the protein film is fully formed. It has been frequently reported that proteins adsorbed at interfaces results in a decrease in the interfacial surface tension as was found here[149, 264].

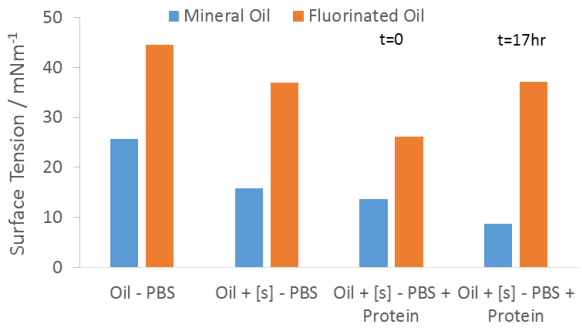

Figure 4.13 Summary of the surface tension values obtained for the mineral and fluorinated oil - PBS interfacial systems characterised, where the surfactants and proteins are PFBC and benzoyl chloride (at concentrations of 0.01 mg/mL and 0.1 mg/mL respectively) and Pll (0.1 mg/mL) and lysozyme (10 mg/mL) for the fluorinated and mineral oil systems respectively.

The addition of PFBC and benzoyl chloride to the fluorinated and mineral oils respectively resulted in similar trends with the addition of surfactant resulting in a decrease surface tension, similar to what has been found by others[265]. However the addition of lysozyme led to a further significant decrease in the surface tension in the mineral oil system the reduction in surface tension resulting from the addition of lysozyme is a phenomenon which has been regularly reported in the literature[156, 260, 261]. Based on the experimental data collected, particularly for interfacial nanoindentation, it was decided that to best understand the mechanical response to normal loading of protein films on liquid-liquid interfaces a theoretical model would be needed. In order to model the interfacial forces the surface tension forces in the absence of a protein film were initially studied.

4.3.4 Interfacial Surface Tension Force Modelling

As the nanoscale mechanics of oil – PBS interfaces is clearly complex, particularly with the introduction of complex protein films, we set out to develop a model that would quantitatively account for the impact of different parameters on AFM nano-indentation profiles. It was first decided to break down the problem into the two contributing factors, the contribution of the film and the contribution of surface ten-

sion forces. To do so, we first proposed to model surface tension forces resisting indentation and then adding the contribution of the protein films as a viscoelastic solid using FEA analysis, *via* superposition. To simplify the complexity of the surface tension forces, we initially simply introduced a linear relationship between displacement acting tangentially along the angle of the colloidal tip, where the length of the displacement is the radius of the tip at the given depth, and the magnitude of the force is proportional to the surface tension, as shown in figure 4.14. The normal force on the colloidal or pyramid AFM tip is then given by equations 4.1 and 4.2.

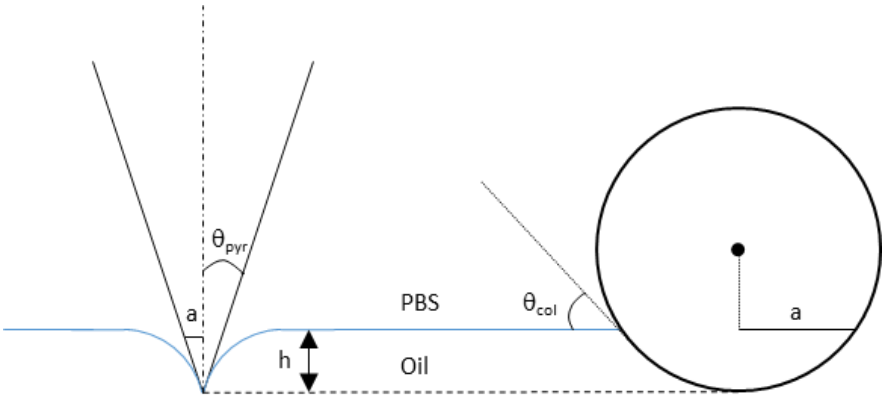

Figure 4.14 Schematic showing the initial contact assumptions for interfacial nanoindentation by AFM using a pyramid indenter (left) and a colloidal probe (right).

$$F_{n,colloid} = 2\gamma\pi \sin\theta_{col} \sqrt{h(2a-h)} \quad [4.1]$$

$$F_{n,pyramid} = 2\gamma\pi h \tan\theta_{pyr} \sin\theta_{pyr} \quad [4.2]$$

where, γ is the surface tension, h is the depth of indentation, a is radius over which the surface tension forces are acting and θ_{pyr} and θ_{col} are the angles at which the surface tension is acting for a pyramidal and colloidal tip respectively, as shown in figure 4.14. Based on these calculations the surface tension forces were calculated for a given indentation depths. However what quickly became apparent was that the surface tension forces found based on these assumptions were massive overestimates,

and in order to get surface tension force responses that were comparable to experimental data the surface tension value needed to be orders of magnitude lower than the values found experimentally or from the literature. As such it was clear that the surface tension modelling needed to be rethought.

Further investigating the interfacial force at the nanoscale revealed that the initial assumptions neglected to take into account short range van der Waals and electrostatic forces, which can result in significant attractive or repulsive interactions between the tip and interface and therefore significantly impact the indentation profile. A previous model of interfacial mechanics, used to model AFM nanoindentation of oil interfaces, was developed to take such interactions into account, although not introducing elastic films at the corresponding interfaces[168, 171, 172]. In such model, the indenter tip and bottom phase never come into contact, i.e. there is always a thin aqueous fluid film between the bead and the oil phase, as shown in figure 4.15. This assumption can only be experimental verified in the total absence of adhesion. The film profile is defined by the augmented Young – Laplace equation[171, 172, 248], which is essentially a pressure balance between the surface tension forces needed to hold a certain shape, the gravitational force and the internal drop pressure. When the surface tension dominates over gravity the contribution from gravitational forces becomes negligible, this is the case when the length scale is significantly below the capillary length. The contribution of the internal drop pressure also becomes negligible if the drop is large relative to the capillary length[171, 172, 248, 256]. The augmented Young – Laplace equation can be simplified as a function of the interfacial gap, as shown in equation 4.3.

$$D'' + \frac{1}{t}D' - \left(2 - \frac{a\Pi(D)}{\gamma}\right)D_0 = 0 \qquad [4.3]$$

Where D is the distance between the AFM probe and oil phase, as shown in figure 4.15, a is the probe diameter, γ is the surface tension and Π is the disjoining pressure. The forces between the indenter colloid and the oil droplet here are related using the Derjaguin approximation. The Derjaguin approximation relates the force balance between two spheres to the interaction energy per area of parallel plate. The disjoining pressure is the rate of change of the interaction energy over the plate separation. The disjoining pressure has been shown to be the sum of a number of forces, here only Van der Waals and electrostatic forces are considered[171, 248].

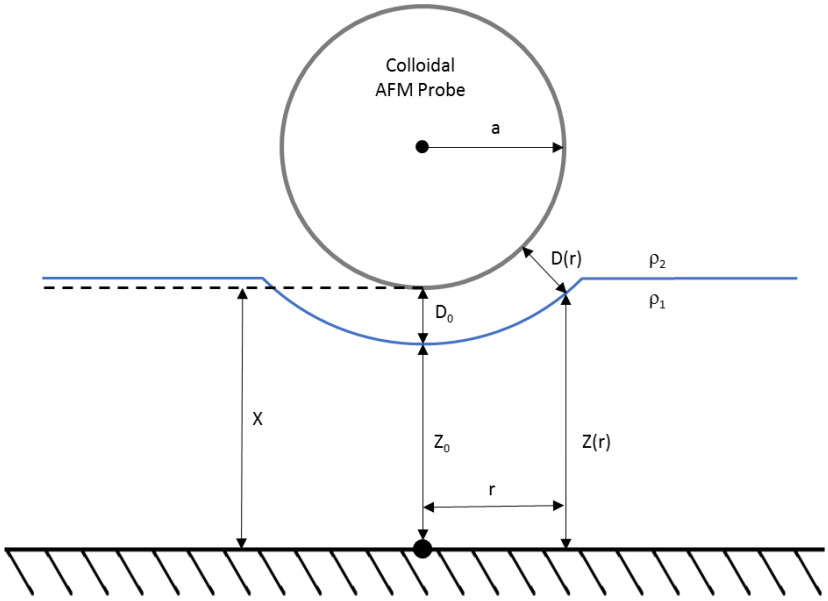

Figure 4.15 Schematic of the AFM probe – interface mechanics during nanoindentation experiments

Characterising the interfacial surface tension using the augmented Young – Laplace treats the fluid interface as a zero thickness surface and describes the pressure balance using a non-linear partial differential equation. From the augmented Young – Laplace we can see that the disjoining pressure is a critical factor in the shape profile. The disjoining pressure can include many short range forces, however in this study it has been simplified to the combination of the electrostatic interaction forces and the van der Waals forces, as described in equations 4.4 and 4.5 below. It can also include

factors such as hydrodynamic drainage and hydrophobic interactions[172]. The electrostatic double layer forces are modelled using the DVLO theory with the Debye – Huckel approximation allowing for surfaces with dissimilar surface potentials, and is given by equation 4.4.

$$\Pi_{el} = \frac{\varepsilon\varepsilon_0 k^2[2\psi_{1o}\psi_{2o}(e^{-kD} + e^{-3kD}) + (\psi_{1o}^2 + \psi_{2o}^2)e^{-2kD}]}{(1 - e^{-2kD})^2} \qquad [4.4]$$

Where, ε is the relative permittivity, ε_0 is the permittivity of free space, k is the Debye length and ψ_{1o} and ψ_{2o} are the surface potentials of the indenter and oil respectively. The van der Waals forces are then given by,

$$\Pi_{vdW} = \frac{A}{6\pi D^3} \qquad [4.5]$$

Where A is the Hamaker constant which is of the order of 10^{-20} J. The augmented Young – Laplace can then be solved once the disjoining pressure is defined for the conditions in question. From the solution to the augmented Young Laplace the force on the indenter probe and the piezo electric crystal movement can be obtained according to equations 4.6 – 4.10.

$$G = \frac{aD_0}{\gamma}\int_0^\infty t\Pi\big(D(t)\big)dt \qquad [4.6]$$

$$H = \frac{aD_0}{\gamma}\int_0^\infty tln(t)\Pi\big(D(t)\big)dt \qquad [4.7]$$

$$X(D_0) = X_\infty + D_0 + H(D_0) + G(D_0)(1/2\ln(D_0) + B) \qquad [4.8]$$

$$Where, B = C + ln\left(\frac{a^{1/2}}{2\lambda}\right) \qquad [4.9]$$

$$F(D_0 = 2\pi\gamma G(D_0) \qquad [4.10]$$

Where, C is Euler's constant = 0.57721566, λ is the capillary length, X is the distance from the substrate to the lowest point of the colloidal probe, B is a constant

dependent on the properties of the isolated interface, and *t* is non-dimensional radius, such that $t = \frac{r}{\sqrt{D_0 a}}$. Here, *G* and *H* are the pressure difference across the interface within the deformation and externally respectively. The equations for *G* and *H* are repeated until they converge at the edge of the deformation. Using these calculations the force on the indenter probe can be plotted against the piezo crystal movement and hence compared to experimental data. The model used here is take from the work by Chan *et al.* who give the full derivation of this solution in their paper published in 2001[171].

Figure 4.16a shows how the shape of the disjoining pressure curve can vary with changing surface potential, illustrating how small changes in the surface potential can result in significant changes in the disjoining pressure profile, and hence potentially big differences in the interfacial stiffness. While figure 4.16b shows how those changes to the surface potential influence the force – piezo movement curves, and figure 4.16c shows how varying the Debye length can vary the force – piezo crystal movement relationship. The full list of variable used in these models can be seen in table 4.2 and 4.3.

Table 4.2 List of constants used for modelling changes to the interfacial force with varying surface potentials

Varying ψ_{01}/ψ_{02}			
Relative Permittivity of water	**Permittivity of free space**	**Debye Length**	**Hamaker Function**
ε_r	ε_0 (N/V^3)	k^{-1} (nm)	A (N.m)
80	8.85 X 10^{-12}	96.2	4.00 X 10^{-20}

Table 4.3 List of constants used for modelling changes to the interfacial force with varying Debye length

Varying k^{-1}				
Zeta Potential		**Relative Permittivity of water**	**Permittivity of free space**	**Hamaker Function**
Ψ_{01} (V)	Ψ_{02} (V)	ε_r	ε_0 (N/V^3)	A (N.m)
-0.02	-0.02	80	8.85 X 10^{-12}	4.00 X 10^{-20}

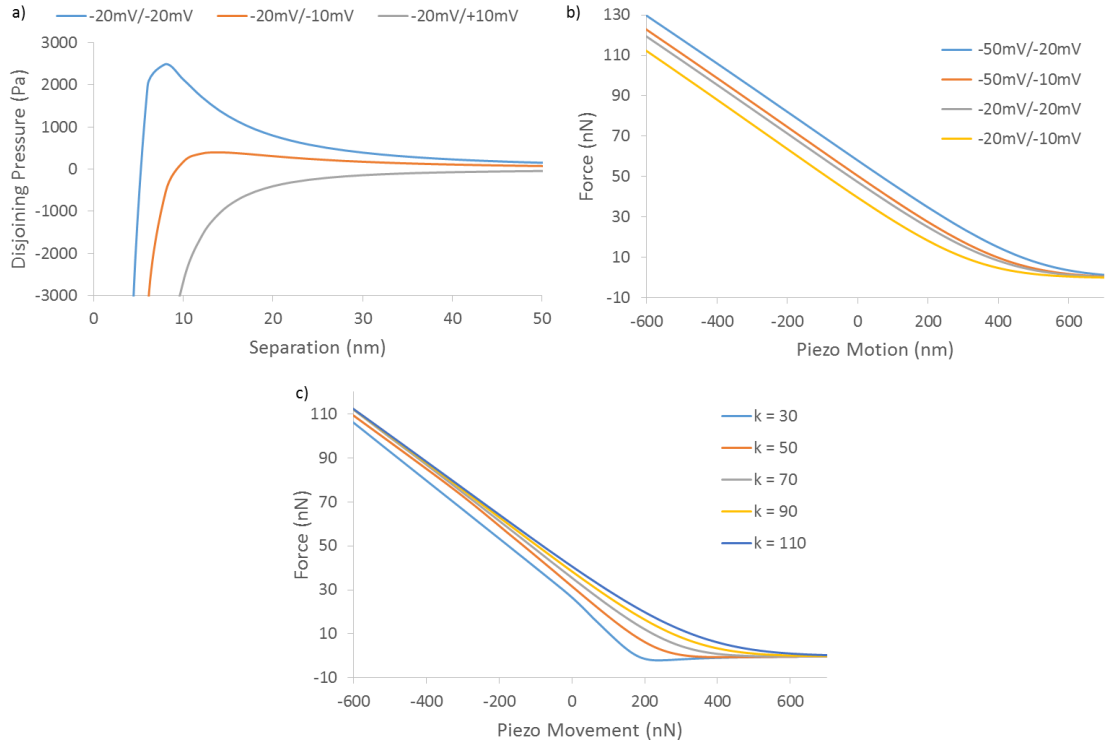

Figure 4.16 a) graph of the disjoining pressure against interfacial separation for varying surface potentials, b) and c) force against piezo crystal motion with varying surface potentials, and Debye length respectively with details of the values used to model the data shown in table 4.2 and 4.3

These traces illustrate the sensitivity of interfacial mechanics to small variations in the surface chemistry and oil/PBS fluid composition. As such, when studying interfacial mechanics with colloidal nanoindentation by AFM, it is not trivial to study the impact of nanofilm assembled at the corresponding interfaces. As such, values of the surface potential for the PLL, BSA and lysozyme interfaces were obtained. For the lysozyme this was done by taking the zeta potential of oil – PBS emulsions coated with the proteins, and the values obtained were in good agreement with values found in the literature, -4.5 mV found via experimentally compared to -10 mV[266] from the

literature. However for the PLL and BSA the droplet size of the emulsion was too large and as a result very unreliable results were obtained on the surface potential of the emulsion droplets. As PLL and BSA are very thoroughly characterised materials it was decided to take the surface potential based on values in the literature and were found to be of the order of 10 – 40 mV[267] and -13 mV[268] respectively.

An initial study to model the interfacial mechanics of fluorinated oil – PBS and mineral oil – PBS interfaces was first carried out using the values of surface tension and surface potential obtained by pendent droplet and zeta potential experiments. The results of this modelling compared with experimental data on the mineral and fluorinated oil systems without protein are shown in figure 4.17, the Hamaker Constant, dielectric permittivity and Debye length were all kept constant using the same values shown in table 4.2.

Table 4.4 List of constants used for modelling changes to the interfacial force for interfaces with fluorinated oil and mineral oil with and without surfactant.

Interface	Zeta Potential		Surface Tension
	Ψ_{01} (mV)	Ψ_{02} (mV)	γ (mN/m)
fOil - PBS	-10.0	-5.0	44.5
fOil + [s] - PBS	-10.0	-5.0	37.0
mOil - PBS	-20.0	-4.5	25.0
mOil + [s] - PBS	-20.0	-4.5	16.0

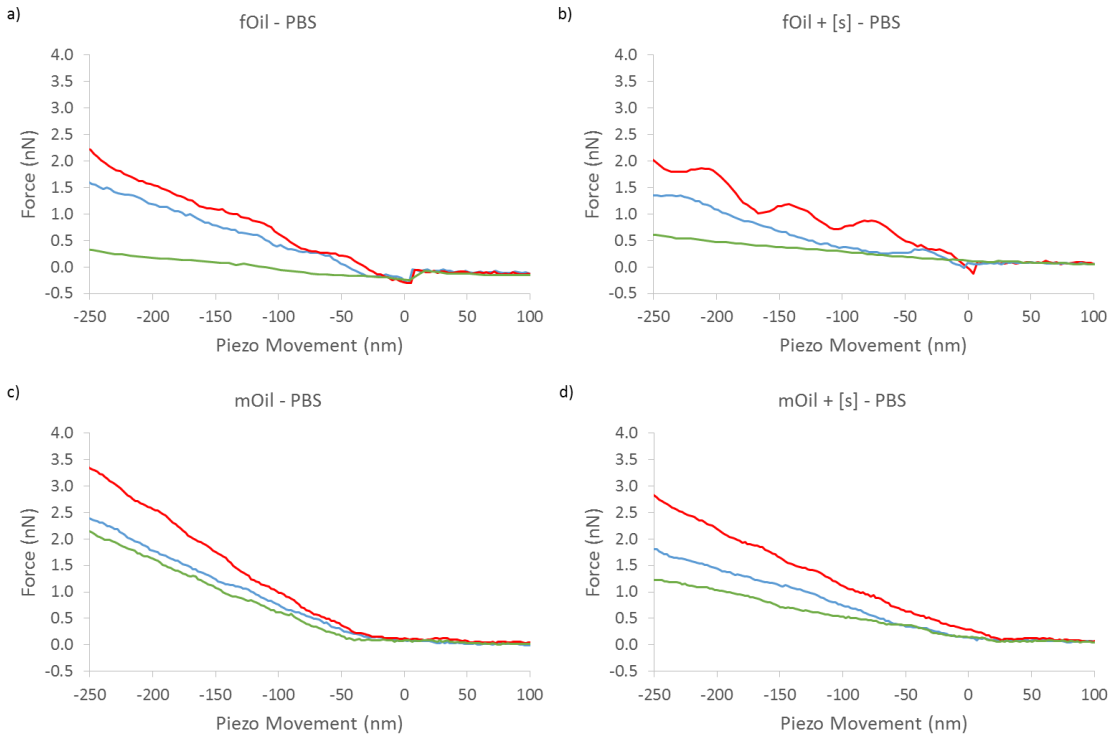

Figure 4.17 Comparison between representative experimental Force – Piezo movement AFM curves to modelled results using the analysis outlined for, a) Fluorinated Oil – PBS, b) Fluorinated Oil + [s] – PBS, c) Mineral Oil - PBS and d) Mineral Oil + [s] – PBS interfaces. Red lines show representative curves for the upper quartile for each of these conditions, green for the lower quartile and blue the average. The modelled data is shown by the black dotted line with yellow error bars showing the standard error of the estimate. Details of the values for the variables used for the numerical model are shown in table 4.4.

From the results shown in figure 4.17, it is clear that the analytical model used for the Mineral and Fluorinated Oil systems are good approximations with the experimental data for the conditions tested without protein. Figure 4.18a - d show the results of our calculations, compared to representative experimental data along with representative curves for the upper and lower quartile, for the Mineral/Fluorinated Oil – PBS and Mineral/Fluorinated Oil + [s] – PBS interfaces. For all of these conditions the model is very accurate at large indentation depths, with the modelled response overlapping very well with the experimental data. In both of these cases at the point where initial 'contact' is felt there is a marked difference between the experimental data and predictions from the model as, in both cases, the initial response is overestimated by the model.

The modelled data shown in figure 4.17 shows very good agreement with the experimental data for all the conditions tested. However it is clear that the sample to sample variability is significant, shown by the difference between representative upper and lower quartile experimental AFM data. This suggests that the spread in the data is a result of the experimental set up or technique. From figures 4.4g and 4.6 it can be seen that where the adhesion seen by AFM is lowest, in the cases where BSA is present, the spread in the data is also lowest. This suggests that the large spread in the experimental data may be resulting from changes in the contact between the interface and the colloid.

The modelled results here only takes into account the interfacial mechanics, according to the model outlined by Chan et al[171], and hence does not include any contribution from the protein film. In order to quantify the contribution of the protein film to the mechanical response under nanoindentation it was modelled using an FEA model.

4.3.5 FEA Modelling of the Mechanical Response of Protein Films under Normal Loading Conditions

The total force acting on the probe was considered to be the sum of the surface tension force and the resistance to deformation from the protein film. It was decided to model the protein film mechanical response using FEA analysis as an axisymmetric viscoelastic membrane, using the viscoelastic profile obtained from the interfacial rheology. Figure 4.18 shows the normalised (normalised as this is how it is required by ABAQUS) relaxation profiles used to govern the viscoelasticity modelled. The elastic modulus used was the shear moduli obtained by interfacial rheology. Modelling the film as a membrane assumes that the film cannot carry any bending load and hence only resists load through stretching, so the shear moduli was used. As the radius of

the oil droplet was very large compared to the AFM tip (ratio > 1000), the interface was modelled as a flat film and the length of the film used was the capillary length of the interface as this is considered to be the length over which the displacement dissipates. The contact between the colloid and the film was assumed frictionless, which, if a fluid film remains between the indenter and the interface can be considered the case.

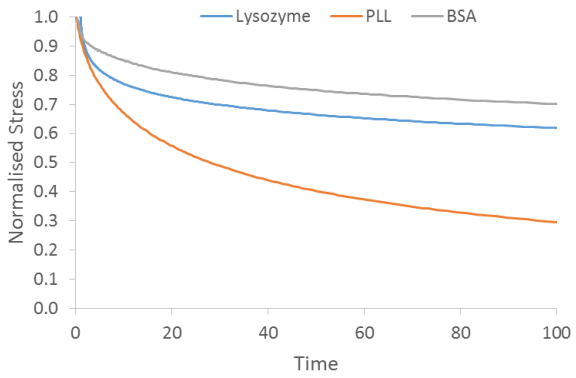

Figure 4.18 Normalised stress relaxation profiles for the lysozyme (on mineral oil) and PLL and BSA (on fluorinated oil) films used to model their viscoelasticity in ABAQUS

The results of this FEA analysis compared to representative experimental data are shown in figure 4.19. Here we see that the total force measured experimentally is greater than resistance offered by any of the protein films studied. However, as the spread in the experimental data is large this is not the always the case for lysozyme and PLL. The reasons behind the large spread in data are not clear, however, it is clear that the interfaces at which the proteins bind are sensitive to small changes in surface properties. As such there may be significant sample to sample variability resulting from seemingly insignificant changes to the surface chemistry, protein film or aqueous phase. Furthermore, there is clear adhesion in the AFM traces, particularly in the absence of any protein and with the addition of PLL. The adhesion could be causing

changes to the contact area which are resulting in significant scan to scan variability. Interestingly the BSA films resulted in no adhesion to the indenter, this could be a result of the negative surface potential of both BSA and silicon beads resulting in purely repulsive forces that ensured no contact between the tip and the protein film. The formation of these protein films could also be resulting in heterogeneity resulting from the manner in which the films are unfolding and binding.

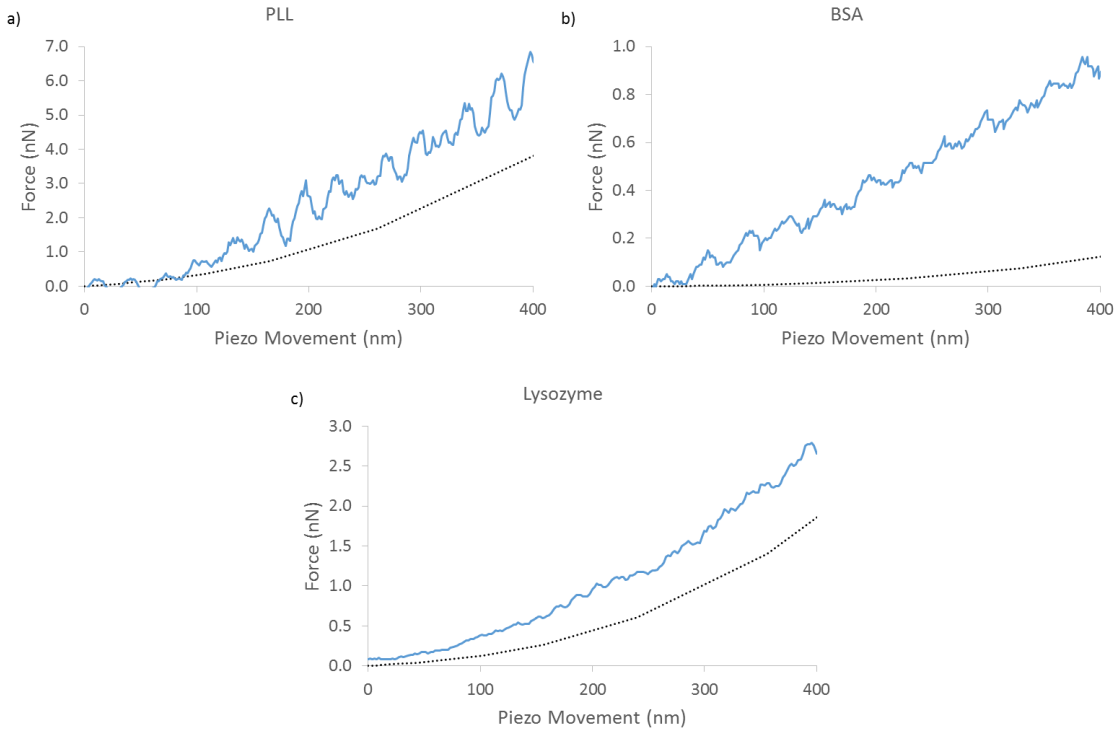

Figure 4.19 Comparison between representative experimental data (blue line) and the theoretical viscoelastic response of film membranes to colloidal indentation for a) and b) PLL and BSA films deposited on fluorinated oil at 0.1 and 1 mg/mL concentration respectively with PFBC as the surfactant at 0.01 mg/mL and c) lysozyme (10 mg/mL) on mineral oil with 0.1 mg/mL benzoyl chloride

The fact that figure 4.19 shows an underestimate suggests that the total resistance to indentation results from the combined interfacial surface tension forces and the film mechanics combined. Finally the combined theoretical response to indentation of protein films at liquid-liquid interfaces is shown in figure 4.20, where the force obtained by AFM is superimposed with interfacial forces using the analytical model outlined in section 4.3.4. The values of surface potential and tension used to model

the interfacial response for these fits is shown in table 4.5, the values for Debye length, relative permittivity and Hamaker constant are the same as those in table 4.2.

Table 4.5 List of constants used to fit the modelled interfacial surface tension force combined with the protein film forces to the experimental data

Interface	Zeta Potential		Surface Tension
	Ψ_{01} (mV)	Ψ_{02} (mV)	γ (mN/m)
PLL	-10	-10	25
BSA	-10	-5	15
Lysozyme	-15	-4.5	10

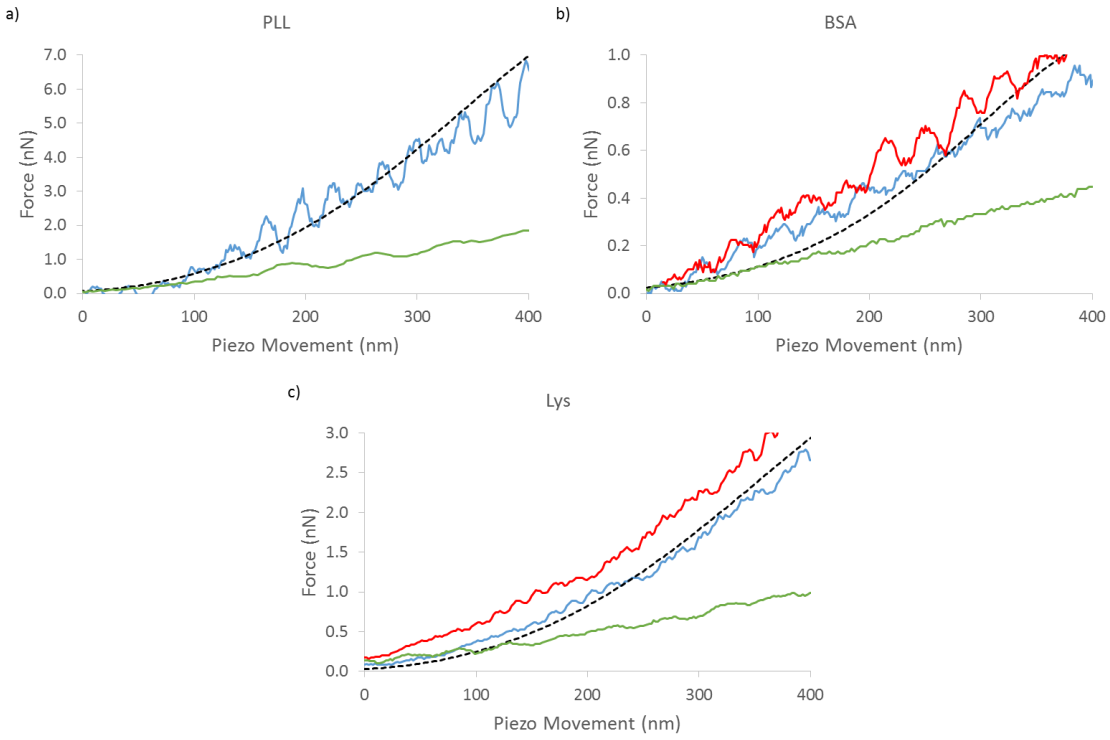

Figure 4.20 Comparison between representative experimental data for a) PLL, b) BSA and c) Lysozyme to the modelled response, where the modelled response consists of the superposition of the film forces obtained from FEA modelling with the theoretical interfacial surface tension forces obtained using the method outlined is section 4.3.4. Red lines show representative curves for the upper quartile for each of these conditions, green for the lower quartile and blue the average. The modelled data is shown by the black dotted line with yellow error bars showing the standard error of the estimate. Details of the values for the variables used for the numerical model are shown in table 4.5. Note: for PLL the upper quartile is not included as the overlap between the average and the upper quartile made it difficult to read the graph.

From figure 4.20 it can be seen that the fits for all the cases studied are in good agreement with the experimental data. The range in the experimental data is represented by the interquartile range, where in figure 2.1, the red curves are representative

upper quartile curves and the green lower quartile. In order to gain a better understanding into why the experimental data is so spread the effects of changes to the surface potential, surface tension and storage modulus on the theoretical model were investigated as shown in figures 4.21, 4.22 and 4.23.

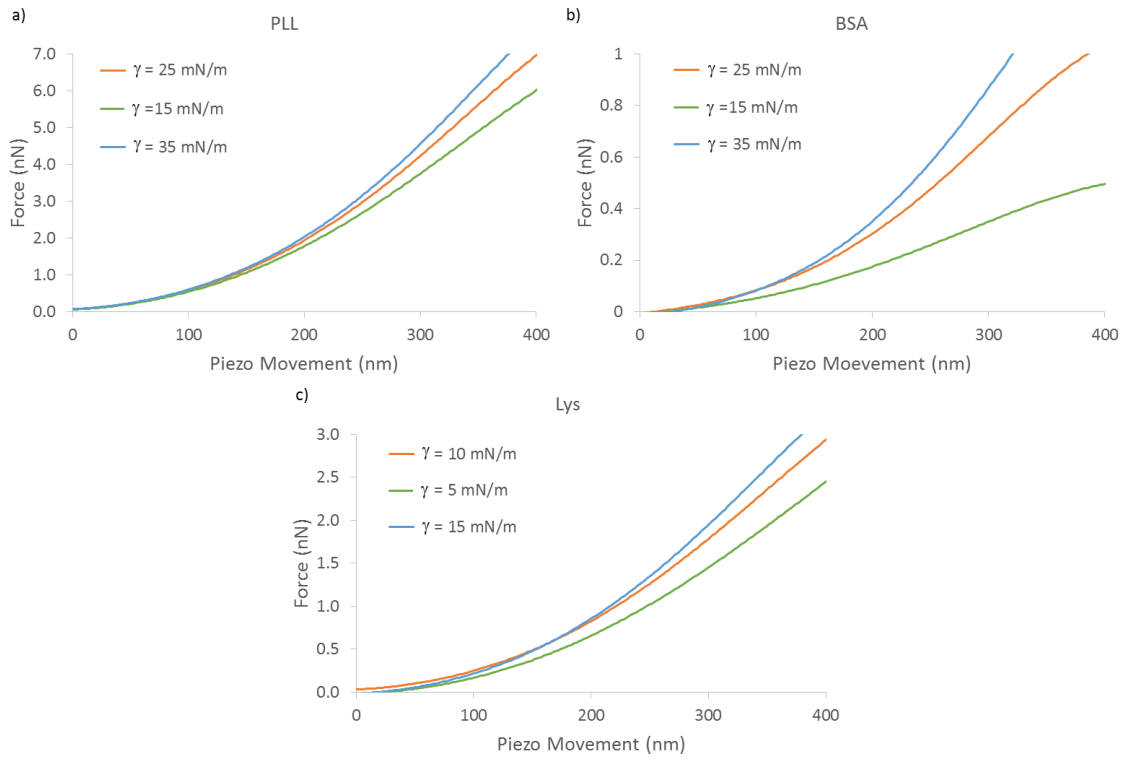

Figure 4.21 Effect of changing the interfacial surface tension on modelled data for a) PLL b) BSA and c) Lysozyme protein films deposited at oil-PBS interfaces (mineral oil in the case of lysozyme and fluorinated oil for BSA and PLL). The orange curves here are the same as the fits shown in figure 4.21 and the blue and green curves show theoretical values with varying surface tension according to the legend.

Figure 4.21 shows how varying the interfacial surface tension, γ, varies the modelled force-displacement response for PLL and BSA deposited on fluorinated oil-PBS and lysozyme deposited at mineral oil-PBS interfaces. The impact on varying the surface tension has the greatest impact on the BSA curves. This is perhaps not surprising as BSA had the lowest interfacial shear modulus of the three proteins studied and as a result the contribution of interfacial surface forces was greatest for BSA. PLL

and lysozyme show some sensitivity to changes in the surface tension but only modestly. The effects of varying the surface potential were next examined as shown in figure 4.22.

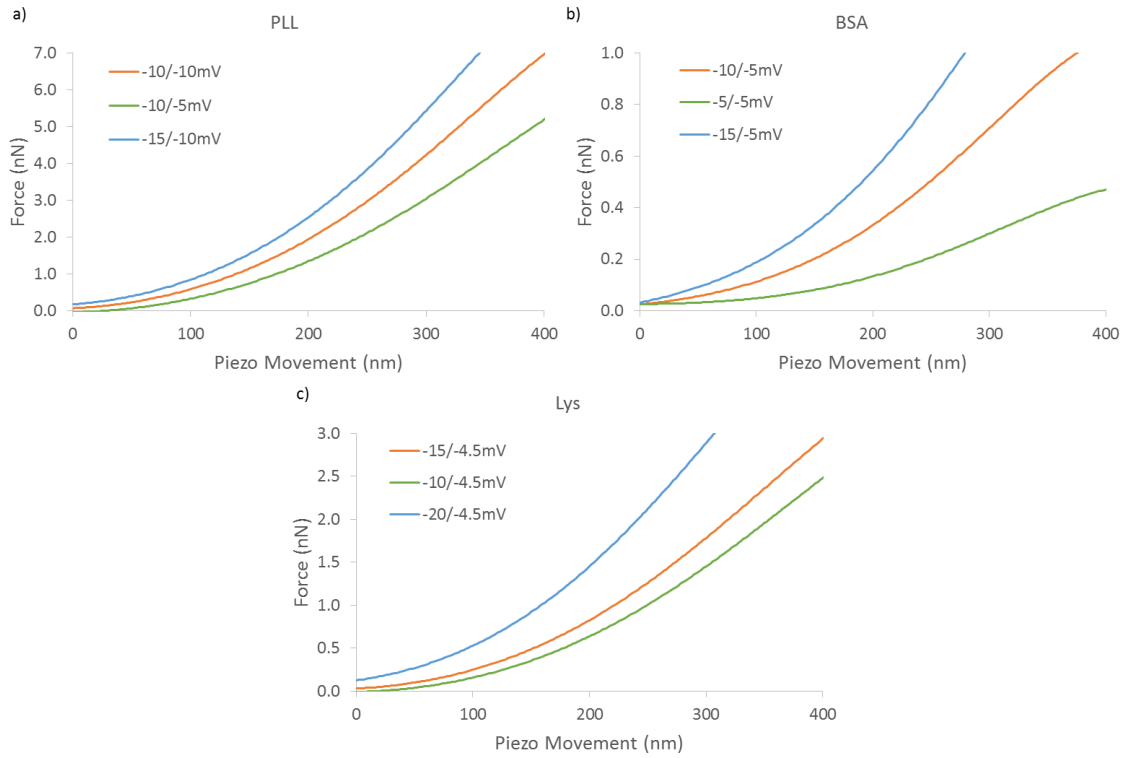

Figure 4.22 Effect of changing the surface potential on modelled data for a) PLL b) BSA and c) Lysozyme protein films deposited at oil-PBS interfaces (mineral oil in the case of lysozyme and fluorinated oil for BSA and PLL). The orange curves here are the same as the fits shown in figure 4.21 and the blue and green curves show theoretical values with varying surface potential according to the legend.

Figure 4.22 shows how varying the surface potential varies the force displacement response for PLL, BSA and lysozyme films deposited at oil water interfaces. From figure 4.23 it can be seen that by varying the surface potential quite modestly, by only 5mV, the theoretical response changes significantly. Sensitivity to the surface potential could explain the wide range in values obtained experimentally particularly in the case of PLL, where the spread in data was greatest. Again here it can be seen that the impact on the BSA films is greatest which is understandable as the interfacial surface tension forces account for a far greater proportion of the force contribution in this case due to the relatively low interfacial shear modulus of BSA films. As the

surface potential is linked to the charge of the surrounding fluid this may suggest that modest changes in the salt concentration of the surrounding fluid could result in significant changes to the interfacial mechanics. Finally we examined the impact of varying the shear moduli used in the FEA model as shown in figure 4.23.

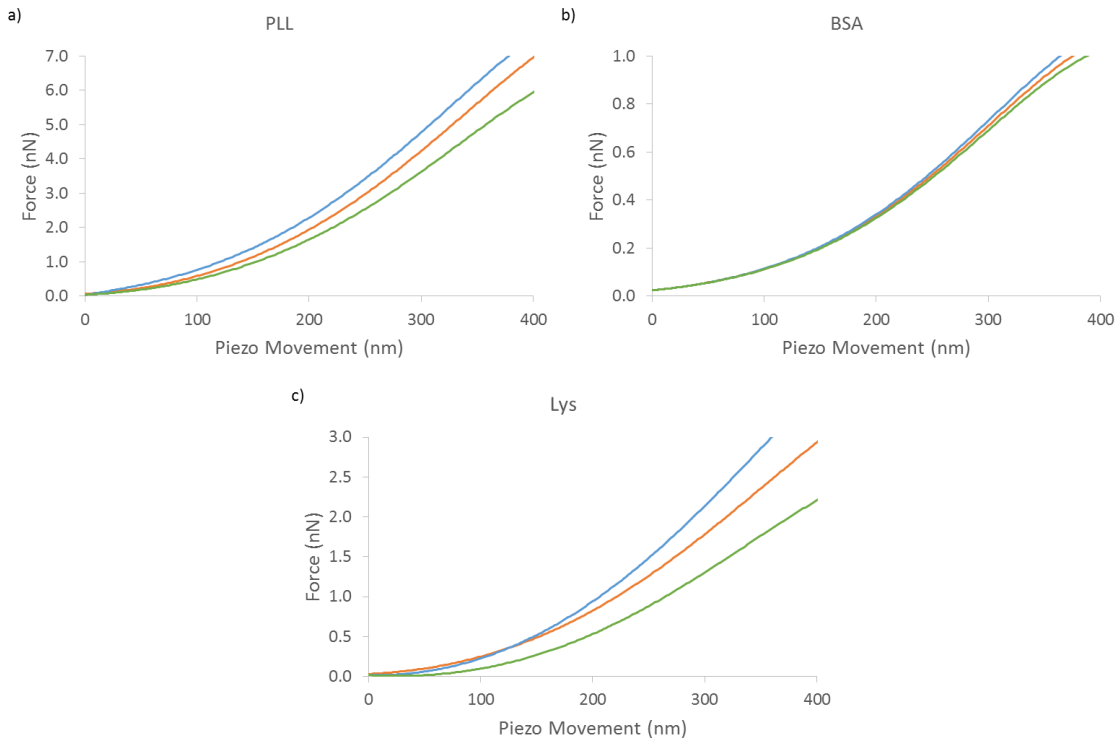

Figure 4.23 Effect of changing the shear moduli used in the FEA on modelled data for a) PLL b) BSA and c) Lysozyme protein films deposited at oil-PBS interfaces (mineral oil in the case of lysozyme and fluorinated oil for BSA and PLL). The orange curves here are the same as the fits shown in figure 4.21 and the blue and green curves show theoretical values with the modulus increased or decreased by 20% respectively.

Figure 4.23 shows the impact of changing the shear moduli used to model the film forces in the FEA model for PLL, BSA and lysozyme. The blue curves are with a 20% increase and the green a 20% decrease in the shear moduli. Here the impact on the BSA curves is negligible, which is expected due to the overall low modulus of the BSA films and hence their modest contribution to the overall interfacial mechanics. What is apparent from figures 4.21 – 4.23 is that the overall film mechanics at interfaces with proteins adsorbed is clearly sensitive to numerous factors. Small changes

to a combination of factors could therefore result in large changes to the response observed experimentally which could explain the large spread in data we obtained.

However there are certainly limitations and assumptions used in this model that need to be investigated further. First, when modelling the interfacial surface tension forces the force response is based on the film thickness, or gap, between the probe and oil droplet[171, 172]. This was not monitored in our experiments and as a result could be a source of inaccuracies in the models used. The interfacial surface tension model used here also only considers DVLO forces in the disjoining pressure, ignoring any contribution from non-DVLO forces like, hydrodynamic or hydrophobic interactions[171]. These forces may be playing a significant role in the nature of the tip-oil drop interactions and should be investigated further in the future. The contribution of the protein film forces is perhaps also too simplistic, assuming that the forces combine simply by superposition needs to be further investigated and justified. Finally, the introduction of the protein film potentially leads to the introduction of a second interface, where there would be the interface between the indenter tip and the film and a second interface between the film and the underlying oil droplet. This could have a significant impact on the indenter-droplet film profile and hence the overall mechanical response.

That being said combining the film forces modelled by FEA with the surface tension forces modelled gave curves in very good agreement with the experimental data and the analytical model in the absence of protein was in excellent agreement with experimental data. While there is certainly work still to be done to both refine the model and justify some assumptions made it is a promising first approximation and lead to some interesting results. The initial motivation behind this study was to

better understand why it was that the trends seen in the mechanics of proteins deposited at liquid-liquid interfaces was so different when testing with oscillatory interfacial rheology compared to interfacial nanoindentation by AFM. When testing by oscillatory rheology the deposition of protein resulted in an extremely large increase in interfacial shear moduli, by 4-5 orders of magnitude in some cases, however when tested by nanoindentation the presence of proteins appeared to be softening the interfaces. The use of the model developed has shown that this may be a result of complex mechanics seen at interfaces. By adding protein films there was also a surfactant effect resulting in a softening of the interface, as has been shown for other proteins[149], as a result when the proteins are deposited they form a viscoelastic cross-linked film however the overall normal stiffness of the interface is decreased due to the surfactant effect. Hence the decrease in interfacial stiffness observed by nanoindentation in the presence of BSA and lysozyme films and the lack of change in the presence of PLL. Hence a combination of mechanical and chemical forces occurs when proteins unfold at the interface. With the model developed here utilising nanoindentation by AFM these forces can be separated and their relative contribution to the observed mechanics found albeit not exactly. The overall result is that when testing by nanoindentation it is like having a soft substrate, while the interfacial rheology doesn't deform the interface in a way that results in a change in surface area and as a result only the viscoelastic film contributes to the mechanical response.

4.4 Conclusions

The aim of this chapter was to characterise the effect of adding protein films at liquid-liquid interfaces on the macroscale and localised interfacial mechanics. The interfacial mechanics of liquid-liquid interfaces was studied by oscillatory interfacial rheology and interfacial nanoindentation by AFM and the proteins studied were PLL,

BSA and lysozyme. As expected the introduction of protein films greatly increased the mechanical strength of the interfaces when studied by oscillatory rheology, with the interfacial shear storage moduli increasing by up to 5 orders of magnitude. However, the protein films had a very different impact on the mechanics as studied by colloidal nanoindentation. Here it was found that the addition of proteins either had no significant impact on the interfacial mechanics or resulted in weakening the mechanical response. In order to better understand these finding it was decided to model the interfacial mechanics of proteins adsorbed at interfaces.

In developing the model to represent proteins adsorbed at interfaces it was decided to model the mechanical response as the superposition of the film forces acting on the protein and the interfacial surface tension forces. The film forces were obtained by FEA modelling the protein films as viscoelastic membranes. While the interfacial surface tension forces were modelled according to the model developed by Chan *et al*[171]. This model showed that the interfacial mechanics is a complex force resulting from a combination of DVLO and non-DVLO forces. Using the analytical model to model the interfaces in the absence of any protein gave excellent agreement, while combining it with the film forces obtained by FEA was also in very good agreement for the PLL, BSA and lysozyme protein films.

Based on these modelled result it became apparent that when testing by oscillatory rheology the clearly measured increase in interfacial moduli resulting from the addition of proteins results overwhelmingly from the film mechanics. However when testing in by nanoindentation the surface area changes result in significant force response by interfacial surface tension forces. The addition of proteins and surfactants then plays a significant role and weakens the interface hence why we get very different trends comparing nanoindentation to oscillatory rheology.

In conclusion we found that interfacial mechanics are clearly the result of a complex combination of forces and interactions. When testing by nanoindentation the contribution of the interfacial surface tension forces must be considered in order to fully understand the relative contributions to the overall mechanical response. The addition of proteins to interfaces changes many important factors which define interfacial forces and hence must be carefully monitored and controlled in order to understand the mechanical strength of protein adsorbed interfaces.

Chapter Five

Conclusions and Outlook

Here a brief conclusion of the findings of this thesis will be given and a discussion of the outlook and future work from this research project

5.1 Conclusions

In this thesis we first studied the mechanical properties of soft biomaterials across different length scales. It has been found that soft materials, like PDMS, show significant discrepancies between their bulk and nanoscale mechanical properties. As a result a side-by-side comparison of the mechanics of soft materials at different length scales was performed. The techniques used for these analyses were, microindentation, oscillatory rheology and nanoindentation by AFM, and PAAm, PDMS and CMC hydrogels were chosen to be tested. This study highlighted the importance of surface adhesion and the resulting changes in contact area, and sample microstructural heterogeneity as key parameters for the mechanical characterisation of ultra-soft substrates at the nano- to micro-scale. Specifically it was shown that when mechanical testing on the micro to nano scale the surface chemistry of the testing geometry and the sample being tested plays a significant role. In the case of soft PDMS where adhesion was present it resulted in significant changes to the contact mechanics, giving the appearance of a much higher moduli compared to the bulk properties, however this discrepancy can be mitigated so long as measures are taken both to minimise adhesion and by using suitable models to characterise the data. On the other hand, where there is significant heterogeneity materials may have locally much stiffer domains within a

soft matrix which may give rise to greater stiffness on a nanoscale, as was shown comparing the CMC gels with and without silicon nanoparticles.

The impact of inorganic divalent cationic and organic cationic polyelectrolyte cross-linkers on the rheological and adhesive properties of CMC hydrogels was next studied. The inorganic cations used in this study were Sr^{2+} and Ca^{2+}, and caused the CMC to chains to collapse into complexes, resulting in no significant change in the bulk rheological properties but an increase in the adhesive strength. The introduction of organic polyelectrolytes caused complex coacervation with the CMC polymer chains, where some CMC chain bridging occurred, but the interactions between the polyelectrolytes and CMC chains caused complexes to be form, resulting in polymer rich complexes to form within a more dilute matrix. The introduction of organic polyelectrolyte cross-links failed to increase the bulk mechanical properties studied by rheology but did increase the adhesive strength. Most interestingly here it was shown how, despite not changing the bulk mechanical properties of the gels, the structural changes resulting from the organic and inorganic crosslinkers gave very different interfacial properties ultimately giving rise to enhanced adhesive properties.

Finally the impact of protein adsorption on interfacial mechanics was studied. The interfacial mechanics was studied by interfacial rheology and interfacial nanoindentation by AFM, and PLL, BSA and lysozyme were the proteins chosen for this study. It was found that proteins adsorbed at the interface resulted in a significant increase in the interfacial shear moduli recorded by rheology, however the same trend was not seen by nanoindentation. By modelling the interfacial mechanics as the superposition of the film forces and the interfacial surface tension forces it was shown that when testing by nanoindentation changes in factors like the surface tension and surface potential have a significant impact on the interfacial mechanics. The addition

of protein films has a surfactant effect on interfaces, and can also change the surface potential, essentially softening them, this results in the films having soft substrates and is proposed as the main cause of discrepancies between interfacial rheology and nanoindentation by AFM. These result were very interesting on two fronts, first, the fact that interfaces behave so differently in shear and under indentation can be explained as in shear it is purely the mechanical strength of the interface that is probed, while under indentation chemical forces arising from the disjoining pressure have a significant impact. Secondly, it was shown that when testing by nanoindentation these two phenomenon, of chemical and mechanical forces, can be probed simultaneously and by using appropriate modelling the relative contributions of these two phenomenon found. Within the context of the Gautrot group this is particularly interesting as it gives a far better understanding of what cells sense and hence sheds light on much of the cell culture work done in our lab adding to our understanding of the importance of mechanotranduciton to cell culture.

7.2 Outlook

In this thesis we have developed a robust protocol for characterising the mechanics of soft materials across different length scales. We have highlighted the importance of surface adhesion and sample heterogeneity on the mechanical characterisation of ultra-soft substrates, particularly at nano to micro length scale testing. Given the importance of substrate mechanics to cell studies this may help shed light on what cells actually sense at the nanoscale and help better understand the factors which control mechano-transduction.

CMC hydrogels are extensively used in industrial applications, in particular as denture adhesives. What we found suggests that the addition of ionic cross-links caused CMC chains to complex into coacervates or coacervate like structures. These

changes resulted in no significant change to the bulk mechanics but an increased adhesive strength. To further this study mechanical characterisation of the local mechanical properties could be done to highlight the heterogeneity caused by coacervation, using a technique like nanoindentation. Further studies could also be conducted using a combination of ionic and covalent cross-links, the covalent cross-links may restrict chain collapse and hence encourage ionic cross-links to form across chains giving a more significant increase in the bulk mechanics.

Finally a model was developed to better understand the mechanical properties of protein adsorbed interfaces. Here we found that when changing the shape and surface area of interfaces, like under indentation testing, the interfacial mechanics resulting from surface tension forces significantly impacts the mechanical response, whereas under shear loading the surface tension forces have a negligible impact. In order to improve the model developed here including the contribution of non-DVLO forces, like hydrophobic and hydrodynamic, would be useful to make the modelling more rounded and complete. Furthermore finding ways to accurately determine the surface potential across an oil-water interface would be extremely useful in order to be sure we are appropriately modelling the interfaces in question. Finally finding methods to monitor the AFM indenter geometry to oil drop separation would be useful particularly to validate the model being used, as the force response is a function of the film separation. As recent studies have shown cells to be able to adhere and spread on protein films adsorbed at liquid-liquid interfaces understanding the mechanics of such interfaces is clearly very important to fully understand how cells are responding to their microstructure.

6 References

1. Rowley, J.A., Madlambayan, G. & Mooney, D.J. Alginate hydrogels as synthetic extracellular matrix materials. *Biomaterials* **20**, 45-53 (1999).
2. Lee, K.Y. & Mooney, D.J. Alginate: Properties and biomedical applications. *Progress in Polymer Science* **37**, 106-126 (2012).
3. Berger, J. et al. Structure and interactions in covalently and ionically crosslinked chitosan hydrogels for biomedical applications. *European Journal of Pharmaceutics and Biopharmaceutics* **57**, 19-34 (2004).
4. Drury, J.L. & Mooney, D.J. Hydrogels for tissue engineering: scaffold design variables and applications. *Biomaterials* **24**, 4337-4351 (2003).
5. Dash, M., Chiellini, F., Ottenbrite, R.M. & Chiellini, E. Chitosan-A versatile semi-synthetic polymer in biomedical applications. *Progress in Polymer Science* **36**, 981-1014 (2011).
6. Trappmann, B. et al. Extracellular-matrix tethering regulates stem-cell fate. *Nature Materials* **11**, 642-649 (2012).
7. Engler, A.J., Sen, S., Sweeney, H.L. & Discher, D.E. Matrix elasticity directs stem cell lineage specification. *Cell* **126**, 677-689 (2006).
8. Yim, E.K.F., Darling, E.M., Kulangara, K., Guilak, F. & Leong, K.W. Nanotopography-induced changes in focal adhesions, cytoskeletal organization, and mechanical properties of human mesenchymal stem cells. *Biomaterials* **31**, 1299-1306 (2010).
9. Hoffman, A.S. Hydrogels for biomedical applications. *Advanced Drug Delivery Reviews* **64**, 18-23 (2012).
10. Bush, B.G., Shapiro, J.M., DelRio, F.W., Cook, R.F. & Oyen, M.L. Mechanical measurements of heterogeneity and length scale effects in PEG-based hydrogels. *Soft Matter* **11**, 7191-7200 (2015).
11. de Molina, P.M., Lad, S. & Helgeson, M.E. Heterogeneity and its Influence on the Properties of Difunctional Poly(ethylene glycol) Hydrogels: Structure and Mechanics. *Macromolecules* **48**, 5402-5411 (2015).
12. Di Lorenzo, F., Hellwig, J., von Klitzing, R. & Seiffert, S. Macroscopic and Microscopic Elasticity of Heterogeneous Polymer Gels. *Acs Macro Letters* **4**, 698-703 (2015).
13. Galli, M. & Oyen, M.L. Fast Identification of Poroelastic Parameters from Indentation Tests. *Cmes-Computer Modeling in Engineering & Sciences* **48**, 241-269 (2009).
14. Galli, M., Comley, K.S.C., Shean, T.A.V. & Oyen, M.L. Viscoelastic and poroelastic mechanical characterization of hydrated gels. *Journal of Materials Research* **24**, 973-979 (2009).
15. Discher, D.E., Janmey, P. & Wang, Y.-l. Tissue cells feel and respond to the stiffness of their substrate. *Science* **310**, 1139-1143 (2005).
16. Gumbiner, B.M. Cell adhesion: the molecular basis of tissue architecture and morphogenesis. *Cell* **84**, 345-357 (1996).
17. Trappmann, B. & Chen, C.S. How cells sense extracellular matrix stiffness: a material's perspective. *Current opinion in biotechnology* **24**, 948-953 (2013).
18. Wozniak, M.A. & Chen, C.S. Mechanotransduction in development: a growing role for contractility. *Nature reviews Molecular cell biology* **10**, 34-43 (2009).

19. Paszek, M.J. & Weaver, V.M. The tension mounts: mechanics meets morphogenesis and malignancy. *Journal of mammary gland biology and neoplasia* **9**, 325-342 (2004).
20. Critchley, D.R. Focal adhesions–the cytoskeletal connection. *Current opinion in cell biology* **12**, 133-139 (2000).
21. Zamir, E. & Geiger, B. Molecular complexity and dynamics of cell-matrix adhesions. *Journal of cell science* **114**, 3583-3590 (2001).
22. Vicente-Manzanares, M., Webb, D.J. & Horwitz, A.R. Cell migration at a glance. *Journal of Cell Science* **118**, 4917-4919 (2005).
23. Parfitt, A. Age-related structural changes in trabecular and cortical bone: cellular mechanisms and biomechanical consequences. *Calcified Tissue International* **36**, S123-S128 (1984).
24. Chen, C.S., Mrksich, M., Huang, S., Whitesides, G.M. & Ingber, D.E. Geometric control of cell life and death. *Science* **276**, 1425-1428 (1997).
25. McBeath, R., Pirone, D.M., Nelson, C.M., Bhadriraju, K. & Chen, C.S. Cell shape, cytoskeletal tension, and RhoA regulate stem cell lineage commitment. *Developmental cell* **6**, 483-495 (2004).
26. Watt, F.M., Jordan, P.W. & O'Neill, C.H. Cell shape controls terminal differentiation of human epidermal keratinocytes. *Proceedings of the National Academy of Sciences* **85**, 5576-5580 (1988).
27. Jiang, X., Bruzewicz, D.A., Wong, A.P., Piel, M. & Whitesides, G.M. Directing cell migration with asymmetric micropatterns. *Proceedings of the National Academy of Sciences of the United States of America* **102**, 975-978 (2005).
28. Théry, M. et al. The extracellular matrix guides the orientation of the cell division axis. *Nature cell biology* **7**, 947-953 (2005).
29. Nelson, C.M., VanDuijn, M.M., Inman, J.L., Fletcher, D.A. & Bissell, M.J. Tissue geometry determines sites of mammary branching morphogenesis in organotypic cultures. *Science* **314**, 298-300 (2006).
30. Pelham, R.J. & Wang, Y.-l. Cell locomotion and focal adhesions are regulated by substrate flexibility. *Proceedings of the National Academy of Sciences* **94**, 13661-13665 (1997).
31. Engler, A. et al. Substrate compliance versus ligand density in cell on gel responses. *Biophysical journal* **86**, 617-628 (2004).
32. Gray, D.S., Tien, J. & Chen, C.S. Repositioning of cells by mechanotaxis on surfaces with micropatterned Young's modulus. *Journal of biomedical materials research Part A* **66**, 605-614 (2003).
33. Chaudhuri, O. et al. Substrate stress relaxation regulates cell spreading. *Nature communications* **6** (2015).
34. Levental, K.R. et al. Matrix crosslinking forces tumor progression by enhancing integrin signaling. *Cell* **139**, 891-906 (2009).
35. Solon, J., Levental, I., Sengupta, K., Georges, P.C. & Janmey, P.A. Fibroblast adaptation and stiffness matching to soft elastic substrates. *Biophysical journal* **93**, 4453-4461 (2007).
36. Huebsch, N. et al. Harnessing traction-mediated manipulation of the cell/matrix interface to control stem-cell fate. *Nature materials* **9**, 518-526 (2010).
37. Bozec, L., van der Heijden, G. & Horton, M. Collagen fibrils: nanoscale ropes. *Biophysical journal* **92**, 70-75 (2007).

38. Flemming, R., Murphy, C., Abrams, G., Goodman, S. & Nealey, P. Effects of synthetic micro-and nano-structured surfaces on cell behavior. *Biomaterials* **20**, 573-588 (1999).
39. Wolf, K., Müller, R., Borgmann, S., Bröcker, E.-B. & Friedl, P. Amoeboid shape change and contact guidance: T-lymphocyte crawling through fibrillar collagen is independent of matrix remodeling by MMPs and other proteases. *Blood* **102**, 3262-3269 (2003).
40. Teixeira, A.I., Abrams, G.A., Bertics, P.J., Murphy, C.J. & Nealey, P.F. Epithelial contact guidance on well-defined micro-and nanostructured substrates. *Journal of cell science* **116**, 1881-1892 (2003).
41. Bettinger, C.J., Langer, R. & Borenstein, J.T. Engineering substrate topography at the micro-and nanoscale to control cell function. *Angewandte Chemie International Edition* **48**, 5406-5415 (2009).
42. Xia, Y. & Whitesides, G.M. Soft lithography. *Annual review of materials science* **28**, 153-184 (1998).
43. Zhang, Y., Lo, C.-W., Taylor, J.A. & Yang, S. Replica molding of high-aspect-ratio polymeric nanopillar arrays with high fidelity. *Langmuir* **22**, 8595-8601 (2006).
44. Mrksich, M. & Whitesides, G.M. Patterning self-assembled monolayers using microcontact printing: a new technology for biosensors? *Trends in biotechnology* **13**, 228-235 (1995).
45. James, C. et al. Patterned protein layers on solid substrates by thin stamp microcontact printing. *Langmuir* **14**, 741-744 (1998).
46. Zhao, B. & Brittain, W.J. Polymer brushes: surface-immobilized macromolecules. *Progress in Polymer Science* **25**, 677-710 (2000).
47. Milner, S. Polymer brushes. *Science* **251**, 905-914 (1991).
48. Xu, F., Zhong, S., Yung, L., Kang, E. & Neoh, K. Surface-active and stimuli-responsive polymer-Si (100) hybrids from surface-initiated atom transfer radical polymerization for control of cell adhesion. *Biomacromolecules* **5**, 2392-2403 (2004).
49. Matyjaszewski, K., Patten, T.E. & Xia, J. Controlled/"living" radical polymerization. Kinetics of the homogeneous atom transfer radical polymerization of styrene. *Journal of the American Chemical Society* **119**, 674-680 (1997).
50. Iwata, R. et al. Control of nanobiointerfaces generated from well-defined biomimetic polymer brushes for protein and cell manipulations. *Biomacromolecules* **5**, 2308-2314 (2004).
51. Trmcic-Cvitas, J. et al. Biofunctionalized protein resistant oligo (ethylene glycol)-derived polymer brushes as selective immobilization and sensing platforms. *Biomacromolecules* **10**, 2885-2894 (2009).
52. Lee, K.Y. & Mooney, D.J. Hydrogels for tissue engineering. *Chemical reviews* **101**, 1869-1880 (2001).
53. Miron-Mendoza, M., Seemann, J. & Grinnell, F. The differential regulation of cell motile activity through matrix stiffness and porosity in three dimensional collagen matrices. *Biomaterials* **31**, 6425-6435 (2010).
54. Tse, J.R. & Engler, A.J. Preparation of hydrogel substrates with tunable mechanical properties. *Current protocols in cell biology*, 10.16. 11-10.16. 16 (2010).
55. Beningo, K.A. & Wang, Y.-L. Flexible substrata for the detection of cellular traction forces. *Trends in cell biology* **12**, 79-84 (2002).

56. Munevar, S., Wang, Y.-l. & Dembo, M. Traction force microscopy of migrating normal and H-ras transformed 3T3 fibroblasts. *Biophysical journal* **80**, 1744-1757 (2001).
57. Beningo, K.A., Lo, C.-M. & Wang, Y.-L. Flexible polyacrylamide substrata for the analysis of mechanical interactions at cell-substratum adhesions. *Methods in cell biology* **69**, 325-339 (2002).
58. Brown, X.Q., Ookawa, K. & Wong, J.Y. Evaluation of polydimethylsiloxane scaffolds with physiologically-relevant elastic moduli: interplay of substrate mechanics and surface chemistry effects on vascular smooth muscle cell response. *Biomaterials* **26**, 3123-3129 (2005).
59. Ai, H. et al. Coating and selective deposition of nanofilm on silicone rubber for cell adhesion and growth. *Cell biochemistry and biophysics* **38**, 103-114 (2003).
60. Yim, E.K. et al. Nanopattern-induced changes in morphology and motility of smooth muscle cells. *Biomaterials* **26**, 5405-5413 (2005).
61. Tzvetkova-Chevolleau, T. et al. The motility of normal and cancer cells in response to the combined influence of the substrate rigidity and anisotropic microstructure. *Biomaterials* **29**, 1541-1551 (2008).
62. Oyen, M.L. Mechanical characterisation of hydrogel materials. *International Materials Reviews* **59**, 44-59 (2014).
63. Baroli, B. Hydrogels for tissue engineering and delivery of tissue-inducing substances. *Journal of Pharmaceutical Sciences* **96**, 2197-2223 (2007).
64. Normand, V., Lootens, D.L., Amici, E., Plucknett, K.P. & Aymard, P. New insight into agarose gel mechanical properties. *Biomacromolecules* **1**, 730-738 (2000).
65. Gu, W.Y., Yao, H., Huang, C.Y. & Cheung, H.S. New insight into deformation-dependent hydraulic permeability of gels and cartilage, and dynamic behavior of agarose gels in confined compression. *Journal of Biomechanics* **36**, 593-598 (2003).
66. Ross, K.A. & Scanlon, M.G. Analysis of the elastic modulus of agar gel by indentation. *Journal of Texture Studies* **30**, 17-27 (1999).
67. Roberts, J.J., Earnshaw, A., Ferguson, V.L. & Bryant, S.J. Comparative study of the viscoelastic mechanical behavior of agarose and poly(ethylene glycol) hydrogels. *Journal of Biomedical Materials Research Part B-Applied Biomaterials* **99B**, 158-169 (2011).
68. Callister, W.D. & Rethwisch, D.G. Materials science and engineering: an introduction, Vol. 7. (Wiley New York, 2007).
69. Anseth, K.S., Bowman, C.N. & BrannonPeppas, L. Mechanical properties of hydrogels and their experimental determination. *Biomaterials* **17**, 1647-1657 (1996).
70. Flory, P.J. & Rehner Jr, J. Statistical Mechanics of Cross-Linked Polymer Networks I. Rubberlike Elasticity. *The Journal of Chemical Physics* **11**, 512-520 (1943).
71. Flory, P.J. & Rehner Jr, J. Statistical mechanics of cross-linked polymer networks II. Swelling. *The Journal of Chemical Physics* **11**, 521-526 (1943).
72. Deiber, J.A., Ottone, M.L., Piaggio, M.V. & Peirotti, M.B. Characterization of cross-linked polyampholytic gelatin hydrogels through the rubber elasticity and thermodynamic swelling theories. *Polymer* **50**, 6065-6075 (2009).
73. Basu, A. et al. Nonaffine Displacements in Flexible Polymer Networks. *Macromolecules* **44**, 1671-1679 (2011).

74. Lakes, R.S. Viscoelastic solids, Vol. 9. (CRC press, 1998).
75. Chen, Q.S., Suki, B. & An, K.N. Dynamic mechanical properties of agarose gels modeled by a fractional derivative model. *Journal of Biomechanical Engineering-Transactions of the Asme* **126**, 666-671 (2004).
76. Kavanagh, G.M. & Ross-Murphy, S.B. Rheological characterisation of polymer gels. *Progress in Polymer Science* **23**, 533-562 (1998).
77. Mak, A.F., Lai, W.M. & Mow, V.C. BIPHASIC INDENTATION OF ARTICULAR-CARTILAGE .1. THEORETICAL-ANALYSIS. *Journal of Biomechanics* **20**, 703-714 (1987).
78. Hui, C.Y., Lin, Y.Y., Chuang, F.C., Shull, K.R. & Lin, W.C. A contact mechanics method for characterizing the elastic properties and permeability of gels. *Journal of Polymer Science Part B-Polymer Physics* **44**, 359-370 (2006).
79. Hu, Y., Zhao, X., Vlassak, J.J. & Suo, Z. Using indentation to characterize the poroelasticity of gels. *Applied Physics Letters* **96** (2010).
80. Chen, D.T.N., Wen, Q., Janmey, P.A., Crocker, J.C. & Yodh, A.G. in Annual Review of Condensed Matter Physics, Vol 1, Vol. 1. (ed. J.S. Langer) 301-322 (Annual Reviews, Palo Alto; 2010).
81. Dae Han, C. & Kim, J.K. On the use of time-temperature superposition in multicomponent/multiphase polymer systems. *Polymer* **34**, 2533-2539 (1993).
82. Van Gurp, M. & Palmen, J. Time-temperature superposition for polymeric blends. *Rheol Bull* **67**, 5-8 (1998).
83. Han, J.M. et al. The adhesive strength and initial viscosity of denture adhesives. *Acta Odontologica Scandinavica* **72**, 839-845 (2014).
84. Tyrrell, J.W. & Attard, P. Viscoelastic study using an atomic force microscope modified to operate as a nanorheometer. *Langmuir* **19**, 5254-5260 (2003).
85. Nayar, V.T., Weiland, J.D., Nelson, C.S. & Hodge, A.M. Elastic and viscoelastic characterization of agar. *Journal of the Mechanical Behavior of Biomedical Materials* **7**, 60-68 (2012).
86. Kloxin, A.M., Kloxin, C.J., Bowman, C.N. & Anseth, K.S. Mechanical Properties of Cellularly Responsive Hydrogels and Their Experimental Determination. *Advanced Materials* **22**, 3484-3494 (2010).
87. Constantinides, G., Chandran, K.S.R., Ulm, F.J. & Van Vliet, K.J. Grid indentation analysis of composite microstructure and mechanics: Principles and validation. *Materials Science and Engineering a-Structural Materials Properties Microstructure and Processing* **430**, 189-202 (2006).
88. Olberding, J.E. & Suh, J.K.F. A dual optimization method for the material parameter identification of a biphasic poroviscoelastic hydrogel: Potential application to hypercompliant soft tissues. *Journal of Biomechanics* **39**, 2468-2475 (2006).
89. Seidlits, S.K. et al. The effects of hyaluronic acid hydrogels with tunable mechanical properties on neural progenitor cell differentiation. *Biomaterials* **31**, 3930-3940 (2010).
90. Ebenstein, D.M. & Pruitt, L.A. Nanoindentation of biological materials. *Nano Today* **1**, 26-33 (2006).
91. Oyen, M.L. Nanoindentation of Biological and Biomimetic Materials. *Experimental Techniques* **37**, 73-87 (2013).
92. Oyen, M.L. & Cook, R.F. A practical guide for analysis of nanoindentation data. *Journal of the mechanical behavior of biomedical materials* **2**, 396-407 (2009).

93. Butt, H.J., Cappella, B. & Kappl, M. Force measurements with the atomic force microscope: Technique, interpretation and applications. *Surface Science Reports* **59**, 1-152 (2005).
94. Oliver, W.C. & Pharr, G.M. An improved technique for determining hardness and elastic modulus using load and displacement sensing indentation experiments. *Journal of materials research* **7**, 1564-1583 (1992).
95. Oliver, W.C. & Pharr, G.M. Measurement of hardness and elastic modulus by instrumented indentation: Advances in understanding and refinements to methodology. *Journal of materials research* **19**, 3-20 (2004).
96. Sneddon, I.N. The relation between load and penetration in the axisymmetric Boussinesq problem for a punch of arbitrary profile. *International journal of engineering science* **3**, 47-57 (1965).
97. Tabor, D. A simple theory of static and dynamic hardness. *Proceedings of the Royal Society of London. Series A. Mathematical and Physical Sciences* **192**, 247-274 (1948).
98. Stilwell, N. & Tabor, D. Elastic recovery of conical indentations. *Proceedings of the Physical Society* **78**, 169 (1961).
99. Bulychev, S. & Alekhin, V. Method of Kinetic Hardness and Microhardness in Testing Impression by an Indentor.(Translation). *Ind. Lab.(USSR)* **53**, 1091-1096 (1987).
100. Grierson, D.S., Flater, E.E. & Carpick, R.W. Accounting for the JKR-DMT transition in adhesion and friction measurements with atomic force microscopy. *Journal of Adhesion Science and Technology* **19**, 291-311 (2005).
101. Jin, F., Guo, X. & Gao, H. Adhesive contact on power-law graded elastic solids: The JKR–DMT transition using a double-Hertz model. *Journal of the Mechanics and Physics of Solids* **61**, 2473-2492 (2013).
102. Barthel, E. Adhesive elastic contacts: JKR and more. *Journal of Physics D: Applied Physics* **41**, 163001 (2008).
103. Shull, K.R. Contact mechanics and the adhesion of soft solids. *Materials Science & Engineering R-Reports* **36**, 1-45 (2002).
104. Sirghi, L. & Rossi, F. Adhesion and elasticity in nanoscale indentation. *Applied physics letters* **89**, 243118 (2006).
105. Chang, C.Y. & Zhang, L.N. Cellulose-based hydrogels: Present status and application prospects. *Carbohydrate Polymers* **84**, 40-53 (2011).
106. Patel, A. & Mequanint, K. Hydrogel biomaterials. (INTECH Open Access Publisher, 2011).
107. Deligkaris, K., Tadele, T.S., Olthuis, W. & van den Berg, A. Hydrogel-based devices for biomedical applications. *Sensors and Actuators B-Chemical* **147**, 765-774 (2010).
108. Wichterle, O. & Lim, D. Hydrophilic Gels for Biological Use. *Nature* **185**, 117-118 (1960).
109. Corkhill, P.H., Hamilton, C.J. & Tighe, B.J. SYNTHETIC HYDROGELS .6. HYDROGEL COMPOSITES AS WOUND DRESSINGS AND IMPLANT MATERIALS. *Biomaterials* **10**, 3-10 (1989).
110. Gupta, P., Vermani, K. & Garg, S. Hydrogels: from controlled release to pH-responsive drug delivery. *Drug Discovery Today* **7**, 569-579 (2002).
111. Lin, C.-C. & Anseth, K.S. PEG Hydrogels for the Controlled Release of Biomolecules in Regenerative Medicine. *Pharmaceutical Research* **26**, 631-643 (2009).

112. Hoffman, A.S. Hydrogels for biomedical applications. *Advanced Drug Delivery Reviews* **54**, 3-12 (2002).
113. Brandl, F., Sommer, F. & Goepferich, A. Rational design of hydrogels for tissue engineering: Impact of physical factors on cell behavior. *Biomaterials* **28**, 134-146 (2007).
114. Peppas, N.A., Huang, Y., Torres-Lugo, M., Ward, J.H. & Zhang, J. Physicochemical, foundations and structural design of hydrogels in medicine and biology. *Annual Review of Biomedical Engineering* **2**, 9-29 (2000).
115. Utech, S. & Boccaccini, A.R. A review of hydrogel-based composites for biomedical applications: enhancement of hydrogel properties by addition of rigid inorganic fillers. *Journal of Materials Science* **51**, 271-310 (2016).
116. Grattoni, C.A., Al-Sharji, H.H., Yang, C.H., Muggeridge, A.H. & Zimmerman, R.W. Rheology and permeability of crosslinked polyacrylamide gel. *Journal of Colloid and Interface Science* **240**, 601-607 (2001).
117. Knapp, D.M. et al. Rheology of reconstituted type I collagen gel in confined compression. *Journal of Rheology* **41**, 971-993 (1997).
118. Hellio, D. & Djabourov, M. Physically and chemically crosslinked gelatin gels. *Macromolecular Symposia* **241**, 23-27 (2006).
119. Kong, H.J., Lee, K.Y. & Mooney, D.J. Decoupling the dependence of rheological/mechanical properties of hydrogels from solids concentration. *Polymer* **43**, 6239-+ (2002).
120. Ruoslahti, E. RGD and other recognition sequences for integrins. *Annual Review of Cell and Developmental Biology* **12**, 697-715 (1996).
121. Zhao, X., Huebsch, N., Mooney, D.J. & Suo, Z. Stress-relaxation behavior in gels with ionic and covalent crosslinks. *Journal of Applied Physics* **107** (2010).
122. Klemm, D., Schumann, D., Udhardt, U. & Marsch, S. Bacterial synthesized cellulose - artificial blood vessels for microsurgery. *Progress in Polymer Science* **26**, 1561-1603 (2001).
123. Zhang, L.M. New water-soluble cellulosic polymers: A review. *Macromolecular Materials and Engineering* **286**, 267-275 (2001).
124. Taubner, T., Synytsya, A. & Čopíková, J. Preparation of amidated derivatives of carboxymethylcellulose. *International journal of biological macromolecules* **72**, 11-18 (2015).
125. Clasen, C. & Kulicke, W.M. Determination of viscoelastic and rheo-optical material functions of water-soluble cellulose derivatives. *Progress in Polymer Science* **26**, 1839-1919 (2001).
126. Reuben, J. & Conner, H.T. Analysis of the carbon-13 n.m.r. spectrum of hydrolyzed O-(carboxymethyl)cellulose: monomer composition and substitution patterns. *Carbohydrate Research* **115**, 1-13 (1983).
127. Zabivalova, N.M., Bochek, A.M., Kalyuzhnaya, L.M., Vlasova, E.N. & Volchek, B.Z. Carboxymethyl cellulose amides and their properties. *Russian Journal of Applied Chemistry* **76**, 1998-2002 (2003).
128. Heinze, T. & Koschella, A. Carboxymethyl Ethers of Cellulose and Starch – A Review. *Macromolecular Symposia* **223**, 13-40 (2005).
129. Klemm, D., Heublein, B., Fink, H.P. & Bohn, A.J.A.C.I.E. Cellulose: fascinating biopolymer and sustainable raw material. **44**, 3358-3393 (2005).
130. Lee, K.Y. et al. Controlling mechanical and swelling properties of alginate hydrogels independently by cross-linker type and cross-linking density. *Macromolecules* **33**, 4291-4294 (2000).

131. Drury, J.L., Dennis, R.G. & Mooney, D.J. The tensile properties of alginate hydrogels. *Biomaterials* **25**, 3187-3199 (2004).
132. Schmitt, C. & Turgeon, S.L. Protein/polysaccharide complexes and coacervates in food systems. *Advances in Colloid and Interface Science* **167**, 63-70 (2011).
133. Ye, A.J.I.j.o.f.s. & technology Complexation between milk proteins and polysaccharides via electrostatic interaction: principles and applications–a review. **43**, 406-415 (2008).
134. Turgeon, S.L., Schmitt, C. & Sanchez, C. Protein–polysaccharide complexes and coacervates. *Current Opinion in Colloid & Interface Science* **12**, 166-178 (2007).
135. Wang, Y., Kimura, K., Huang, Q., Dubin, P.L. & Jaeger, W. Effects of Salt on Polyelectrolyte−Micelle Coacervation. *Macromolecules* **32**, 7128-7134 (1999).
136. Krogstad, D.V. et al. Small Angle Neutron Scattering Study of Complex Coacervate Micelles and Hydrogels Formed from Ionic Diblock and Triblock Copolymers. *Journal of Physical Chemistry B* **118**, 13011-13018 (2014).
137. Priftis, D., Farina, R. & Tirrell, M. Interfacial Energy of Polypeptide Complex Coacervates Measured via Capillary Adhesion. *Langmuir* **28**, 8721-8729 (2012).
138. Krogstad, D.V. et al. Effects of Polymer and Salt Concentration on the Structure and Properties of Triblock Copolymer Coacervate Hydrogels. *Macromolecules* **46**, 1512-1518 (2013).
139. Marcì, G., Mele, G., Palmisano, L., Pulito, P. & Sannino, A. Environmentally sustainable production of cellulose-based superabsorbent hydrogels. *Green Chemistry* **8**, 439-444 (2006).
140. Sun, J.-Y. et al. Highly stretchable and tough hydrogels. *Nature* **489**, 133-136 (2012).
141. Smeds, K.A. & Grinstaff, M.W. Photocrosslinkable polysaccharides for in situ hydrogel formation. *Journal of biomedical materials research* **54**, 115-121 (2001).
142. Webber, G.B. et al. Dynamic Forces between a Moving Particle and a Deformable Drop. *The Journal of Physical Chemistry C* **112**, 567-574 (2008).
143. Bos, M.A. & van Vliet, T. Interfacial rheological properties of adsorbed protein layers and surfactants: a review. *Advances in Colloid and Interface Science* **91**, 437-471 (2001).
144. Gautrot, J., Kong, D., Nguyen, K., Megone, W. & Peng, L. The culture of HaCaT cells on liquid substrates is mediated by a mechanically strong liquid-liquid interface. *Faraday Discussions* (2017).
145. Kong, D. et al. Protein Nanosheet Mechanics Controls Cell Adhesion and Expansion on Low-Viscosity Liquids. *Nano Letters* **18**, 1946-1951 (2018).
146. Kong, D., Peng, L., Di Cio, S., Novak, P. & Gautrot, J.E. Stem Cell Expansion and Fate Decision on Liquid Substrates Are Regulated by Self-Assembled Nanosheets. *ACS Nano* **12**, 9206-9213 (2018).
147. Mitropoulos, V., Mütze, A. & Fischer, P. Mechanical properties of protein adsorption layers at the air/water and oil/water interface: A comparison in light of the thermodynamical stability of proteins. *Advances in Colloid and Interface Science* **206**, 195-206 (2014).

148. Raffaele Mezzenga and Peter, F. The self-assembly, aggregation and phase transitions of food protein systems in one, two and three dimensions. *Reports on Progress in Physics* **76**, 046601 (2013).
149. Mitropoulos, V., Mutze, A. & Fischer, P. Mechanical properties of protein adsorption layers at the air/water and oil/water interface: A comparison in light of the thermodynamical stability of proteins. *Advances in Colloid and Interface Science* **206**, 195-206 (2014).
150. Bryant, C.M. & McClements, D.J. Molecular basis of protein functionality with special consideration of cold-set gels derived from heat-denatured whey. *Trends in Food Science & Technology* **9**, 143-151 (1998).
151. Damodaran, S. Adsorbed layers formed from mixtures of proteins. *Current Opinion in Colloid & Interface Science* **9**, 328-339 (2004).
152. Krägel, J., Derkatch, S.R. & Miller, R. Interfacial shear rheology of protein–surfactant layers. *Advances in Colloid and Interface Science* **144**, 38-53 (2008).
153. Fainerman, V.B. & Miller, R. Equilibrium and dynamic characteristics of protein adsorption layers at gas-liquid interfaces: Theoretical and experimental data. *Colloid Journal* **67**, 393-404 (2005).
154. Lu, J.R., Su, T.J. & Thomas, R.K. Structural Conformation of Bovine Serum Albumin Layers at the Air–Water Interface Studied by Neutron Reflection. *Journal of Colloid and Interface Science* **213**, 426-437 (1999).
155. Beverung, C.J., Radke, C.J. & Blanch, H.W. Protein adsorption at the oil/water interface: characterization of adsorption kinetics by dynamic interfacial tension measurements. *Biophysical Chemistry* **81**, 59-80 (1999).
156. Malcolm, A.S., Dexter, A.F. & Middelberg, A.P.J. Mechanical Properties of Interfacial Films Formed by Lysozyme Self-Assembly at the Air−Water Interface. *Langmuir* **22**, 8897-8905 (2006).
157. Murray, B.S. in Studies in Interface Science, Vol. 7. (eds. D. Möbius & R. Miller) 179-220 (Elsevier, 1998).
158. Burgess, D.J. & Sahin, N.O. Interfacial Rheological and Tension Properties of Protein Films. *Journal of Colloid and Interface Science* **189**, 74-82 (1997).
159. Raman, B. et al. Critical Balance of Electrostatic and Hydrophobic Interactions Is Required for β2-Microglobulin Amyloid Fibril Growth and Stability. *Biochemistry* **44**, 1288-1299 (2005).
160. Alahverdjieva, V.S. et al. Adsorption behaviour of hen egg-white lysozyme at the air/water interface. *Colloids and Surfaces A: Physicochemical and Engineering Aspects* **323**, 167-174 (2008).
161. Liu, J. & Messow, U. Diffusion-controlled adsorption kinetics at the air/solution interface. *Colloid and Polymer Science* **278**, 124-129 (2000).
162. Murray, B.S. Rheological properties of protein films. *Current Opinion in Colloid & Interface Science* **16**, 27-35 (2011).
163. Jones, D.B. & Middelberg, A.P.J. Micromechanical Testing of Interfacial Protein Networks Demonstrates Ensemble Behavior Characteristic of a Nanostructured Biomaterial. *Langmuir* **18**, 5585-5591 (2002).
164. Reynaert, S., Brooks, C.F., Moldenaers, P., Vermant, J. & Fuller, G.G. Analysis of the magnetic rod interfacial stress rheometer. *Journal of Rheology* **52**, 261-285 (2008).
165. Derjaguin, B.J.A.P.U. BV Derjaguin and L. Landau, Acta Physicochim. URSS 14, 633 (1941). **14**, 633 (1941).

166. Derjaguin, B.J.D.o.t.F.S. A theory of the heterocoagulation, interaction and adhesion of dissimilar particles in solutions of electrolytes. **18**, 85-98 (1954).
167. Verwey, E.J.T.J.o.P.C. Theory of the stability of lyophobic colloids. **51**, 631-636 (1947).
168. Wang, W. et al. Review and perspectives of AFM application on the study of deformable drop/bubble interactions. *Advances in Colloid and Interface Science* **225**, 88-97 (2015).
169. Manica, R. et al. Hydrodynamic forces involving deformable interfaces at nanometer separations. *Physics of Fluids* **20**, 032101 (2008).
170. Kirmizis, D. & Logothetidis, S. Atomic force microscopy probing in the measurement of cell mechanics. *International journal of nanomedicine* **5**, 137-145 (2010).
171. Chan, D.Y.C., Dagastine, R.R. & White, L.R. Forces between a Rigid Probe Particle and a Liquid Interface: I. The Repulsive Case. *Journal of Colloid and Interface Science* **236**, 141-154 (2001).
172. Dagastine, R.R. & White, L.R. Forces between a Rigid Probe Particle and a Liquid Interface: II. The General Case. *Journal of Colloid and Interface Science* **247**, 310-320 (2002).
173. Dagastine, R.R., Stevens, G.W., Chan, D.Y.C. & Grieser, F. Forces between two oil drops in aqueous solution measured by AFM. *Journal of Colloid and Interface Science* **273**, 339-342 (2004).
174. Vakarelski, I.U. et al. Bubble Colloidal AFM Probes Formed from Ultrasonically Generated Bubbles. *Langmuir* **24**, 603-605 (2008).
175. Gunning, A., Mackie, A., Wilde, P. & Morris, V. Atomic Force Microscopy of Emulsion Droplets: Probing Droplet− Droplet Interactions. *Langmuir* **20**, 116-122 (2004).
176. Tabor, R.F. et al. Combined AFM−Confocal Microscopy of Oil Droplets: Absolute Separations and Forces in Nanofilms. *The Journal of Physical Chemistry Letters* **2**, 961-965 (2011).
177. Shi, C. et al. Measuring Forces and Spatiotemporal Evolution of Thin Water Films between an Air Bubble and Solid Surfaces of Different Hydrophobicity. *ACS Nano* **9**, 95-104 (2015).
178. Amoroso, N.J.D.A., Antonio. Hong, Yi. Microstructural manipulation of electrospun scaffolds for specific bending stiffness for heart valve tissue engineering. *Acta biomaterialia* **8**, 4268-4277.
179. Amoroso, N.J. et al. Microstructural manipulation of electrospun scaffolds for specific bending stiffness for heart valve tissue engineering. *Acta Biomaterialia* **8**, 4268-4277 (2012).
180. Gutierrez, E. & Groisman, A. Measurements of Elastic Moduli of Silicone Gel Substrates with a Microfluidic Device. *PLoS ONE* **6**, e25534 (2011).
181. Wen, J.H. et al. Interplay of matrix stiffness and protein tethering in stem cell differentiation. *Nat Mater* **13**, 979-987 (2014).
182. Cesa, C.M. et al. Micropatterned silicone elastomer substrates for high resolution analysis of cellular force patterns. *Review of scientific instruments* **78**, 034301 (2007).
183. Lee, W.S., Yeo, K.S., Andriyana, A., Shee, Y.G. & Mahamd Adikan, F.R. Effect of cyclic compression and curing agent concentration on the stabilization of mechanical properties of PDMS elastomer. *Materials & Design* **96**, 470-475 (2016).

184. Seo, J.-H., Sakai, K. & Yui, N. Adsorption state of fibronectin on poly (dimethylsiloxane) surfaces with varied stiffness can dominate adhesion density of fibroblasts. *Acta biomaterialia* **9**, 5493-5501 (2013).
185. Wang, Z., Volinsky, A.A. & Gallant, N.D. Crosslinking effect on polydimethylsiloxane elastic modulus measured by custom-built compression instrument. *Journal of Applied Polymer Science* **131** (2014).
186. Chen, J., Wright, K. & Birch, M. Nanoscale viscoelastic properties and adhesion of polydimethylsiloxane for tissue engineering. *Acta Mechanica Sinica* **30**, 2-6 (2014).
187. Williams, A.D. & Flory, P.J. Configurational statistics of poly(ethylene terephthalate) chains. *Journal of Polymer Science Part A-2: Polymer Physics* **5**, 417-424 (1967).
188. Flory, P.J. Molecular theory of rubber elasticity. *Polymer* **20**, 1317-1320 (1979).
189. Erman, B. & Flory, P.J. Relationships between stress, strain, and molecular constitution of polymer networks. Comparison of theory with experiments. *Macromolecules* **15**, 806-811 (1982).
190. Flory, P.J. & Erman, B. Silicone networks with junctions of high functionality and the theory of rubber elasticity. *Journal of Polymer Science: Polymer Physics Edition* **22**, 49-55 (1984).
191. Cail, J.I. & Stepto, R.F.T. Molecular modelling of the elastic behaviour of poly(ethylene terephthalate) network chains. *Polymer* **44**, 6077-6087 (2003).
192. Sirghi, L. & Rossi, F. The effect of adhesion on the contact radius in atomic force microscopy indentation. *Nanotechnology* **20**, 365702 (2009).
193. Versaevel, M., Grevesse, T., Riaz, M., Lantoine, J. & Gabriele, S. in Micropatterning in Cell Biology, Pt C, Vol. 121. (eds. M. Piel & M. Thery) 33-+ (Elsevier Academic Press Inc, San Diego; 2014).
194. Roca-Cusachs, P. et al. Stability of microfabricated high aspect ratio structures in poly (dimethylsiloxane). *Langmuir* **21**, 5542-5548 (2005).
195. Johnson, K. Contact Mechanics Cambridge Univ. *Press, Cambridge* (1985).
196. Plotnikov, Sergey V., Pasapera, Ana M., Sabass, B. & Waterman, Clare M. Force Fluctuations within Focal Adhesions Mediate ECM-Rigidity Sensing to Guide Directed Cell Migration. *Cell* **151**, 1513-1527 (2012).
197. Moore, S.W., Roca-Cusachs, P. & Sheetz, M.P. Stretchy Proteins on Stretchy Substrates: The Important Elements of Integrin-Mediated Rigidity Sensing. *Developmental Cell* **19**, 194-206 (2010).
198. Baker, B.M. et al. Cell-mediated fiber recruitment drives extracellular matrix mechanosensing in engineered fibrillar microenvironments. *Nature materials* **14**, 1262-1268 (2015).
199. Chaudhuri, O. et al. Hydrogels with tunable stress relaxation regulate stem cell fate and activity. *Nature materials* **15**, 326-334 (2016).
200. Di Cio, S. & Gautrot, J.E. Cell sensing of physical properties at the nanoscale: Mechanisms and control of cell adhesion and phenotype. *Acta biomaterialia* (2015).
201. Peyton, S.R. & Putnam, A.J. Extracellular matrix rigidity governs smooth muscle cell motility in a biphasic fashion. *Journal of Cellular Physiology* **204**, 198-209 (2005).
202. Huang, X.W. et al. Matrix Stiffness-Induced Myofibroblast Differentiation Is Mediated by Intrinsic Mechanotransduction. *American Journal of Respiratory Cell and Molecular Biology* **47**, 340-348 (2012).

203. Jiang, F.X., Yurke, B., Firestein, B.L. & Langrana, N.A. Neurite outgrowth on a DNA crosslinked hydrogel with tunable stiffnesses. *Annals of Biomedical Engineering* **36**, 1565-1579 (2008).
204. Schrader, J. et al. Matrix Stiffness Modulates Proliferation, Chemotherapeutic Response, and Dormancy in Hepatocellular Carcinoma Cells. *Hepatology* **53**, 1192-1205 (2011).
205. Hoyle, C. & E Thiol-Ene Click Chemistry. *Angewandte Chemie (International ed.)* **49**, 1540-1573.
206. Khetan, S. Degradation-mediated cellular traction directs stem cell fate in covalently crosslinked three-dimensional hydrogels. *Nature materials* **12**, 458-465.
207. Colak, B. Impact of the Molecular Environment on Thiol–Ene Coupling For Biofunctionalization and Conjugation. *Bioconjugate chemistry* **27**, 2111-2123.
208. Nguyen, K.D.Q., Megone, W.V., Kong, D. & Gautrot, J. Thiol-ene cross-linking and functionalisation of Polydimethylsiloxane for biomedical applications. *Frontiers in Bioengineering and Biotechnology*.
209. Lionetto, F., Sannino, A., Mensitieri, G. & Maffezzoli, A. in Macromolecular Symposia, Vol. 200 199-208 (Wiley Online Library, 2003).
210. Pushpamalar, V., Langford, S.J., Ahmad, M. & Lim, Y.Y. Optimization of reaction conditions for preparing carboxymethyl cellulose from sago waste. *Carbohydrate Polymers* **64**, 312-318 (2006).
211. Desmarais, A.J. (Google Patents, 1991).
212. Kulak, Y., Özcan, M. & Arikan, A.J.J.o.P.I., Esthetic and Reconstructive Dentistry Subjective assessment by patients of the efficiency of two denture adhesive pastes. **14**, 248-252 (2005).
213. An, Y.R., Li, D.Y., Roohpour, N., Gautrot, J.E. & Barber, A.H. Failure mechanisms in denture adhesives. *Dental Materials* **32**, 615-623 (2016).
214. de Oliveira, N.M. et al. MASTICATORY PERFORMANCE OF COMPLETE DENTURE WEARERS AFTER USING TWO ADHESIVES: A CROSSOVER RANDOMIZED CLINICAL TRIAL. *Journal of Prosthetic Dentistry* **112**, 1182-1187 (2014).
215. Papadiochou, S., Emmanouil, L. & Papadiochos, L. Denture adhesives: A systematic review. *Journal of Prosthetic Dentistry* **113**, 391-397 (2015).
216. Adinugraha, M.P., Marseno, D.W. & Haryadi Synthesis and characterization of sodium carboxymethylcellulose from cavendish banana pseudo stem (Musa cavendishii LAMBERT). *Carbohydrate Polymers* **62**, 164-169 (2005).
217. Benchabane, A. & Bekkour, K. Rheological properties of carboxymethyl cellulose (CMC) solutions. *Colloid and Polymer Science* **286**, 1173-1180 (2008).
218. Choppe, E., Puaud, F., Nicolai, T. & Benyahia, L. Rheology of xanthan solutions as a function of temperature, concentration and ionic strength. *Carbohydrate Polymers* **82**, 1228-1235 (2010).
219. Nickerson, M.T., Paulson, A.T. & Speers, R.A. Rheological properties of gellan solutions: effect of calcium ions and temperature on pre-gel formation. *Food Hydrocolloids* **17**, 577-583 (2003).
220. Augst, A.D., Kong, H.J. & Mooney, D.J.J.M.b. Alginate hydrogels as biomaterials. **6**, 623-633 (2006).
221. Weinbreck, F., Tromp, R.H. & de Kruif, C.G. Composition and Structure of Whey Protein/Gum Arabic Coacervates. *Biomacromolecules* **5**, 1437-1445 (2004).

222. Zhivkov, A.M. in Cellulose-Fundamental Aspects (InTech, 2013).
223. Hoogendam, C.W. et al. Persistence Length of Carboxymethyl Cellulose As Evaluated from Size Exclusion Chromatography and Potentiometric Titrations. *Macromolecules* **31**, 6297-6309 (1998).
224. Shang, J., Shao, Z. & Chen, X. Electrical Behavior of a Natural Polyelectrolyte Hydrogel: Chitosan/Carboxymethylcellulose Hydrogel. *Biomacromolecules* **9**, 1208-1213 (2008).
225. Zhao, Q. et al. Synthesis and characterization of soluble chitosan/sodium carboxymethyl cellulose polyelectrolyte complexes and the pervaporation dehydration of their homogeneous membranes. *Journal of Membrane Science* **333**, 68-78 (2009).
226. Feng, X., Pelton, R. & Leduc, M. Mechanical Properties of Polyelectrolyte Complex Films Based on Polyvinylamine and Carboxymethyl Cellulose. *Industrial & Engineering Chemistry Research* **45**, 6665-6671 (2006).
227. Chollakup, R., Smitthipong, W., Eisenbach, C.D. & Tirrell, M. Phase Behavior and Coacervation of Aqueous Poly(acrylic acid)−Poly(allylamine) Solutions. *Macromolecules* **43**, 2518-2528 (2010).
228. Wang, Q. & Schlenoff, J.B. The Polyelectrolyte Complex/Coacervate Continuum. *Macromolecules* **47**, 3108-3116 (2014).
229. Attard, P., Antelmi, D. & Larson, I. Comparison of the Zeta Potential with the Diffuse Layer Potential from Charge Titration. *Langmuir* **16**, 1542-1552 (2000).
230. Tang, Y.-F., Du, Y.-M., Hu, X.-W., Shi, X.-W. & Kennedy, J.F. Rheological characterisation of a novel thermosensitive chitosan/poly(vinyl alcohol) blend hydrogel. *Carbohydrate Polymers* **67**, 491-499 (2007).
231. Ramazani-Harandi, M.J., Zohuriaan-Mehr, M.J., Yousefi, A.A., Ershad-Langroudi, A. & Kabiri, K. Rheological determination of the swollen gel strength of superabsorbent polymer hydrogels. *Polymer Testing* **25**, 470-474 (2006).
232. Kuo, C.K. & Ma, P.X. Ionically crosslinked alginate hydrogels as scaffolds for tissue engineering: Part 1. Structure, gelation rate and mechanical properties. *Biomaterials* **22**, 511-521 (2001).
233. Silva-Correia, J. et al. Gellan gum-based hydrogels for intervertebral disc tissue-engineering applications. **5**, e97-e107 (2011).
234. Steed, J.W. First- and second-sphere coordination chemistry of alkali metal crown ether complexes. *Coordination Chemistry Reviews* **215**, 171-221 (2001).
235. Key, P. & Sellen, D. A laser light-scattering study of the structure of agarose gels. *Journal of Polymer Science: Polymer Physics Edition* **20**, 659-679 (1982).
236. Sellen, D. Laser light scattering study of polyacrylamide gels. *Journal of Polymer Science Part B: Polymer Physics* **25**, 699-716 (1987).
237. Qi, L., Chapel, J.-P., Castaing, J.-C., Fresnais, J. & Berret, J.-F.J.S.M. Organic versus hybrid coacervate complexes: co-assembly and adsorption properties. **4**, 577-585 (2008).
238. Fouissac, E., Milas, M., Rinaudo, M. & Borsali, R.J.M. Influence of the ionic strength on the dimensions of sodium hyaluronate. **25**, 5613-5617 (1992).
239. Matsumoto, T., Mashiko, K.J.P.E. & Science Influence of added salt on dynamic viscoelasticity of carboxymethylcellulose aqueous systems. **28**, 393-402 (1988).

240. Coutinho, D.F. et al. Modified Gellan Gum hydrogels with tunable physical and mechanical properties. *Biomaterials* **31**, 7494-7502 (2010).
241. Ru, Q., Wang, Y., Lee, J., Ding, Y. & Huang, Q. Turbidity and rheological properties of bovine serum albumin/pectin coacervates: Effect of salt concentration and initial protein/polysaccharide ratio. *Carbohydrate Polymers* **88**, 838-846 (2012).
242. Chai, C., Lee, J. & Huang, Q. The effect of ionic strength on the rheology of pH-induced bovine serum albumin/κ-carrageenan coacervates. *LWT - Food Science and Technology* **59**, 356-360 (2014).
243. Qazvini, N.T., Bolisetty, S., Adamcik, J. & Mezzenga, R. Self-Healing Fish Gelatin/Sodium Montmorillonite Biohybrid Coacervates: Structural and Rheological Characterization. *Biomacromolecules* **13**, 2136-2147 (2012).
244. Huang, G.Q., Xiao, J.X., Wang, S.Q. & Qiu, H.W. Rheological properties of O-carboxymethyl chitosan – gum Arabic coacervates as a function of coacervation pH. *Food Hydrocolloids* **43**, 436-441 (2015).
245. Sjöblom, J. et al. Our current understanding of water-in-crude oil emulsions.: Recent characterization techniques and high pressure performance. *Advances in Colloid and Interface Science* **100-102**, 399-473 (2003).
246. Tabor, R.F. et al. Homo-and hetero-interactions between air bubbles and oil droplets measured by atomic force microscopy. **7**, 8977-8983 (2011).
247. Almatroushi, E. & Borhan, A. Interaction and Coalescence of Drops and Bubbles Rising through a Tube. *Industrial & Engineering Chemistry Research* **45**, 398-406 (2006).
248. Aston, D.E. & Berg, J.C. Quantitative Analysis of Fluid Interface–Atomic Force Microscopy. *Journal of Colloid and Interface Science* **235**, 162-169 (2001).
249. Benjamins, J., Lyklema, J. & Lucassen-Reynders, E.H. Compression/Expansion Rheology of Oil/Water Interfaces with Adsorbed Proteins. Comparison with the Air/Water Surface. *Langmuir* **22**, 6181-6188 (2006).
250. Maldonado-Valderrama, J. & Patino, J.M.R. Interfacial rheology of protein–surfactant mixtures. *Current Opinion in Colloid & Interface Science* **15**, 271-282 (2010).
251. Langevin, D. Influence of interfacial rheology on foam and emulsion properties. *Advances in Colloid and Interface Science* **88**, 209-222 (2000).
252. Bush, J.W.M., Hu, D.L. & Prakash, M. in Advances in Insect Physiology, Vol. 34. (eds. J. Casas & S.J. Simpson) 117-192 (Academic Press, 2007).
253. Lee, D.-G. & Kim, H.-Y.J.J.o.F.M. The role of superhydrophobicity in the adhesion of a floating cylinder. **624**, 23-32 (2009).
254. Vella, D.J.L. Floating objects with finite resistance to bending. **24**, 8701-8706 (2008).
255. Keller, J.B.J.P.o.F. Surface tension force on a partly submerged body. **10**, 3009-3010 (1998).
256. Snyder, B.A., Aston, D.E. & Berg, J.C.J.L. Particle− drop interactions examined with an atomic force microscope. **13**, 590-593 (1997).
257. Sader, J.E., Chon, J.W.M. & Mulvaney, P. Calibration of rectangular atomic force microscope cantilevers. *Review of Scientific Instruments* **70**, 3967-3969 (1999).
258. Keese, C.R. & Giaever, I. Substrate mechanics and cell spreading. *Experimental Cell Research* **195**, 528-532 (1991).

259. Choi, J.-H. et al. Influence of pH and Surface Chemistry on Poly(l-lysine) Adsorption onto Solid Supports Investigated by Quartz Crystal Microbalance with Dissipation Monitoring. *The Journal of Physical Chemistry B* **119**, 10554-10565 (2015).
260. Roberts, S.A., Kellaway, I.W., Taylor, K.M.G., Warburton, B. & Peters, K. Combined Surface Pressure−Interfacial Shear Rheology Study of the Effect of pH on the Adsorption of Proteins at the Air−Water Interface. *Langmuir* **21**, 7342-7348 (2005).
261. Erickson, J.S., Sundaram, S. & Stebe, K.J. Evidence that the Induction Time in the Surface Pressure Evolution of Lysozyme Solutions Is Caused by a Surface Phase Transition. *Langmuir* **16**, 5072-5078 (2000).
262. Martin, A.H., Meinders, M.B.J., Bos, M.A., Cohen Stuart, M.A. & van Vliet, T. Conformational Aspects of Proteins at the Air/Water Interface Studied by Infrared Reflection−Absorption Spectroscopy. *Langmuir* **19**, 2922-2928 (2003).
263. Wilde, P.J. Interfaces: their role in foam and emulsion behaviour. *Current Opinion in Colloid & Interface Science* **5**, 176-181 (2000).
264. Serrien, G., Geeraerts, G., Ghosh, L. & Joos, P. Dynamic surface properties of adsorbed protein solutions: BSA, casein and buttermilk. *Colloids and Surfaces* **68**, 219-233 (1992).
265. Eastoe, J. & Dalton, J.S. Dynamic surface tension and adsorption mechanisms of surfactants at the air–water interface. *Advances in Colloid and Interface Science* **85**, 103-144 (2000).
266. Koch, S., Woias, P., Meixner, L.K., Drost, S. & Wolf, H. Protein detection with a novel ISFET-based zeta potential analyzer. *Biosensors and Bioelectronics* **14**, 413-421 (1999).
267. Volodkin, D., Ball, V., Schaaf, P., Voegel, J.-C. & Mohwald, H. Complexation of phosphocholine liposomes with polylysine. Stabilization by surface coverage versus aggregation. *Biochimica et Biophysica Acta (BBA) - Biomembranes* **1768**, 280-290 (2007).
268. Jachimska, B. & Pajor, A. Physico-chemical characterization of bovine serum albumin in solution and as deposited on surfaces. *Bioelectrochemistry* **87**, 138-146 (2012).